Journal Pre-proof

A Comprehensive Electrochemical Study of 2-Mercaptobenzoheterocyclic Derivatives. Air-Assisted Electrochemical Synthesis of New Sulfonamide Derivatives

Nesa Yousefloui, Saber Alizadeh, Mahmood Masoudi-Khoram, Davood Nematollahi, Hojjat Alizadeh

PII: S0013-4686(20)30844-6

DOI: https://doi.org/10.1016/j.electacta.2020.136451

Reference: EA 136451

To appear in: *Electrochimica Acta*

Received Date: 5 March 2020

Revised Date: 11 May 2020

Accepted Date: 12 May 2020

Please cite this article as: N. Yousefloui, S. Alizadeh, M. Masoudi-Khoram, D. Nematollahi, H. Alizadeh, A Comprehensive Electrochemical Study of 2-Mercaptobenzoheterocyclic Derivatives. Air-Assisted Electrochemical Synthesis of New Sulfonamide Derivatives, *Electrochimica Acta*, https://doi.org/10.1016/j.electacta.2020.136451.

A Comprehensive Electrochemical Study of 2-Mercaptobenzoheterocyclic Derivatives. Air-Assisted Electrochemical Synthesis of New Sulfonamide Derivatives

Nesa Yousefloui,a Saber Alizadeh,a Mahmood Masoudi-Khoram,a Davood Nematollahi*a and Hojjat Alizadehb

Graphical Abstract

In this work, we have introduced a green air-assisted electrochemical method for the synthesis of new sulfonamide derivatives via oxidative coupling of heterocyclic thiols and amines.

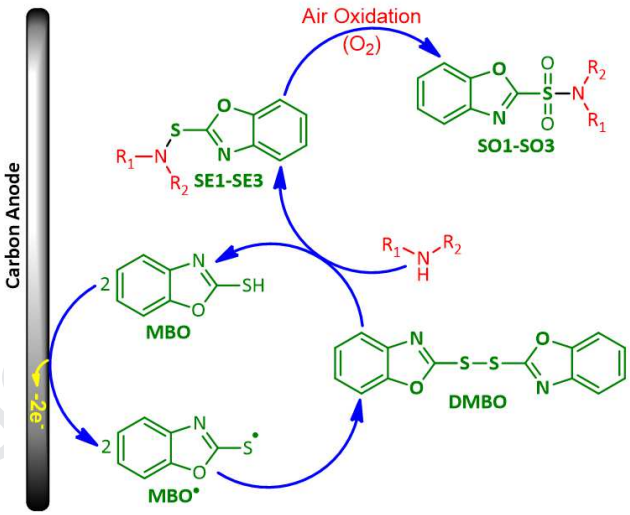

Highlights

- Electrochemical synthesis of new sulfonamide derivatives.
- Comprehensive electrochemical study of 2-mercaptobenzoheterocyclic derivatives.
- Antimicrobial activity of synthesized sulfonamide and sulfonamide derivatives.
- Scaling up experiments.
- Mechanistic studies.

A Comprehensive Electrochemical Study of 2-Mercaptobenzoheterocyclic Derivatives. Air-Assisted Electrochemical Synthesis of New Sulfonamide Derivatives

Nesa Yousefloui,[a] Saber Alizadeh,[a] Mahmood Masoudi-Khoram,[a] Davood Nematollahi[*a] and Hojjat Alizadeh[b]

E-Mail: nemat@basu.ac.ir

[a]Faculty of Chemistry, Bu-Ali Sina University, Hamedan, Iran. Zip Code 65178-38683

[b]Rooyana veterinary laboratory, Saqqez, Kurdistan, Iran

[*]Corresponding author. Tel.: + 0098 813 8271541; fax: +0098 813 8272404.

E-mail addresses: *nemat@basu.ac.ir, dnematollahi@yahoo.com* (D. Nematollahi).

Fax: +0098 813 8257407, Tel: +0098 813 8282807.

ABSTRACT

In this work, we have introduced a green air-assisted electrochemical method for the synthesis of new sulfonamide derivatives via oxidative coupling of heterocyclic thiols and amines. The synthetic method was designed based on the data collected from electrochemical oxidation of heterocyclic thiols in the absence and presence of amines. These compounds have been successfully synthesized in water/ethanol mixture solutions in an undivided cell, at carbon rod electrodes, by constant current electrolysis at room temperature. The proposed method does not need to use toxic solvent, metal, catalyst and challenging workups. This method is easy to scale-up and the products have antibacterial activity.

Keywords: 2-Mercaptobenzoheterocyclic compounds, Sulfonamide derivatives, Green chemistry, Electrochemical synthesis, Cyclic voltammetry, Sulfenamide derivatives.

1. Introduction

Sulfonamides are the first group of antibiotics to be used systemically in the treatment of bacterial infections [1]. In addition, they are used as anticancer, anti-inflammatory and antiviral agents [2-6]. Some of them, also used for the treatment of type II diabetes [7], coronary artery disease and asthma [8], Alzheimer's disease [9] and respiratory diseases [10]. Despite the importance of these compounds, the methods used to synthesize sulfonamides have serious problems [11]. A literature survey reveals that the conventional methods for the synthesis of sulfonamides are the reaction of amines with sulfonyl chlorides [12-14], palladium-catalyzed sulfination of aryl and heteroaryl halides [15,16], gold(I)-catalyzed sulfination of aryl boronic acids [17], palladium-catalyzed reaction of haloarenes bearing amino groups with sulfur dioxide [18], three-component reaction of sodium

metabisulfite, sodium azide and aryldiazonium [19], Cu(II)-catalyzed reaction of (hetero)aryl boronic acids and amines, along with sulfur dioxide [20], copper-catalyzed regioselective cleavage of C−X and C−H bonds [21], copper-catalyzed reaction of tri-arylbismuth, $Na_2S_2O_5$ and nitro compounds in a deep eutectic solvent [22], cobalt-phthalocyanine-catalyzed aerobic oxidative coupling of thiols and amines [23], I_2O_5-mediated oxidative coupling of aryl thiols and amines [24] and electrochemical methods [25,26]. Although some of these methods are efficient but they include compounds such as sulfonyl chlorides, DABSO (SO_2 surrogate) and choline chloride that are expensive, unstable and unsafe. In addition, these methods have the disadvantages such as heavy metal pollution, strongly acidic/basic media, unsafe solvent, tedious work-up, high temperature and long reaction time. A very interesting paper recently published on the electrochemical synthesis of sulfonamide compounds via oxidative coupling of thiols with amines [27]. Although many problems have been addressed in this paper, there still exist problems associated with this paper including the use of toxic acetonitrile solvent, strong acidic media and the inability to synthesis of sulfonamide based on 2-mercaptobenzoheterocyclic compounds.

Another series of compounds synthesized in this study are sulfenamides. These compounds containing divalent sulfur bonded to trivalent nitrogen, which have been widely used in the vulcanization of rubbers as accelerator [28]. For example, *N-tert*-butyl-2-benzothiazole sulfenamide (TBBS) is the most widely used sulfonamide in the rubber industry as vulcanization accelerator [29,30]. In addition to rubber industry, sulfenamides are widely used in agriculture as plant growth regulators, pesticides and fungicides [28,31,32]. They have also shown many important biological activities such as antitumor, antiplatelet, antiasthmatic, antimicrobial and lipoxygenase activities [28,31-36].

The importance of sulfonamide and sulfenamide compounds has prompted many researchers to search for new compounds with higher activity and/or develop efficient methods of synthesis. Our literature survey shows that methods for the synthesis of sulfenamide consist of metal-assisted synthesis [37,38], hypervalent iodine(III) activated method [39], microwave-assisted synthesis [40], reaction of amines with thiophthalimides [41], transamination of *N*-unsubstituted sulfonamides [42], copper-catalyzed [43,44]. These methods [37-44], have the disadvantages such as heavy metal pollution, tedious work-up, low atom economy, safety problems, high temperatures, toxic and expensive reagents. However, the development of a simple and environmentally friendly methodology is still required for the synthesis of sulfonamide and sulfenamide compounds. The present work describes an air-assisted electrochemical method for the synthesis of titled compounds via electrochemical oxidation of 2-mercaptobenzoxazole in the presence of some amines under simple and green conditions, without toxic solvents and reagents, using carbon electrode in water/ethanol mixture. Another feature of the proposed method is its amenability to scaling up which is discussed in the text.

In addition, a comprehensive study on the electrochemical behavior of 2-mercaptobenzoxazole (**MBO**), 2-mercaptobenzothiazole (**MBT**) and 2-mercaptobenzimidazole (**MBI**) in water/ethanol mixture were carried out by cyclic voltammetry. This work proposed the mechanisms for the electrochemical oxidation of **MBO**, **MBT** and **MBI** in the absence and presence of amines.

2. Experimental

2.1. Reagents and apparatus

2-Mercaptobenzoxazole (**MBO**) (95%), 2-mercapto benzothiazole (**MBT**) (97%), 2-mercaptobenzimidazole (**MBI**) (98%), diethylamine (**AM1**) (≥99.5%), cyclohexylamine (**AM2**) (≥99%), piperidine (**AM3**) (≥99%), sodium hydrogen phosphate (99%) and sodium dihydrogen phosphate (99%) were obtained from Sigma-Aldrich. Ethanol, sodium bicarbonate (98%), sodium carbonate (98%), hydrochloric acid (37%), sodium hydroxide (99%) were obtained from Merck (Darmstadt, Germany). These chemicals were used without further purification. The buffered solutions were prepared based on Kolthoff tables.

The glassy carbon electrode was polished using alumina slurry (3.0 – 0.1 µm). Melting points were measured with a Barnstead Electrothermal 9100 apparatus. IR spectra (KBr) were recorded on Perkin–Elmer GX FT-IR spectrometer. ^{1}H and ^{13}C NMR spectra were recorded on a Bruker Avance DRX-400 spectrometer at 400 MHz and INOVA 500 MHz. The mass spectra were recorded on MS Model: 5975C VL MSD with Tripe-Axis Detector. Cyclic voltammetry was performed using a Sama-500 potentiostat/galvanostat. Typical voltammetry experiments were carried out on a classical three electrode undivided cell configuration with a platinum auxiliary electrode and a glassy carbon (GC) working electrode (surface area = 1.8 mm^2). The working electrode potentials were measured versus Ag/AgCl (3M KCl) (all electrodes from AZAR electrode). The Macro-scale electrolysis was carried out with a two electrode system under constant current condition by a dc power supply Dazheng ps-303D. The working electrode (anode) used in macro-scale electrolysis was an assembly of five ordinary soft carbon rods (38 cm^2), placed circularly around a stainless steel cylinder cathode (25 cm^2 area).

Autolab model PGSTAT302N potentiostat/galvanostat was used for preparative electrolysis, controlled-potential coulometry and cyclic voltammetry. A glassy carbon disc (1.8 mm^2 areas) and a platinum wire were used as working and counter electrodes, respectively. An assembly of four graphite rods (30 cm^2) and a large stainless steel gauze were used as working and counter

electrodes in controlled-potential coulometry and macro scale electrolysis, respectively. The potential of the working electrode was measured against Ag/AgCl (AZAR electrode). All chemicals were purchased from commercial sources and used without further purification.

2.2. Characteristic of the products

***N,N*-diethylbenzo[d]oxazole-2-sulfonamide (SO1) ($C_{11}H_{14}N_2O_3S$).** Light yellow oil, yield: 59%, ^{1}H NMR (400 MHz, DMSO-d_6) δ/ppm: 7.48 (d, *J* = 8 Hz, 2H, aromatic), 7.25 (d, *J* = 8 Hz, 2H, aromatic), 2.94 (q, 4H, methylene), 1.17 (t, 6H, methyl). ^{13}C NMR (100 MHz, DMSO-d_6) δ/ppm: 11.0, 41.3, 109.7, 110.8, 123.4, 124.9, 132.2, 148.3, 180.2. IR (KBr) v/cm^{-1}: 2971, 2823, 2776, 1764, 1618, 1507, 1449, 1279, 1247, 1132, 1096, 1008, 931, 744, 647, 607. MS (EI, 70 eV) m/z (%): 256 (M, 3), 192 (3), 151 (100), 91 (26), 58 (62).

***N*-Cyclohexyl-2-benzoxazole sulfonamide (SO2) ($C_{13}H_{16}N_2O_3S$).** Light yellow oil, yield: 79%. ^{1}H NMR (500 MHz, DMSO-d_6) δ/ppm: 7.62 (d, *J* = 7.8, 1H, NH), 7.21 (d, *J* = 7.7 Hz, 1H, aromatic), 7.16 (d, *J* = 7.5 Hz, 1H, aromatic), 7.04 (t, *J* = 7.5 Hz, 1H, aromatic), 6.96 (t, *J* = 7.3 Hz, 1H, aromatic), 3.01 (s, 1H, CH), 1.92 (d, *J* = 10.1 Hz, 2H, CH), 1.70 (d, *J* = 12.1 Hz, 2H, CH), 1.55 (d, *J* = 12.8 Hz, 1H, CH), 1.37 - 1.14 (m, 5H, CH). ^{13}C NMR (100 MHz, DMSO-d_6) δ/ppm: 182.1, 150.8, 142.1, 123.2, 121.0, 113.5, 108.2, 49.9, 30.8, 25.0, 24.2. IR (KBr) v/cm^{-1}: 3476, 2935, 2854, 2588, 2523, 2048, 1890, 1759, 1698, 1643, 1538, 1507, 1464, 1431, 1381, 1346, 1252, 1132, 1114, 1070, 1003, 890, 741, 625, 605, 552, 450, 417. MS (EI, 70 eV) m/z (%): 279 (M, 3), 41 (75), 57 (86), 76 (16), 104 (25), 132 (7), 149 (100), 167 (15).

***N*-Piperidin-2-benzoxazole sulfonamide (SO3) ($C_{12}H_{14}N_2O_3S$).** Light yellow oil, yield: 62%. ^{1}H NMR (500 MHz, DMSO-d_6) δ/ppm: 7.31 (d, *J* = 7.9 Hz, 1H, aromatic), 7.21 (d, *J* = 7.7 Hz, 1H, aromatic), 7.12 (t, *J* = 7.1 Hz, 1H, aromatic), 7.06 (t, *J* = 7.1 Hz, 1H, aromatic), 3.09 - 2.73 (m, 4H, CH), 1.68 - 1.51 (m, 6H, CH). ^{13}C NMR (126 MHz, DMSO-d_6) δ/ppm: 181.6, 150.0, 138.3, 124.0, 122.2, 112.6, 109.0, 44.1, 22.7, 22.1. IR (KBr) v/cm^{-1}: 3445, 3049, 2941,

2855, 1774, 1640, 1578, 1501, 1451, 1424, 1248, 1131, 1069, 1004, 921, 743, 627, 552, 418. MS (EI, 70 eV) *m/z* (%): 266 (M, 0.2), 41 (32), 64 (74), 91 (65), 84 (62), 134 (48), 151 (100), 173 (10), 202 (35), 256 (10).

***N,N*-diethylbenzo[d]thiazole-2-sulfenamide (SE4) ($C_{11}H_{14}N_2S_2$).** Light yellow oil, yield: 65%. ^{1}H NMR (500 MHz, DMSO-d_6) δ/ppm: 7.95 (d, J = 7.9 Hz, 1H, aromatic), 7.76 (d, J = 8.1 Hz, 1H, aromatic), 7.39 (t, J = 7.7 Hz, 1H, aromatic), 7.28 (t, J = 7.6 Hz, 1H, aromatic), 3.08 (q, J = 7.0 Hz, 4H, methylene), 1.14 (t, J = 7.1 Hz, 6H, methyl). ^{13}C NMR (126 MHz, DMSO-d_6) δ/ppm: 178.3, 155.1, 134.9, 126.4, 124.1, 122.0, 121.6, 52.3, 13.7. IR (KBr) v/cm^{-1}: 2972, 2931, 2855, 1563, 1468, 1429, 1376, 1310, 1273, 1159, 1081, 1023, 1009, 756, 727, 669, 432. MS (EI, 70 eV) *m/z* (%): 239 (M, 33), 167 (20), 108 (4), 72 (100), 42 (15).

***N*-Cyclohexyl-2-benzothiazole sulfenamide (SE5) ($C_{13}H_{16}N_2S_2$).** White solid, yield: 88%, isolated yield: 53%. mp: 95-97 ℃. ^{1}H NMR (500 MHz, DMSO-d_6) δ/ppm: 7.98 (d, J = 8.5 Hz, 1H, aromatic), 7.73 (d, J = 8.1 Hz, 1H, aromatic), 7.41 (t, 1H, aromatic), 7.29 (t, 1H, aromatic), 5.49 (d, J = 5.8 Hz, 1H, NH), 2.77 (m, J = 9.2, 4.4 Hz, 1H, CH), 1.97 (s, 2H, CH), 1.70 (s, 2H, CH), 1.54 (d, J = 11.6 Hz, 1H, CH), 1.22 (t, 5H, CH). ^{13}C NMR (126 MHz, DMSO-d_6) δ/ppm: 181.4, 155.3, 134.8, 126.4, 123.9, 122.1, 121.4, 59.9, 33.5, 25.8, 24.8. IR (KBr) v/cm^{-1}: 3443, 3222, 2930, 2850, 1560, 1463, 1427, 1316, 1241, 1187, 1068, 1012, 753, 726. MS (EI, 70 eV) m/z (%): 265 (M, 86), 41 (70), 55 (64), 83 (14), 98 (100), 122 (11), 149 (15), 167 (86), 182 (17), 221 (11).

***N*-Piperidin-2-benzothiazole sulfenamide (SE6) ($C_{12}H_{14}N_2S_2$).** Light yellow oil, yield: 74%. ^{1}H NMR (500 MHz, DMSO-d_6) δ/ppm: 8.00 (d, J = 7.9 Hz, 1H, aromatic), 7.77 (d, J = 8.1 Hz, 1H, aromatic), 7.41 (t, J = 7.6 Hz, 1H, aromatic), 7.30 (t, J = 7.6 Hz, 1H, aromatic), 3.17 - 2.86 (m, 4H, CH), 1.67 - 1.40 (m, 6H, CH). ^{13}C NMR (126 MHz, DMSO-d_6) δ/ppm: 176.9, 155.2, 135.0, 126.5, 124.2, 122.2, 121.7, 57.9,

27.4, 22.9. IR (KBr) v/cm^{-1}: 3064, 2939, 2847, 1559, 1453, 1467, 1427, 1362, 1310, 1271, 1157, 1126, 1081, 1008, 919, 856, 761, 729, 667, 429. MS (EI, 70 eV) m/z (%): 251 (M, 39.5), 42 (36), 69 (6.5), 55 (33), 84 (100), 108 (5.9), 167 (18.3).

3. Results and Discussion

3.1. Electrochemical study of 2-mercaptobenzoheterocyclic compounds

In this work, electrochemical oxidation of **MBO**, **MBT** and **MBI** have been studied in two stages. The first stage involves studying the electrochemical behavior of these compounds in order to better understand the oxidation mechanism, electrochemical properties of the compounds and produced intermediates. The second part involves the electrochemical study of these compounds in the presence of diethylamine, cyclohexanamine and piperidine in order to obtain the necessary information for synthesis of sulfonamide and sulfenamide compounds.

Fig. 1, part I, shows the cyclic voltammograms of **MBO** (1.0 mM) in aqueous phosphate buffer (c = 0.2 M, pH = 7.0) by changing the potential scan rate between 10 and 1000 mV/s. The Figure shows that at the scan rate of 10 mV/s, the voltammogram has two anodic peaks (A_1 and A_2) and one sharp and symmetric cathodic peak (C_1). The effect of increasing scan rate on the voltammetric response is quite complex. At first with increasing scan rate from 10 to 50 mV/s, the anodic peak A_2 removed and both I_{pA1} and I_{pC1} increase linearly with v. With further increase in scan rate, I_{pA1} continues to increase linearly (I_{pA1} = 0.03 v + 1.80, R^2 = 0.9925) (Fig. 1 part II). In order to obtain further data on the adsorption/diffusion behavior of **MBO**, the log I_{pA1}changes were plotted against the log v (Fig. 1 part III).

[Figure 1]

The slope of the line is a measure of the adsorption/diffusion of **MBO** on the surface of electrode. It is found that when the slope of the line is equal to 0.5, the process is pure diffusion-controlled, however, when the slope is 1, the process is pure adsorption-controlled [45]. The slope of the line is 0.75, which are higher than 0.5 and less than one that confirms the adsorption-diffusion process for electrochemical oxidation of **MBO**. With increasing potential scan rate from 50 mV/s, the voltammetric behavior of peak C_1 is quite complex (Fig. 1 parts I and IV).

At low scan rates (10, 25 and 50 mV/s), the peak is sharp and symmetrical and increases linearly with v (characteristic of an adsorption peak [45]). However, with increasing potential scan rate, I_{pC1} changes abnormally (Fig. 1 part I). At high scan rates (500, 750 and 1000 mV/s), the cathodic peak C_1 becomes almost a normal diffusion peak and its current increases linearly with $v^{1/2}$ at high scan rates (characteristic of a diffusion peak [45]) (Fig. 1 part IV, inset).

Figure 2 part I compares the electrochemical behavior of **MBO** in water (phosphate buffer, pH = 7.0 and *c* = 0.2 M), at two different switching potentials. The Figure clearly shows that when the switching potential increases from 0.30 V to 0.65 V, the amount of adsorbed material and adsorption intensity have increased dramatically. Based on these results, it can be concluded that the over-oxidation of **MBO** appears to lead to the formation of materials with a higher adsorption property.

Figure 2 part II compares peak C_1 in different water (phosphate buffer, pH = 8.0, c = 0.2 M)/ethanol mixtures. As can be seen, when the percentage of ethanol in the mixture is zero (curve a), the cathodic peak C_1 shows the characteristic of a complete adsorption peak. However, with increasing ethanol percentage in the solvent mixture, peak C_1 tends to become a normal diffusion peak (curve c).

[Figure 2]

Fig. 3 shows the linear sweep voltammograms of **MBO** at scan rate of 10 mV/s, in ethanol/H_2O (with different pH values) (20/80, v/v) mixture. As can be seen at all studied pHs, the voltammograms show an anodic peak (A_1) in the positive going scan. The shift of peaks towards negative potentials with increasing pH values is a sign of the participation of proton in the redox process. According to these data, and taking into account the previously reported data [27,46,47], we proposed the following mechanism for electrochemical oxidation of **MBO** at different pH solutions.

[Figure 3]

At pH values less than 3.5, the oxidation mechanism of **MBO** is shown in Eq. 1. According to this equation, two protonated **MBOs** become dimer after losing two electrons and four protons. At this condition, the slope for the *E*-pH line is 113 mV/pH, which is close to the theoretical value of 118 mV/pH for a two-electron/four-proton process.

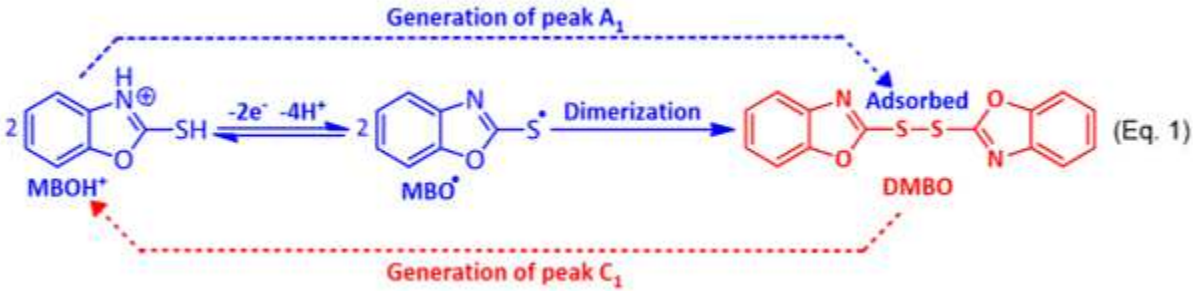

At pH values more than 3.5 and less than 6.9, the oxidation mechanism of **MBO** is shown in Eq. 2. In this condition, the slope for the *E*-pH line is 53 mV/pH, which is close to the theoretical value of 59 mV/pH for a two-electron/two-proton process.

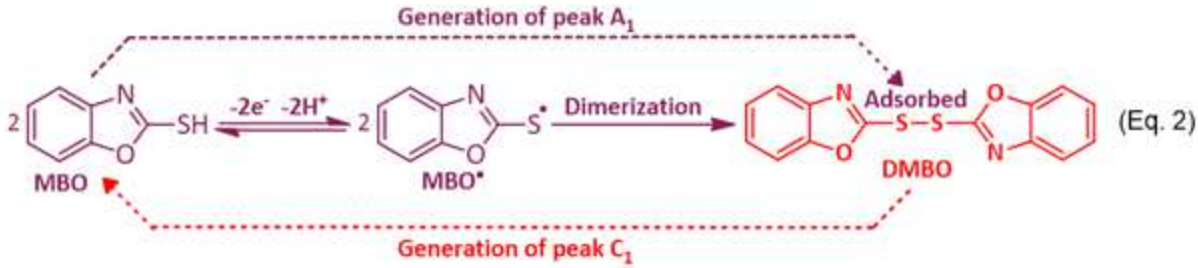

At pH values more than 6.9, the oxidation mechanism of **MBO** is shown in Eq. 3. In this region (pH > 6.9), **MBO** is in its anionic form and in its redox process the proton is not exchanged. In addition, from data shown in Fig. 3 part II, we can conclude that the pK_a values for acid/base equilibria of **MBOH**$^+$/**MBO** and **MBO**/**MBO**$^-$ are 3.5 and 6.9, respectively (Eqs. 4 and 5). These data are in agreement with previously published data [46,48].

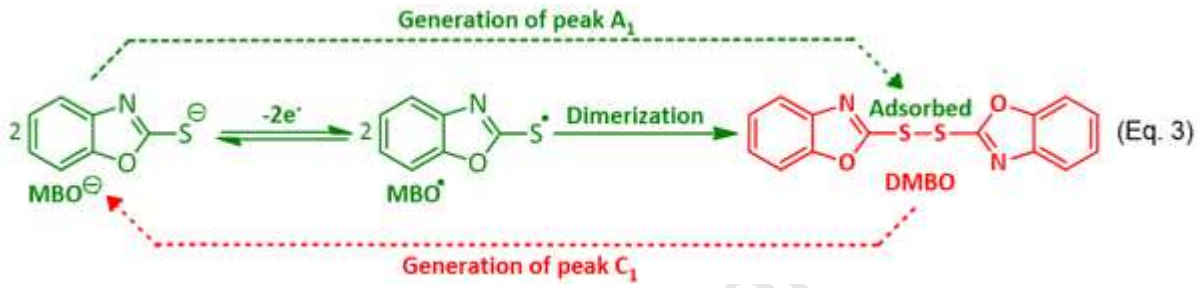

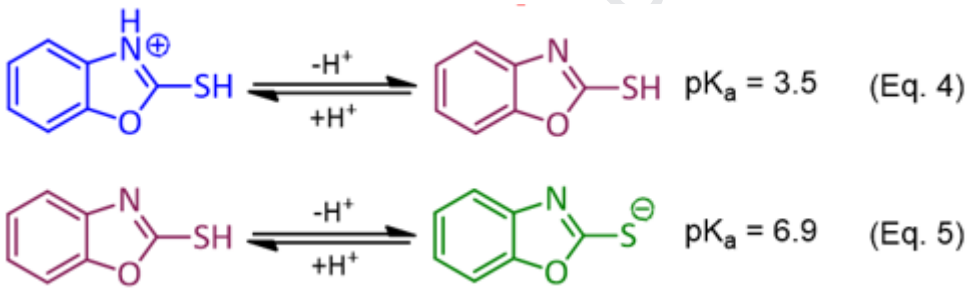

According to our data, the anodic peak A_1 pertains to the oxidation of **MBO** (**MBOH**$^+$ and/or **MBO**$^-$) to the **MBO** radical (**MBO**$^\bullet$). At the next step, the reaction of two **MBO** radicals leads to the formation of 1,2-bis(benzo[d]oxazol-2-yl)disulfane dimer (**DMBO**). So, at slow or moderate potential scan rates, peak C_1 pertains to the reduction of adsorbed **DMBO** to **MBO** (Eqs. 1-3). At high scan rates, however, there is no sufficient time for dimerization reaction, so, diffusion peak C_1 is related to the reduction of **MBO**$^\bullet$ to **MBO**. The change of I_{pC1} at different pH is shown in Fig. 3, part III. As can be seen, with increasing pH from 1.4 to 5.0, the adsorption activity of **DMBO** increases. We think that the relative protonation of **DMBO** and formation of a more suitable medium for hydrogen bonding is important factor for less adsorption activity of **DMBO** in more acidic solutions. The

adsorption activity of **DMBO** decreased with increasing pH from 5.0, so that at pH 9.0, peak C_1 shows the characteristic of a complete diffusion peak.

Figure 4 shows the cyclic voltammograms of **MBT** (curve a) and **MBI** (curve c) in comparison with **MBO** (curve b). As can be seen, these voltammograms are basically similar. However, they have some differences in detail. For example, the oxidation of **MBO** is higher than those of **MBT** and **MBI** due to the more electron donating ability of S and N atoms in the structure of **MBT** and **MBI** in comparison with O atom.

[Figure 4]

Other important differences in the voltammograms of **MBT**, **MBO** and **MBI** are different in adsorption ability of synthesized dimers and peak to peak separation ($\Delta E_p = E_{pA1} - E_{pC1}$). As can be seen, **MBT** shows largest peak-to-peak separation (ΔE_p = 0.68 V) and its dimer have highest adsorption activity. The result can be related to more adsorption activity of S atom in comparison with N and O atoms present in the structures of **MBO** and **MBI**. Figure 4 also shows that the lowest adsorption activity and peak-to-peak separation (ΔE_p = 0.13 V) belongs to **MBI**.

The effect of increasing potential scan rate on the cyclic voltammograms of **MBT** is shown in Fig. 5 part I. As can be seen, **MBT** shows a similar trend with that of *MBO* (Fig. 1). These experiments confirm previous results that at high scan rates, there is no sufficient time for dimerization reaction, so, peak C_1 is attributed to the reduction of **MBT**$^{\bullet}$ to **MBT**. At these scan rates, peak C_1 becomes like a normal diffusion peak and its current increases linearly with $v^{1/2}$.

[Figure 5]

The effect of increasing potential scan rate on the cyclic voltammograms of **MBI** is shown in Fig. 5 part II. Different with **MBO** and **MBT**, the cathodic peak C_1 shows a normal

behavior with increasing scan rate. The presence of two N atoms in the structure of **MBI**, makes **MBI**$^{\bullet}$ more stable than **MBT**$^{\bullet}$ and **MBO**$^{\bullet}$. Consequently, we think that in the time scale of our experiments, **MBI** dimer is not formed and peak C_1 belongs to reduction of **MBI**$^{\bullet}$ to **MBI**.

Fig. 6 shows the linear sweep voltammograms of **MBT** at scan rate of 10 mV/s, in ethanol/H_2O (with different pH values) (20/80, v/v) mixture. The shift of peak A_1 towards negative potentials with increasing pH values confirmed the participation of proton in the redox process. According to the data presented in Fig. 6, the following equations for electrochemical oxidation of **MBT** at different pH values are proposed. At pHs less than 4.0, the oxidation mechanism of **MBT** is shown in Eq. 6. In this range of pH, the slope for the *E*-pH line is 53 mV/pH, which is close to the theoretical value of 59 mV/pH for a two-electron/two-proton process. At pH values more than 4.0 and less than 7.2, the oxidation mechanism of **MBT** is shown in Eq. 7. In this region of pH, the slope for the *E*-pH line is 85 mV/pH, which confirms the occurrence of a two-electron/three-proton process as shown in Eq. 7.

[Figure 6]

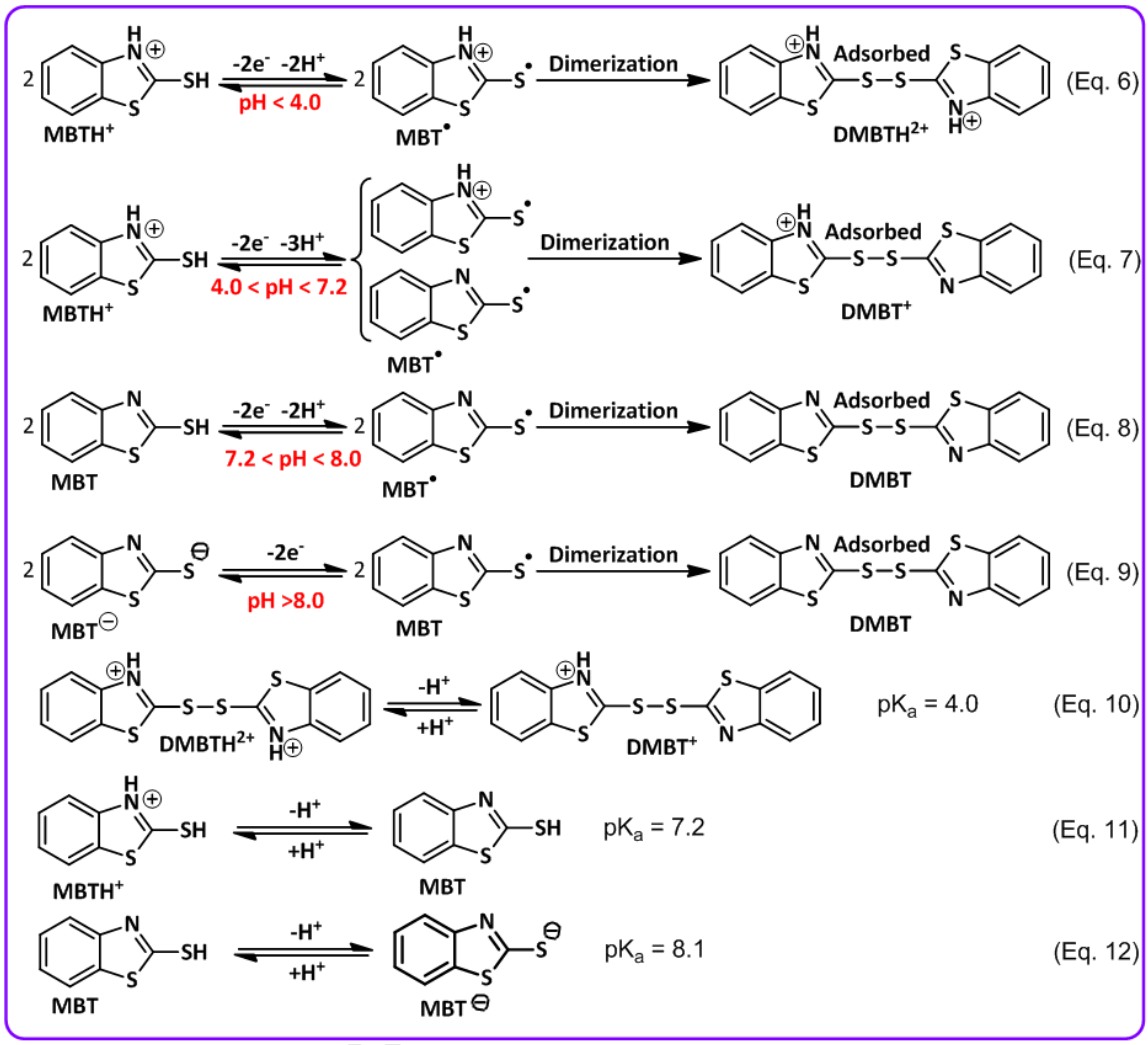

It is necessary to mention that the theoretical value for a two-electron/three-proton process is about 88 mV/pH. At pHs more than 7.2 and less than 8.0, the oxidation mechanism of **MBT** is shown in Eq. 8. In this narrow region of pH, the slope for the *E*-pH line is 50 mV/pH, which confirms the occurrence of a two-electron/two-proton process. In the basic region (pH > 8.0), **MBT** is in its anionic form (**MBT**$^-$) and so its redox process is not dependent on the pH (Eq. 9). In addition, from these data, we can determine the pK_a of the acid/base couples, **DMBTH**$^{2+}$/**DMBTH**$^+$, **MBTH**$^+$/**MBT** and **MBT**/**MBT**$^-$. The calculated pk_a values are 4.0, 7.2 and 8.1, respectively (Eqs. 10-12). These data are in agreement with previously published data [48].

Similar research was conducted on **MBI**. Fig. 7 shows the linear sweep voltammograms of **MBI** in ethanol/H_2O (with different pH values) (20/80, v/v) mixture at scan rate of 10 mV/s. According to the data presented in Fig. 7, the following equations for electrochemical oxidation of **MBI** at different pH values are proposed. At pHs less than 7.9, the oxidation mechanism of **MBI** is shown in Eq. 13. In this range of pH, **MBI** is in its protonated form and the slope for the *E*-pH line is 35 mV/pH, which is close to the theoretical value of 29.5 mV/pH for a one-electron/two-proton process.

[Figure 7]

In the pH ranging from 7.9 to 9.9, the slope for the *E*-pH line is 67 mV/pH, which is close to the theoretical value of 59 mV/pH for a one-electron/one-proton process (Eq. 14). In the basic region (pH > 9.9), **MBI** is in its anionic form (**MBI**$^-$) and so the proton does not get involved in the redox process (Eq. 15). In addition, from these graphs we can calculate the pK_a values for of the acid/base couples, **MBIH**$^+$/**MBI** and **MBI**/**MBI**$^-$. The calculated pk_a values are 7.9 and 9.9, respectively (Eqs. 16 and 17). These data are in agreement with previously published data [48].

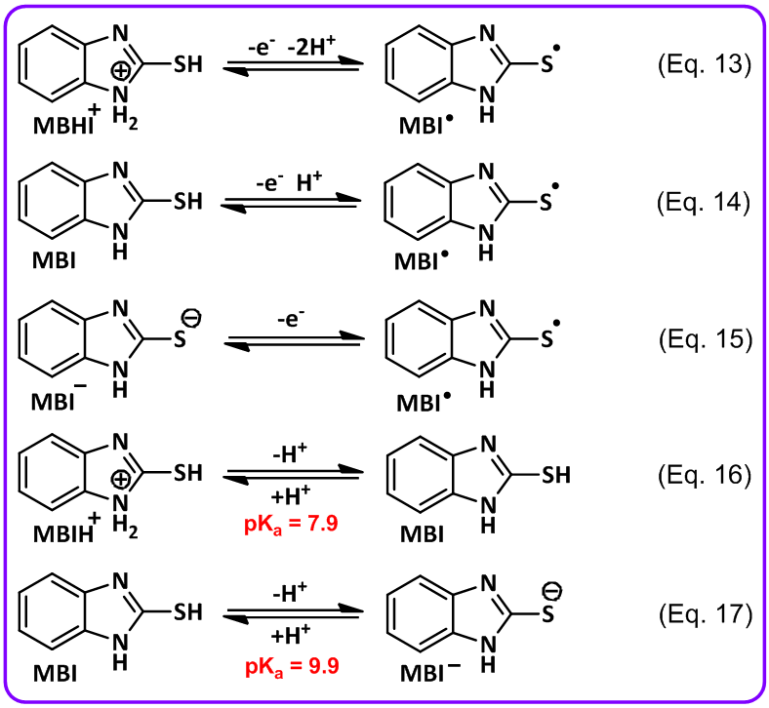

3.2. Electrochemical study of 2-mercaptobenzoheterocyclic compounds in the presence of diethylamine

In this part, to obtain the information needed for the synthesis of new compounds based on **MBO** oxidation, electrochemical study of **MBO** was carried out in the presence of diethylamine (**AM1**) to find the most suitable conditions for the synthesis as well as evaluation of the reaction mechanism. Cyclic voltammograms of **MBO** in the presence of **AM1** are shown in Fig. 8 (part I curve b) and have been compared with that of in the absence of **AM1** (curve a). Comparison of these voltammograms shows that the most important change is the removal of the cathode peak C_1. Since peak C_1 is related to the reduction of dimer (**DMBO**), its disappearance is a sign of the lack of dimer at the electrode surface. In other words, the occurrence of a fast chemical reaction between **AM1** and **DMBO**, removed the dimer from the electrode surface. Our data also show that I_{pC1} depends on the **AM1** concentration so that it decreases with increasing **AM1** concentration. Increasing the **AM1** concentration increases the reaction rate of amine with the dimer

results in the disappearance of the peak C_1 at high amine concentration. We also have found that there is a significant influence of potential sweep rate on the shape of the voltammogram (Fig. 8 part II). It is seen that the current of peak C_1 (I_{pC1}) increase with increasing potential scan rate due to the decrease in the time available for the reaction of amine with dimer at higher scan rates.

[Figure 8]

Constant current electrolysis was performed in water (pH=8.0)/ethanol mixture containing **MBO** and **AM1** at the current density of 0.26 mA.cm^{-2} (10 mA). The electrolysis progress was monitored using cyclic voltammetry (Fig. 9) and thin layer chromatography. It was found that, proportional to the electrolysis progress, the anodic peak current (I_{pA1}) decreased. The electrolysis was ended when the peak A_1 decay more than 95% (after consumption of 190 C electricity). In this condition, the spot of **MBO** disappeared on TLC.

By putting together voltammetric and amount of charge passed along with the results obtained from spectroscopic analysis of the product (mass spectroscopy and NMR), the mechanism shown in Scheme 1, is proposed for the electrochemical oxidation of **MBO** in the presence of **AM1**. According to Scheme 1, sulfonamide **SO1** is synthesized in four steps from **MBO**. First: electrolytic formation of **MBO$_{ox}$**, second: formation of dimer **DMBO**, third: nucleophilic addition of **AM1** to **DMBO**, S-S bond cleavage and formation of corresponding sulfenamide (**SE1**) and fourth: the air oxidation of sulfonamide [49-51] and converting it into the final product (**SO1**). The air oxidation of sulfonamide has caused the main product of **MBO** in the presence of **AM1** to be **SO1** and only a little amount of sulfenamide (**SE1**) was observed chromatographically.

[Figure 9]

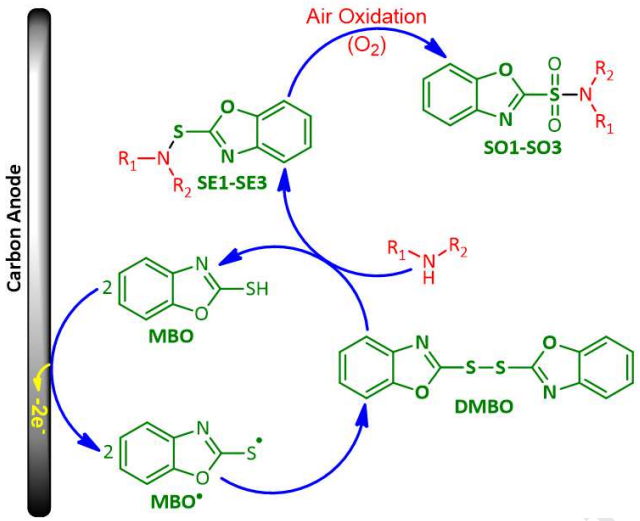

Scheme 1. Electrochemical oxidation pathway of MBO in the presence of the amines.

In the case of **MBT**, the same reaction mechanism was observed, however, the air oxidation process is not carried much. Therefore, when **MBT** is used as the starting material, the main product is sulfenamide (**SE**) and only small amounts of sulfonamide (**SO**) were observed (Scheme 2).

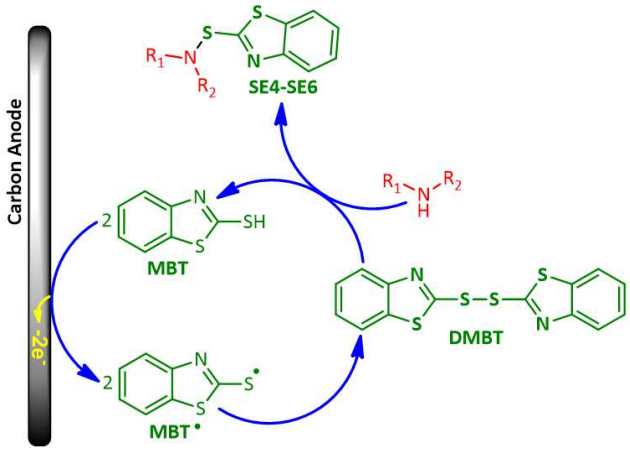

Scheme 2. Electrochemical oxidation pathway of MBT in the presence of the amines.

Different with **MBO** and **MBT**, when **MBI** is used as the starting material, as discussed in the preceding sections, the **MBI** dimer is not formed and we could not synthesize any sulfonamide or sulfenamide compounds from oxidation of **MBI** in the presence of amines.

3.3. Constant current electrolysis

Current density is one of the most important factors controlling yield and purity. The synthesis of **SO2** and **SE5**, were studied at different current densities ranging from 0.06 to 0.72 mA/cm^2, while other parameters (charge: 190 C, temperature: 298 K, **MBO** and **MBT** amount: 0.5 mmol and cyclohexylamine (**AM2**) amount: 1.5 mmol) remain constant (Fig. 10). Our results show that the highest yield for **SO2** (88%) and **SE5** (79%) were obtained at a current density of 0.26 and 0.52 mA/cm^2, respectively. In the synthesis of **SO2**, at the current densities lower than 0.26 mA/cm^2, the amount of **MBO** radicals produced per unit time decreases. As a result, they are less likely to react together to form **DMBO**. In such conditions, the **MBO** radicals participate either in the side reactions or in the back reaction in the cathode surface, therefore, despite equal charge consumption, the production yield is low. On the other hand, at the current densities higher than 0.26 mA/cm^2, the over oxidation of **DMBO** and/or **SE2** reduces the production yield.

[Figure 10]

*3.4. Electrochemical synthesis of sulfonamides (**SO1-SO3**) and sulfenamides (**SE4-SE6**)*

For the synthesis of sulfonamides **SO1**-**SO3**, an 80 ml solution containing phosphate buffer (pH = 8.0, *c* = 0.2 M)/ethanol (20/80 v/v) was pre-electrolyzed in an undivided cell. Then 0.5 mmol of **MBO**, 1.5 mmol of amine (**AM1**, **AM2** or **AM3**) was subjected to electrolysis at constant current of 10 mA (0.26 mA cm^{-2}), in an undivided cell. The progress of the electrolysis was followed by TLC using *n*-hexane/ethyl acetate (2:1) and also cyclic voltammetry. At the end of electrolysis, the reaction mixture was filtered and then the ethanol was removed under vacuum. The residual was extracted with 3 x 10 ml of ethyl acetate. The extracted organic phase was dried over anhydrous sodium sulphate, filtered

and evaporated under reduced pressure. The resulting residue was purified by flash chromatography on silica gel (eluent 2:1 *n*-hexane–ethyl acetate) to afford the corresponding sulfonamide (Table 1).

[Table 1]

For the synthesis of sulfenamides **SE4**-**SE6**, in a solution containing carbonate buffer (pH = 12.0, *c* = 0.2 M)/ethanol (20/80 v/v), **MBT** and amine (**AM1**, **AM2** or **AM3**) was subjected to electrolysis at constant current of 20 mA (0.52 mA cm^{-2}), in an undivided cell. Other conditions for the synthesis of sulfenamides **SE4**-**SE6**, are similar to the synthesis of sulfonamides (Table 2).

[Table 2]

3.5. Scaling up experiments

In this part, we describe the large scale synthesis of **SO2** and **SE5**. Fig. 11 shows the electrochemical cell designed and manufactured for this purpose [52]. The working electrode (anode) used in large-scale electrolysis was an assembly of fifteen ordinary carbon plate (11 cm × 1.5 cm × 0.3 cm), placed beside of fifteen stainless steel plate cathode (11 cm× 1.5 cm × 0.1 cm). Under these conditions, the electrode surface increases up to 247 cm^2. In a typical procedure, for the large scale synthesis of **SO2**, 300 ml solution containing phosphate buffer (pH = 8.0, *c* = 0.2 M)/ethanol (20/80 v/v) was pre-electrolyzed in the cell; then 10 mmol of **MBO**, 30 mmol of **AM2** was subjected to electrolysis at the constant current of 0.22 mA cm^{-2} (yield 72%).

The large scale synthesis of **SE5** was carried out in a 300 ml solution containing carbonate buffer (pH = 12.0, *c* = 0.2 M)/ethanol (20/80 v/v), then 10 mmol of **MBT** and 30

mmol of **AM2** was subjected to electrolysis at the constant current of 0.51 mA cm^{-2} (yield 81%). Other conditions are similar to those of the previous section.

The large scale synthesis of **SE5** was carried out in a 300 ml solution containing carbonate buffer (pH = 12.0, *c* = 0.2 M)/ethanol (20/80 v/v), then 10 mmol of **MBT** and 30 mmol of **AM2** was subjected to electrolysis at the constant current of 0.51 mA cm^{-2} (yield 81%). Other conditions are similar to those of the previous section.

[Figure 11]

3.6. Antibacterial susceptibility

This part of the investigation was initiated to evaluate the antibacterial susceptibility of the synthesized sulfonamide (**SO1**-**SO3**) and sulfenamide (**SE4**-**SE6**) derivatives. Antobiogram studies revealed that all gram positive (*Bacillus cereus* and *Staphylococcus aureus*) and gram negative bacteria (*Escherichia coli* and *Salmonella enteritidis*) were sensitive to **SO2** and **SO3**. Gram positive bacteria were sensitive to **SE4** and **SE6** while, gram negative bacteria showed resistance to **SE4** and **SE6**. Gram negative bacteria were sensitive to **SE5** (see Supplementary Information). All bacteria was resistance to **SO1**. The results of antibacterial activity of **SO1**-**SO3** and **SE4**-**SE6** compounds are summarized in Table 3.

[Table 3]

4. Conclusion

In this work, an efficient and green strategy based on the electrochemical oxidation of 2-mercaptobenzoheterocyclic compounds in the presence of some amines was developed for the synthesis of some new sulfonamide (**SO**) and sulfenamide (**SE**) derivatives. All reactions were carried out in a simple cell, consisting of carbon and stainless steel electrodes in water/ethanol mixture under constant current condition, without using any catalyst. It is

also shown that the products can be easily synthesized in preparative scales with impressive yields. The product type is dependent upon the 2-mercaptobenzoheterocyclic type. When **MBO** is used as the starting material, sulfonamide compounds (**SO**) are the main products. Unlike **MBO**, when **MBT** is the starting material, then sulfenamide (**SE**) derivatives are the main products. It should be noted that Unlike **MBO** and **MBT**, upon the oxidation of **MBI** in the presence of amines, we could not isolate these two types of products. The product yields are dependent upon the current density. In this paper, also, the electrochemical behavior of **MBO**, **MBT** and **MBI** has been comprehensively investigated and unique information has been published.

Acknowledgements

The authors wish to acknowledge Iran National Science Foundation (INSF) for financial support of this work. We also acknowledge the Bu-Ali Sina University Research Council and Center of Excellence in Development of Environmentally Friendly Methods for Chemical Synthesis (CEDEFMCS) for their support of this work.

Appendix A. Supplementary data

Supplementary data including FT-IR, ^{1}H NMR ^{13}C NMR and MS spectra of **SO1-SO3** and **SE4-SE6** and antibacterial activity of products associated with this article can be found, in the online version, at http://dx.doi.org

Reference:

[1] R.J. Anderson, P.W. Groundwater, A. Todd, A.J. Worsley, Antibacterial agents: Chemistry, Mode of Action, Mechanisms of Resistance and Clinical Applications, John Wiley & Sons, Chichester, West Sussex (2012), pp. 105-124.

[2] S. Syed Shoaib Ahmad, G. Rivera, M. Ashfaq, Recent advances in medicinal chemistry of sulfonamides. Rational design as anti-tumoral, anti-bacterial and anti-inflammatory agents, Mini Rev. Med. Chem. 13 (2013) 70-86.

[3] A. Scozzafava, T. Owa, A. Mastrolorenzo, C.T. Supuran, Anticancer and antiviral sulfonamides, Curr. Med. Chem. 10 (2003) 925-953.

[4] C.T. Supuran, A. Casini, A. Scozzafava, Protease inhibitors of the sulfonamide type: anticancer, antiinflammatory, and antiviral agents, Med. Res. Rev. 23 (2003) 535-558.

[5] K.P. Rakesh, S.M. Wang, J. Leng, L. Ravindar, A.M. Asiri, H.M. Marwani, H. L. Qin, Recent development of sulfonyl or sulfonamide hybrids as potential anticancer agents: a key review. Anti-Cancer Agents Med. Chem. 18 (2018) 488–505.

[6] S.M. Pant, A. Mukonoweshuro, B. Desai, M.K. Ramjee, C.N. Selway, G.J. Tarver, A.G. Wright, K. Birchall, T.M. Chapman, T.A. Tervonen, J. Klefstrçm, Design, synthesis, and testing of potent, selective hepsin inhibitors via application of an automated closed-loop optimization platform. J. Med. Chem. 61 (2018) 4335-4347.

[7] H. Nishioka, N. Tooi, T. Isobe, N. Nakatsuji, K. Aiba, BMS-708163 and Nilotinib restore synaptic dysfunction in human embryonic stem cell-derived Alzheimer's disease models, Sci. Rep. 6 (2016) 33427.

[8] L.D. Pennington et al., Discovery and structure-guided optimization of diarylmethanesulfonamide disrupters of glucokinase–glucokinase regulatory protein (GK–GKRP) binding: Strategic use of a N → S ($n_N \rightarrow \sigma^*_{S–X}$) interaction for conformational constraint, J. Med. Chem. 58 (2015) 9663-9679.

[9] K.W. Gillman et al. Discovery and evaluation of BMS-708163, a potent, selective and orally bioavailable γ-secretase inhibitor, ACS Med. Chem. Lett. 1 (2010) 120-124

[10] H. Sugimoto, M. Shichijo, T. Iino, Y. Manabe, A. Watanabe, M. Shimazaki, F. Gantner, K.B. Bacon, An orally bioavailable small molecule antagonist of CRTH2, ramatroban (BAY u3405), inhibits prostaglandin D2-induced eosinophil migration in vitro, J. Pharmacol. Exp. Ther. 305 (2003) 347-352

[11] O.M. Mulina, A.I. Ilovaisky, A.O. Terent'ev, Oxidative Coupling with S–N Bond Formation, Eur. J. Org. Chem. 2018 (2018) 4648–4672.

[12] J. Jiang, S. Zeng, D. Chen, C. Cheng, W. Deng, J. Xiang, Synthesis of *N*-arylsulfonamides via Fe-promoted reaction of sulfonyl halides with nitroarenes in an aqueous medium, Org. Biomol. Chem. 16 (2018) 5016–5020.

[13] K.K. Anderson, Comprehensive Organic Chemistry, Pergamon Press, Oxford (1979).

[14] S. Caddick, J.D. Wilden, D.B. Judd, Direct synthesis of sulfonamides and activated sulfonate esters from sulfonic acids, J. Am. Chem. Soc. 126 (2004) 1024–1025.

[15] A. Shavnya, S.B. Coffey, A.C. Smith, V. Mascitti, Palladium-catalyzed sulfination of aryl and heteroaryl halides: direct access to sulfones and sulfonamides, Org. Lett. 15 (2013) 6226–6229.

[16] E.F. Flegeau, J.M. Harrison, M.C. Willis, One-pot sulfonamide synthesis exploiting the palladium-catalyzed sulfination of aryl iodides, Synlett. 27 (2016) 101–105.

[17] M.W. Johnson, S.W. Bagley, N.P. Mankad, R.G. Bergman, V. Mascitti, F.D. Toste, Application of fundamental organometallic chemistry to the development of a gold-catalyzed synthesis of sulfinate derivatives, Angew. Chem., Int. Ed. 53 (2014) 4404–4407.

[18] H. Konishi, H. Tanaka, K. Manabe, Pd-Catalyzed selective synthesis of cyclic sulfonamides and sulfinamides using $K_2S_2O_5$ as a sulfur dioxide surrogate, Org. Lett. 19 (2017) 1578–1581.

[19] M. Wang, Q. Fan, X. Jiang, Metal-free construction of primary sulfonamides through three diverse salts, Green Chem. 20 (2018) 5469–5473.

[20] Y. Chen, P.R.D. Murray, A.T. Davies, M.C. Willis, Direct copper-catalyzed three-component synthesis of sulfonamides, J. Am. Chem. Soc. 140 (2018) 8781–8787.

[21] D. Yang, P. Sun, W. Wei, F. Liu, H. Zhang, H. Wang, Copper-catalyzed regioselective cleavage of C− X and C− H bonds: a strategy for sulfur dioxide fixation, Chem. Eur. J. 24 (2018) 4423–4427.

[22] X. Marset, J. Torregrosa-Crespo, R.M. Martínez-Espinosa, G. Guillena, D.J. Ramón, Multicomponent synthesis of sulfonamides from triarylbismuthines, nitro compounds and sodium metabisulfite in deep eutectic solvents, Green Chem. 21 (2019) 4127-4132.

[23] Y. Dou, X. Huang, H. Wang, L. Yang, H. Li, B. Yuan, G. Yang, Reusable cobalt-phthalocyanine in water: Efficient catalytic aerobic oxidative coupling of thiols to construct S–N/S–S bonds, Green Chem. 19 (2017) 2491-2495.

[24] M. Zhu, W. Wei, D. Yang, H. Cui, L. Wang, G. Meng, H. Wang, Metal-free I_2O_5-mediated direct construction of sulfonamides from thiols and amines, Org. Biomol. Chem. 15 (2017) 4789–4793.

[25] B. Mokhtari, D. Nematollahi, H. Salehzadeh, A tunable pair electrochemical strategy for the synthesis of new benzenesulfonamide derivatives, Sci. Rep. 9 (2019) Article number: 4537.

[26] S. Khazalpour, D. Nematollahi, A. Ahmad, B. Dowlati, Electroreductive nucleophile acceptor generation. Electrochemical synthesis of N-(4-(dimethylamino) phenyl) benzenesulfonamide, Electrochim. Acta 180 (2015) 909–913.

[27] G. Laudadio, E. Barmpoutsis, C. Schotten, L. Struik, S. Govaerts, D.L. Browne, T. Noël, Sulfonamide synthesis through electrochemical oxidative coupling of amines and thiols, J. Am. Chem. Soc. 141 (2019) 5664-5668.

[28] L. Craine, M. Raban, The chemistry of sulfonamides, Chem. Rev. 89 (1989) 689-712.

[29] N. Zhan, Y. Zhang and X.Z. Wang, Solubility of *N*-tert-butylbenzothiazole-2-sulfenamide in several pure and binary solvents, J. Chem. Eng. Data 64 (2019) 1051-1062.

[30] A.J. Marzocca, M.A. Mansilla, Vulcanization kinetic of styrene–butadiene rubber by sulfur/TBBS, J. Appl. Polym. Sci. 101 92006) 35-41.

[31] L. Ma, G. Li, J. Huang, J. Zhu, Z. Tang, Using sulfinamides as high oxidation state sulfur reagent for preparation of sulfonamides, Tetrahedron lett. 59 (2018) 1600-1603.

[32] M.V. Stasevych, M.Y. Plotnikov, M.O. Platonov, S.I. Sabat, R.Y. Musyanovych, V.P. Novikov, Sulfur-containing derivatives of 1,4-naphthoquinone, part 2: Sulfenyl derivative synthesis, Heteroatom. Chem. 16 (2005) 587-598.

[33] G. Murineddu, F. Deligia, G. Ragusa, L. García-Toscano, M. Gómez-Cañas, B. Asproni, V. Satta, E. Cichero, R. Pazos, P. Fossa, G. Loriga, J. Fernández-Ruiz, G.A. Pinna, Novel sulfenamides and sulfonamides based on pyridazinone and pyridazine scaffolds as CB1 receptor ligand antagonists, Bioorg. Med. Chem. 26 (2018) 295-307.

[34] D.J. Owen, C.B. Davis, R.D. Hartnell, P.D. Madge, R.J. Thomson, A.K.J. Chong, R.L.Coppel, M. VonItzstein, Synthesis and evaluation of galactofuranosyl N,N-dialkyl sulfenamides and sulfonamides as antimycobacterial agents, Bioorg. Med. Chem. Lett. 17 (2007) 2274-2277.

[35] J.L. Shang, H. Guo, Z.S. Li, B. Ren, Z.M. Li, H.G. Dai, L.X. Zhang, J.G. Wang, Synthesis and evaluation of isatin-β-thiosemicarbazones as novel agents against antibiotic-resistant gram-positive bacterial species, Bioorg. Med. Chem. Lett. 23 (2013) 724-727.

[36] A.S. Karwa, A.R. Poreddy, B. Asmelash, T.S. Lin, R.B. Dorshow, R. Rajagopalan, Type 1 phototherapeutic agents. 2. Cancer cell viability and ESR Studies of Tricyclic Diarylamines, ACS Med. Chem. Lett. 211 (2011) 828-833.

[37] F.A. Davis, A.J. Friedman, E.W. Kluger, E.B. Skibo, E.R. Fretz, A.P. Milicia, W.C. LeMasters, M.D. Bentley, J.A. Lacadie, I.B. Douglass, Chemistry of the sulfur-nitrogen bond. 12. Metal-assisted synthesis of sulfenamide derivatives from aliphatic and aromatic disulfides, J. Org. Chem. 42 (1977) 967-972.

[38] K.M. Huttunen, J. Leppänen, K. Laine, J. Vepsäläinen, J. Rautio, Convenient microwave-assisted synthesis of lipophilic sulfenamide prodrugs of metformin, Eur. J. Pharm. Sci. 49 (2013) 624–628.

[39] E. Rattanangkool, W. Krailat, T. Vilaivan, P. Phuwapraisirisan, M. Sukwattanasinitt, S. Wacharasindhu, Hypervalent Iodine (III)-promoted metal-free S–H activation: an approach for the construction of S–S, S–N, and S–C bonds, Eur. J. Org. Chem. 2014 (2014) 4795-4804.

[40] H. Yakan, H. Kutuk, Comparison of conventional and microwave-assisted synthesis of some new sulfenamides under free catalyst and ligand, Monatsh. Chem. 149 (2018) 2047–2057.

[41] D.N.Harpp, T.G. Back, A general synthesis of sulfonamides, Tetrahedron Lett. 12 (1971) 4953-4956.

[42] M. Shimizu, H. Fukazawa, S. Shimada, Y. Abe, The synthesis and reaction of *N*-sulfenyl heterocycles: development of effective sulfenylating reagents, Tetrahedron 62 (2006) 2175-2182.

[43] N. Taniguchi, Unsymmetrical disulfide and sulfenamide synthesis via reactions of thiosulfonates with thiols or amines, Tetrahedron 73 (2017) 2030-2035.

[44] N. Taniguchi, Copper-catalyzed formation of sulfur–nitrogen bonds by dehydrocoupling of thiols with amines, Eur. J. Org. Chem. 2010 (2010) 2670-2673.

[45] A.J. Bard, L.R. Faulkner, Electrochemical Methods, 2nd edn, Wiley, New York (2001).

[46] R.N. Goyal and M.S. Verma, Electrochemical oxidation of 2-mercaptobenzoxazole, Indian J. Chem. 35A (1996) 281-287.

[47] A. Schaufuß, G. Wittstock, Oxidation of 2-mercaptobenzoxazole in aqueous solution: solid phase formation at glassy carbon electrodes, J. Solid State Electrochem. 3 (1999) 361-369.

[48] A.A. Ahmed Boraei, I.T. Ahmed, M.M.A. Hamed, Acid dissociation constants of some mercaptobenzazoles in aqueous-organic solvent mixtures, J. Chem. Eng. Data 41 (1996) 787-790.

[49] Q. Liu, L. Wang, H. Yue, J.S. Li, Z. Luo, W. Wei, Catalyst-free visible-light-initiated oxidative coupling of aryldiazo sulfones with thiols leading to unsymmetrical sulfoxides in air, Green Chem. 21 (2019) 1609-1613.

[50] F. Jensen, A. Greer, E.L. Clennan, Reaction of organic sulfides with singlet oxygen. A revised mechanism, J. Am. Chem. Soc. 120 (1998) 4439-4449.

[51] D.H. Kim, J. Lee, A. Lee, Visible-light-driven silver-catalyzed one-pot approach: A selective synthesis of diaryl sulfoxides and diaryl sulfones, Org. Lett. 20 (2018) 764-767.

[52] B. Karimi, M. Rafiee, S. Alizadeh, H. Vali, Green Chem. 17 (2015) 991-1000.

Tables

Table 1. Products and conditions for the synthesis of sulfonamide compounds (**SO**).

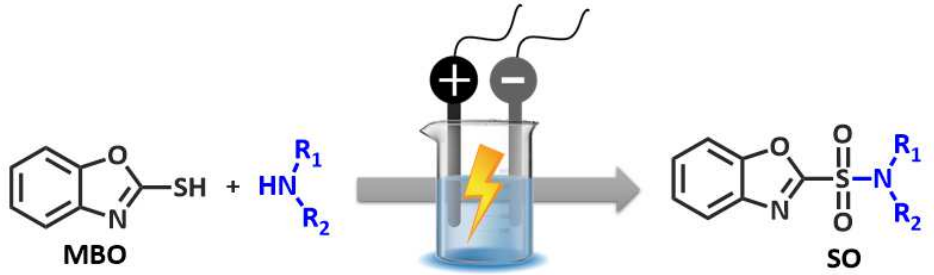

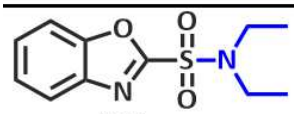 **SO1** Yield: 59%	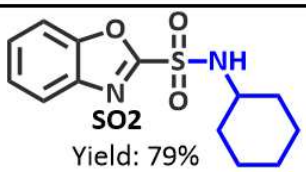 **SO2** Yield: 79%	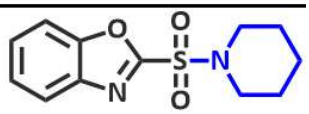 **SO3** Yield: 62%

Table 2. Products and conditions for the synthesis of sulfenamide compounds (**SE**).

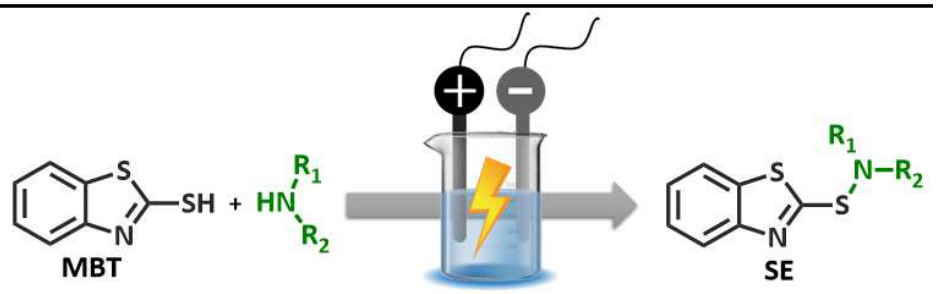

Undivided cell . Anode: carbon . Cathode: stainless steel

Carbonate buffer (pH = 12.0)/ethanol (20/80 v/v)

J = 0.52 mA cm^{-2} . Q = 190 C . Room temperature

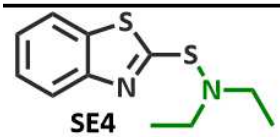 **SE4** Yield: 65%	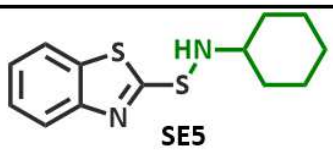 **SE5** Yield: 88%	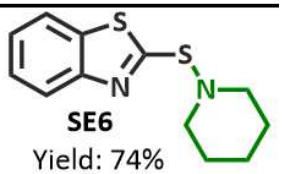 **SE6** Yield: 74%

Table 3. Antibacterial activity of **SO1**-**SO3** and **SE4**-**SE6**.

	Microorganism	Tetracyclne disc 30 µg[a]	well 30 µg[b]	Disc 30 µg	Activity
SO1	*Bacillus cereus*	32	12	11	(-)[c]
	Staphylococcus aureus	26	8	9	(-)
	Escherichia coli	20	8	9	(-)
	Salmonella enteritidis	18	7	10	(-)
SO2	*Bacillus cereus*	26	17	15	(+)[d]
	Staphylococcus aureus	29	19	16	(+)
	Escherichia coli	18	16	14	(+)
	Salmonella enteritidis	22	16	15	(+)
SO3	*Bacillus cereus*	29	16	14	(+)
	Staphylococcus aureus	23	17	14	(+)
	Escherichia coli	18	18	17	(+)
	Salmonella enteritidis	19	16	15	(+)
SE4	*Bacillus cereus*	30	19	17	(+)
	Staphylococcus aureus	27	16	15	(+)
	Escherichia coli	18	8	8	(-)
	Salmonella enteritidis	23	8	7	(-)
SE5	*Bacillus cereus*	35	18	17	(+)
	Staphylococcus aureus	28	9	9	(-)
	Escherichia coli	20	16	15	(+)
	Salmonella enteritidis	22	14	15	(+)
SE6	*Bacillus cereus*	28	18	14	(+)
	Staphylococcus aureus	26	16	15	(+)
	Escherichia coli	18	8	8	(-)
	Salmonella enteritidis	24	7	8	(-)

[a]Diameter of effective zone of inhibition (mm).

[b]Solvent well, DMSO + Tween 20.

[c]Negative activity.

[d]Positive activity

Figures

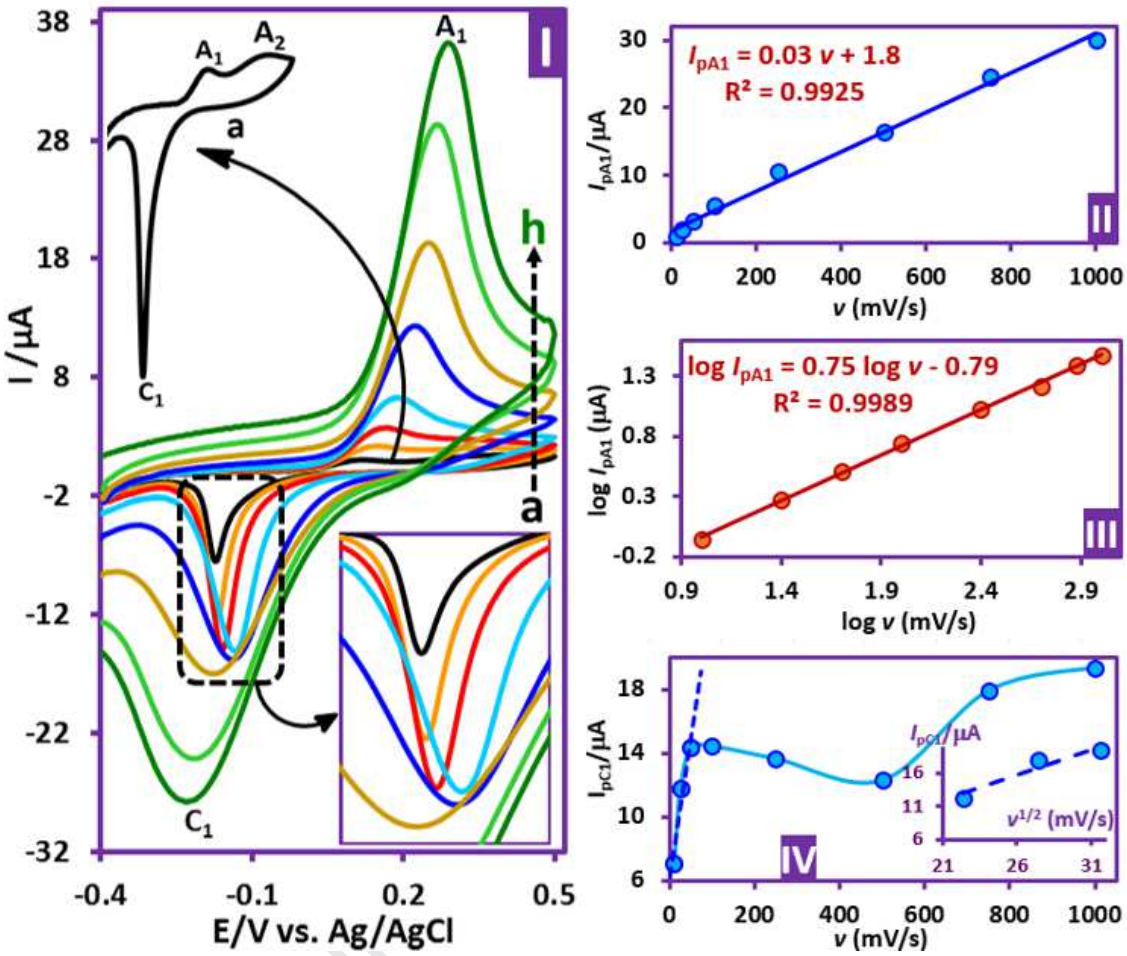

Figure 1. Part I. Cyclic voltammograms of **MBO** (1.0 mM) in aqueous phosphate buffer (*c* = 0.2 M, pH = 7.0), at GC electrode, at different scan rate and at room temperature. Scan rates from a to h are: 10, 25, 50, 100, 250, 500, 750 and 1000 mV/s. Part II, the plot of I_{pA1} versus scan rate. Part III, the plot of log I_{pA1} versus log *v*. Part IV, the plot of I_{pC1} versus scan rate.

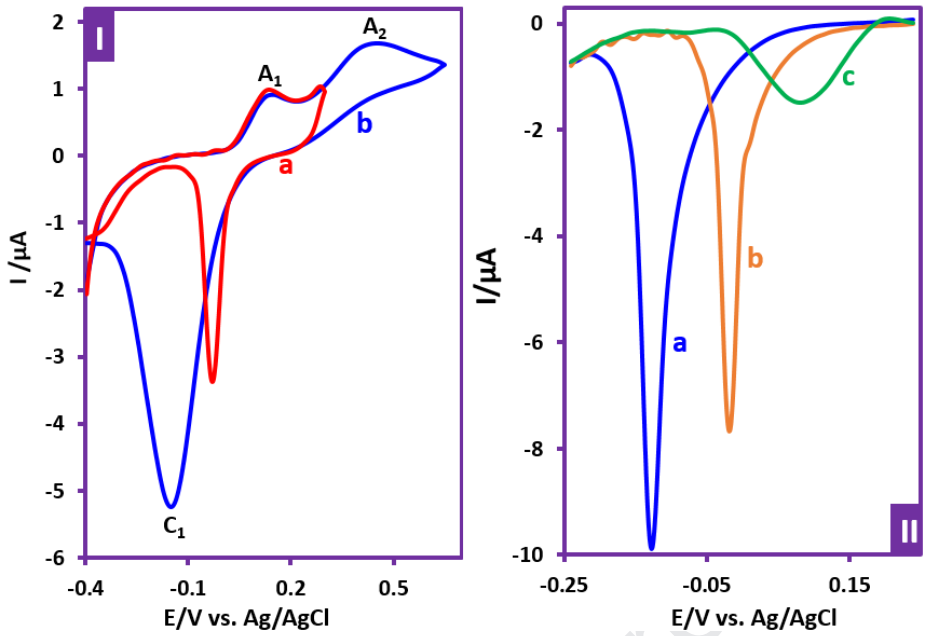

Figure 2. Part I: Cyclic voltammograms of **MBO** (1.0 mM) in water (phosphate buffer, pH = 7.0 and *c* = 0.2 M). Part II: Linear sweep voltammograms of **MBO** (1.0 mM) (peak C_1) in different ethanol/H_2O (phosphate buffer, pH = 8.0 and *c* = 0.2 M) mixtures a) 0%, b) 10% and c) 20% ethanol. Working electrode: GC electrode. Scan rate: 10 mV/s. Temperature = room temperature.

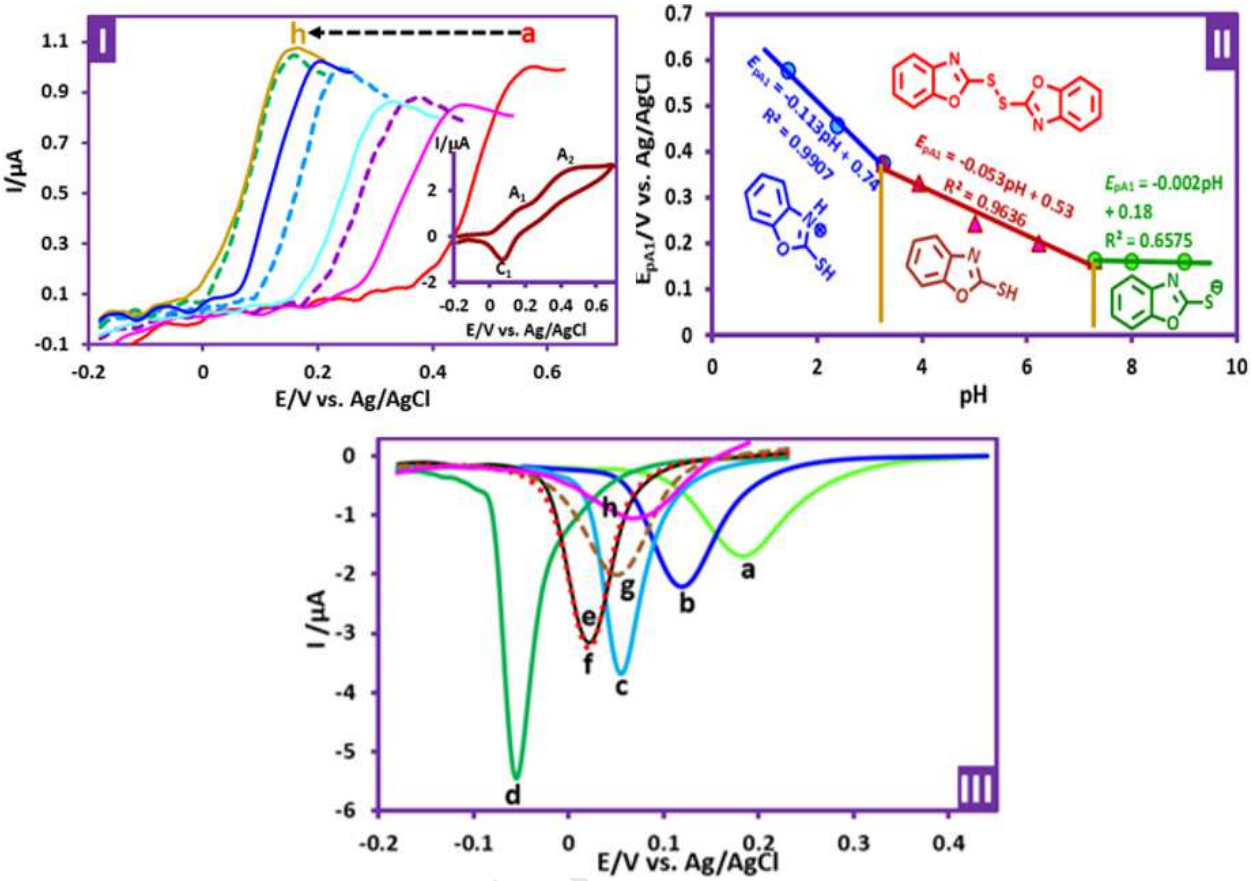

Figure 3. Part I: Linear sweep voltammograms of **MBO** (1.0 mM) in ethanol/H_2O (with different pH values) (20/80, v/v) mixture at GC electrode, at room temperature. Scan rate: 10 mV/s. pH values from a to h are: 1.4, 2.4, 3.3, 3.9, 5.0, 6.2, 7.3 and 8.0. Inset: cyclic voltammogram of **MBO** under above condition at pH = 9.00. Part II: The potential-pH diagram of **MBO**. Part III: The status of peak C_1 at different pHs. pH values from a to h are: 1.4, 2.4, 3.3, 5.0, 6.2, 7.3, 8.0 and 9.0.

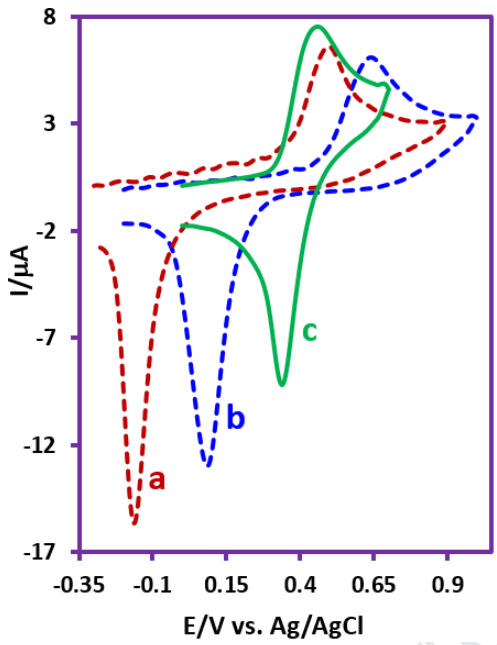

Figure 4. Cyclic voltammograms of 1.0 mM: (a) **MBT**, (b) **MBO** and (c) **MBI** in water ($HClO_4$, pH = 1.0 and *c* = 0.1 M)/ethanol (80/20) mixture at GC electrode, at room temperature. Scan rate: 100 mV/s.

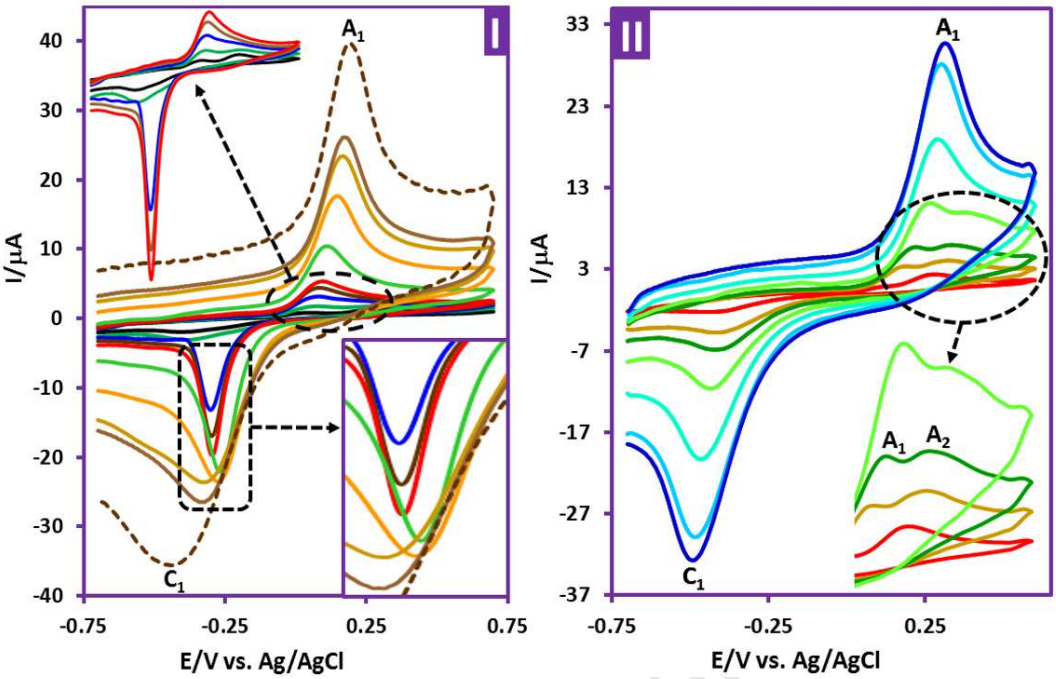

Figure 5. Cyclic voltammograms of 1.0 mM **MBT** (part I) and 1.0 mM **MBI** (part II) in water (phosphate buffer, pH = 8.0 and *c* = 0.2 M)/ethanol (80/20) mixture at GC electrode, at room temperature. Scan rates for **MBT** are: 10, 25, 50, 75, 100, 250, 500, 750, 1000 and 2000 mV/s. Scan rates for **MBI** are: 10, 50, 100, 250, 500, 750 and 1000 mV/s.

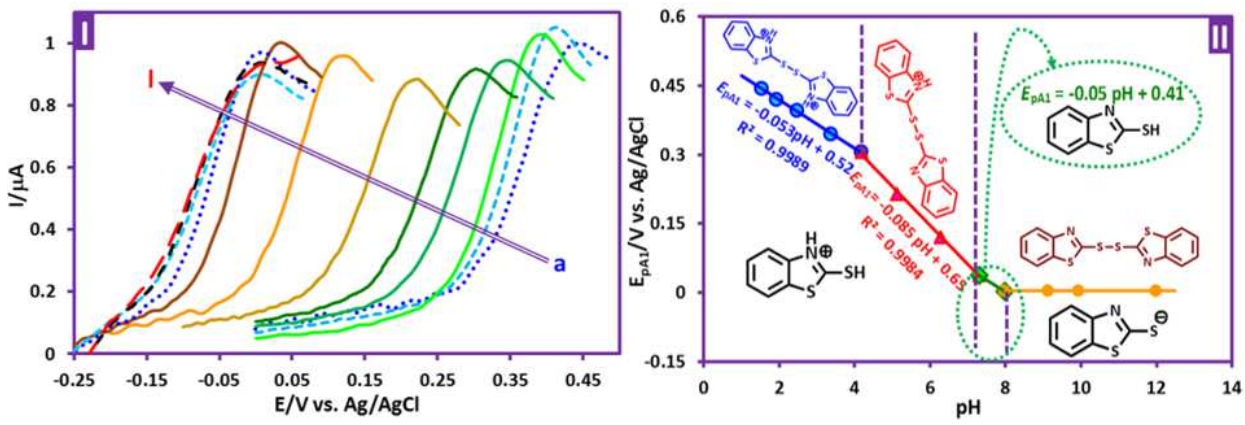

Figure 6. . Part I: Linear sweep voltammograms of **MBT** (1.0 mM) in ethanol/H_2O (with different pH values) (20/80, v/v) mixture at GC electrode, at room temperature. Scan rate: 10 mV/s. pH values from a to I are: 1.54, 1.93, 2.47, 3.37, 4.17, 5.12, 6.27, 7.31, 7.98, 9.13, 9.94 and 12.00. Part II: The potential-pH diagram of **MBT**.

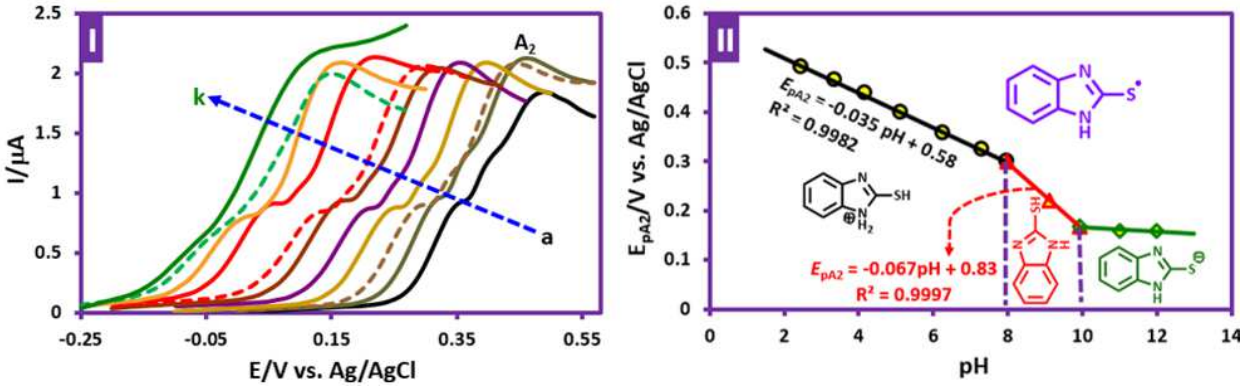

Figure 7. Part I: Linear sweep voltammograms of **MBI** (1.0 mM) in ethanol/H_2O (with different pH values) (20/80, v/v) mixture at GC electrode, at room temperature. Scan rate: 10 mV/s. pH values from a to k are: 2.47, 3.37, 4.17, 5.12, 6.27, 7.31, 7.98, 9.13, 9.94, 11.01 and 12.00. Part II: The potential-pH diagram of **MBI**.

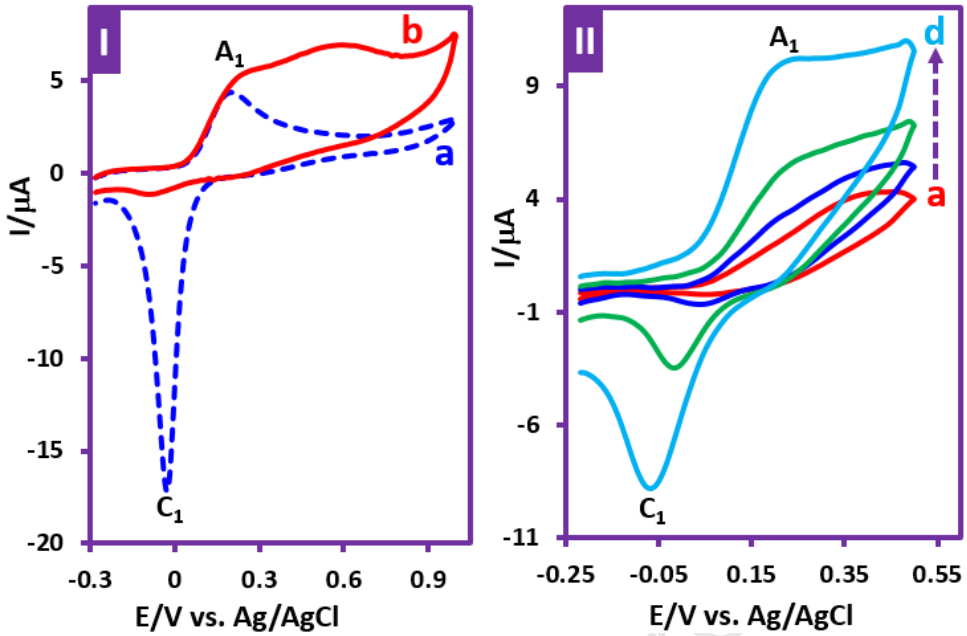

Figure 8. Part I: Cyclic voltammograms of **MBO** (1.0 mM) in the absence of **AM1** (curve a) and in the presence of **AM1** (2.5 mM) (curve b) at scan rate of 100 mV s^{-1}. Part II: Cyclic voltammograms of **MBO** (1.0 mM) in the presence of **AM1** (2.5 mM) at various scan rates. Scan rates from of a to d are: 10, 25, 100 and 250 mV s^{-1}. Solvent: ethanol/H_2O (pH = 8.0) (20/80, v/v) mixture at GC electrode and at room temperature.

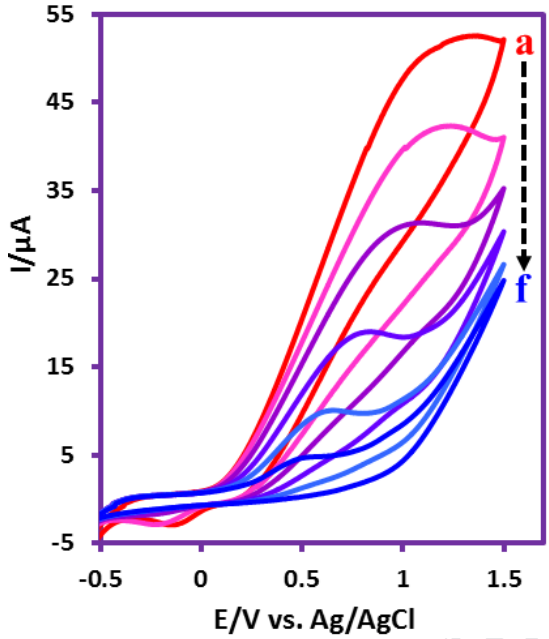

Figure 9. Cyclic voltammograms of **MBO** (0.5 mmol) in the presence of **AM1** (1.5 mmol) during the constant current electrolysis in water (pH=8.0)/ethanol mixture (20/80, v/v) in various time. Time from a to f is: 0, 60, 120, 180, 240 and 330 min. current density: 0.26 mA/cm^2. Scan rate: 100 mV/s at room temperature.

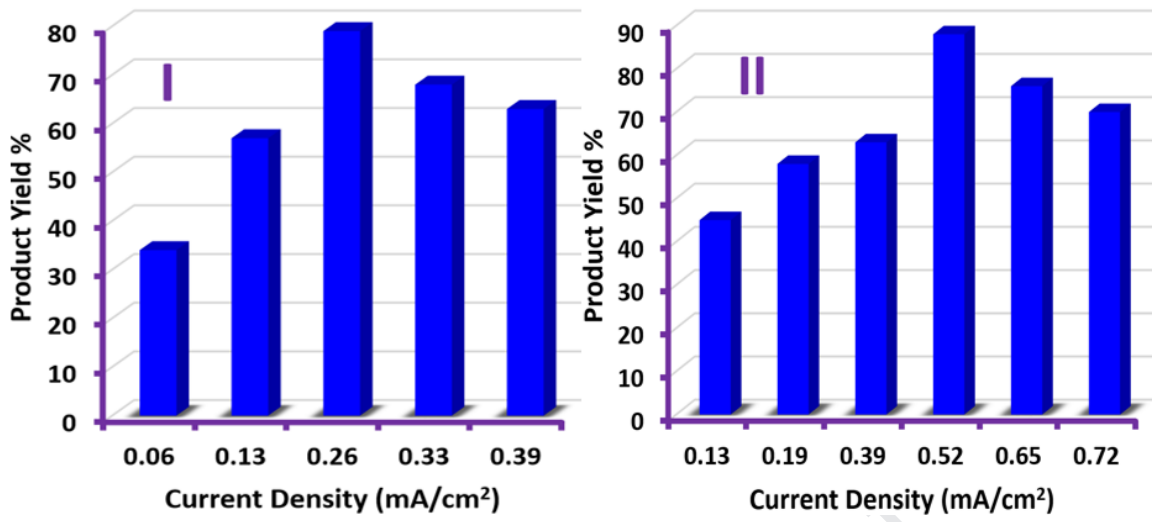

Figure 10. The effect of current density on the yield of **SO2** (part I) and **SE5** (part II). Charge passed: 190 C. **MBO** and **MBT** amount: 0.5 mmol. **AM2** amount: 1.5 mmol at room temperature.

Figure 11. Cell configuration in large scale synthesis.

A Comprehensive Electrochemical Study of 2-Mercaptobenzoheterocyclic Derivatives. Air-Assisted Electrochemical Synthesis of New Sulfonamide Derivatives

Nesa Yousefloui,[a] Saber Alizadeh,[a] Mahmood Masoudi-Khoram,[a] Davood Nematollahi[*a] and Hojjat Alizadeh[b]

E-Mail: nemat@basu.ac.ir

[a]Faculty of Chemistry, Bu-Ali Sina University, Hamedan, Iran. Zip Code 65178-38683

[b]Rooyana veterinary laboratory, Saqqez, Kurdistan, Iran

[*]Corresponding author. Tel.: + 0098 813 8271541; fax: +0098 813 8272404.

E-mail addresses: *nemat@basu.ac.ir, dnematollahi@yahoo.com* (D. Nematollahi).

Fax: +0098 813 8257407, Tel: +0098 813 8282807.

ABSTRACT

In this work, we have introduced a green air-assisted electrochemical method for the synthesis of new sulfonamide derivatives via oxidative coupling of heterocyclic thiols and amines. The synthetic method was designed based on the data collected from electrochemical oxidation of heterocyclic thiols, 2-mercaptobenzoxazole (**MBO**), 2-mercaptobenzothiazole (**MBT**) and 2-mercaptobenzimidazole (**MBI**) in the absence and presence of amines. The electrochemical results indicate that the oxidation of **MBO** and **MBT** lead to the formation of the corresponding dimers, which as an intermediate is essential for sulfonamide synthesis. The results also show that, in the time scale of our voltammetric experiments, oxidation of **MBI** does not lead to dimer formation. Our voltammetric studies suggest that the formed dimer is adsorbed on the electrode surface. The amount and intensity of adsorption depends on the type heterocyclic thiol, solvent, switching potential and solution pH. The mechanism of synthesis of sulfonamide compounds has been established based on the disappearing of the dimer reduction peak in the cyclic voltammogram of **MBO** in the presence of amines along with increasing the number of electrons transferred in this condition, as well as spectroscopic data of the products. These compounds have been successfully synthesized in water/ethanol mixture solutions in an undivided cell, at carbon rod electrodes, by constant current electrolysis at room temperature. The proposed method does not need to use toxic solvent, metal, catalyst and challenging workups. This method is easy to scale-up and the products have antibacterial activity.

Keywords: 2-Mercaptobenzoheterocyclic compounds, Sulfonamide derivatives, Green chemistry, Electrochemical synthesis, Cyclic voltammetry, Sulfenamide derivatives.

1. Introduction

Sulfonamides are the first group of antibiotics to be used systemically in the treatment of bacterial infections [1]. In addition, they are used as anticancer, anti-inflammatory and antiviral agents [2-6]. Some of them, also used for the treatment of type II diabetes [7], coronary artery disease and asthma [8], Alzheimer's disease [9] and respiratory diseases [10]. A literature survey reveals that the conventional methods for the synthesis of sulfonamides are the reaction of amines with sulfonyl chlorides [11,12] (Scheme 1, part I). Although some of these methods are efficient but they have disadvantages, such as the use of sulfonyl chlorides which are sensitive to hydrolysis, difficult to handle and not amenable to long-term storage. Transition metal catalyzed coupling reaction of primary sulfonamides and aryl halides or arylboronic acids is another method of sulfonamide synthesis [13-19] (Scheme 1, part II). These methods are also efficient but the main disadvantage of these methods is heavy metal pollution. The reaction of sodium sulfinates with amines in the presence of copper ions is another way to synthesize sulfonamides, which consequently creates the problem of metal pollution [20,21] (Scheme 1, part III). The oxidative chlorination of an aryl organosulfur compound is also another way to synthesize sulfonamides (Scheme 1, part IV). Although sulfonyl chlorides and transition metal are not used in this method, it has some drawbacks such as harsh acidic and low temperature conditions and harmful reagent [22]. Another method to synthesize sulfonamides, involves the combination of aryl halides, sulfur dioxide and amines [23-29] (Scheme 1, part IV). Although some of these methods are efficient but they may cause heavy metal pollution and are include strongly acidic/basic media, unsafe solvent, and compounds such as DABSO (SO_2 surrogate) that are expensive, unstable and unsafe.

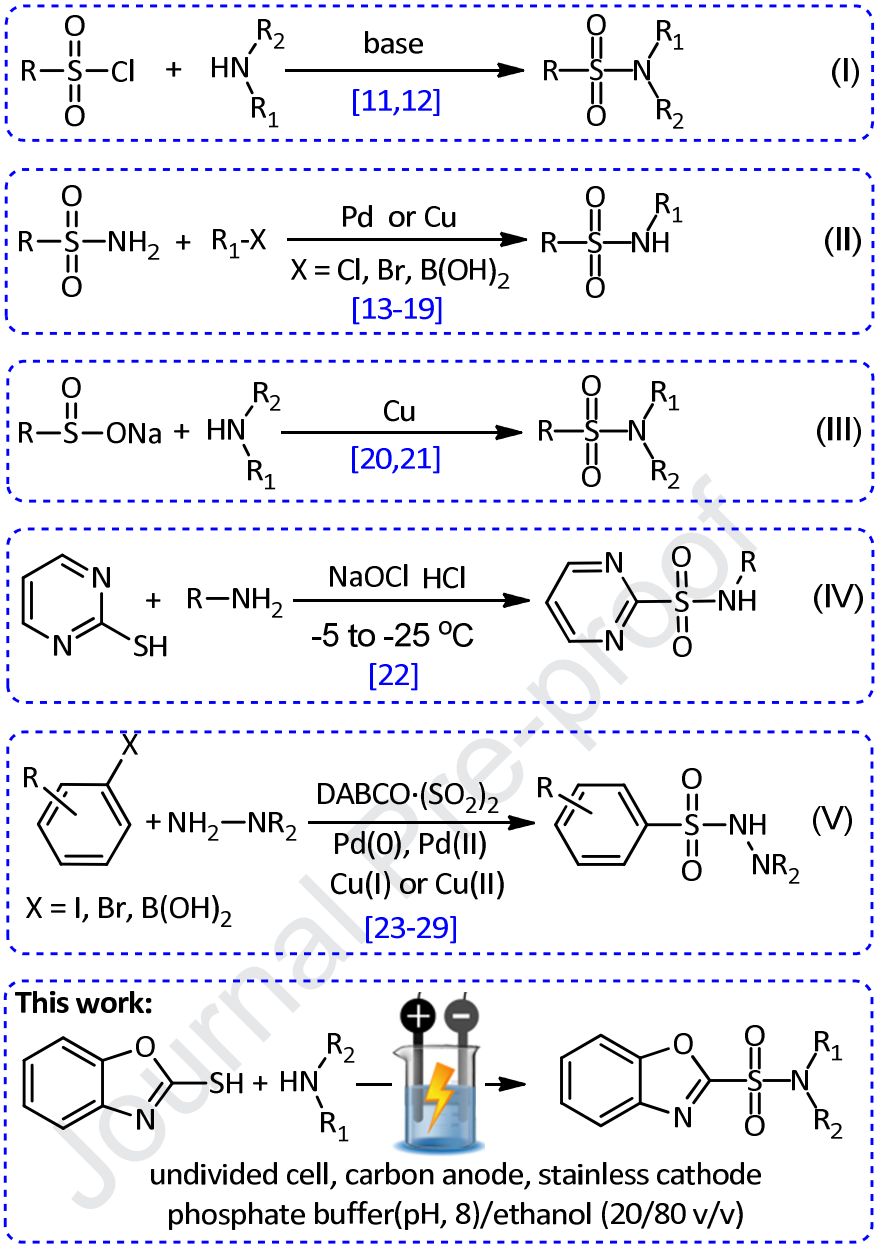

Scheme 1. Overview of the synthetic method for sulfonamides.

In addition to the chemical methods described above, we can list some interesting paper dealing with electrochemical synthesis of sulfonamides [30-32]. Although many problems have been addressed in these papers, there still exist problems associated with these papers including the use of toxic acetonitrile solvent, strong acidic media and the inability to synthesis of sulfonamide based on 2-mercaptobenzoheterocyclic compounds.

Another series of compounds synthesized in this study are sulfenamides. These compounds containing divalent sulfur bonded to trivalent nitrogen, which have been widely used in the vulcanization of rubbers as accelerator [33]. For example, *N-tert*-butyl-2-benzothiazole sulfenamide (TBBS) is the most widely used sulfonamide in the rubber industry as vulcanization accelerator [34]. In addition to rubber industry, sulfenamides are widely used in agriculture as plant growth regulators, pesticides and fungicides [33,35]. They have also shown many important biological activities such as antitumor, antiplatelet, antiasthmatic, antimicrobial and lipoxygenase activities [33,35,36].

Our literature survey shows that methods for the synthesis of sulfenamide consist of metal-assisted synthesis [37,38], hypervalent iodine(III) activated method [39], microwave-assisted synthesis [40], reaction of amines with thiophthalimides [41], transamination of *N*-unsubstituted sulfonamides [42], copper-catalyzed [43,44]. These methods, have the disadvantages such as heavy metal pollution, tedious work-up, low atom economy, safety problems, high temperatures, toxic and expensive reagents. However, the development of a simple and environmentally friendly methodology is still required for the synthesis of sulfonamide and sulfenamide compounds. The present work describes an air-assisted electrochemical method for the synthesis of titled compounds via electrochemical oxidation of 2-mercaptobenzoxazole in the presence of some amines under simple and green conditions, without toxic solvents and reagents, using carbon electrode in water/ethanol mixture. Another feature of the proposed method is its amenability to scaling up which is discussed in the text.

Electrochemistry is a powerful tool for studying reaction mechanisms [44]. In this paper a comprehensive study on the electrochemical behavior of 2-mercaptobenzoxazole (**MBO**), 2-mercaptobenzothiazole (**MBT**) and 2-mercaptobenzimidazole (**MBI**) in water/ethanol

mixture were carried out by cyclic voltammetry at glassy carbon electrode to report the detailed oxidation mechanism as well as detailed potential-pH properties and pK_a values of **MBO**, **MBT** and **MBI** and related compounds. This paper provides experimental details on the synthesis of sulfonamide and sulfenamide compounds with a comprehensive electrochemical data on the oxidation and acid/base behaviors of **MBO**, **MBT** and **MBI** and related compounds.

2. Experimental

2.1. Reagents and apparatus

2-Mercaptobenzoxazole (**MBO**) (95%), 2-mercapto benzothiazole (**MBT**) (97%), 2-mercaptobenzimidazole (**MBI**) (98%), diethylamine (**AM1**) (≥99.5%), cyclohexylamine (**AM2**) (≥99%), piperidine (**AM3**) (≥99%), sodium hydrogen phosphate (99%) and sodium dihydrogen phosphate (99%) were obtained from Sigma-Aldrich. Ethanol, sodium bicarbonate (98%), sodium carbonate (98%), hydrochloric acid (37%), sodium hydroxide (99%) were obtained from Merck (Darmstadt, Germany). These chemicals were used without further purification. The buffered solutions were prepared based on Kolthoff tables.

The glassy carbon electrode was polished using alumina slurry (3.0 – 0.1 µm). Melting points were measured with a Barnstead Electrothermal 9100 apparatus. IR spectra (KBr) were recorded on Perkin–Elmer GX FT-IR spectrometer. ^{1}H and ^{13}C NMR spectra were recorded on a Bruker Avance DRX-400 spectrometer at 400 MHz and INOVA 500 MHz. The mass spectra were recorded on MS Model: 5975C VL MSD with Tripe-Axis Detector. Cyclic voltammetry was performed using a Sama-500 potentiostat/galvanostat. Typical voltammetry experiments were carried out on a classical three electrode undivided cell configuration with a platinum auxiliary electrode and a glassy carbon (GC) working electrode (surface area = 1.8 mm^2). The working electrode potentials were measured versus Ag/AgCl (3M KCl) (all electrodes from AZAR

electrode). The Macro-scale electrolysis was carried out with a two electrode system under constant current condition by a dc power supply Dazheng ps-303D. The working electrode (anode) used in macro-scale electrolysis was an assembly of five ordinary soft carbon rods (38 cm^2), placed circularly around a stainless steel cylinder cathode (25 cm^2 area).

Autolab model PGSTAT302N potentiostat/galvanostat was used for preparative electrolysis, controlled-potential coulometry and cyclic voltammetry. A glassy carbon disc (1.8 mm^2 areas) and a platinum wire were used as working and counter electrodes, respectively. An assembly of four graphite rods (30 cm^2) and a large stainless steel gauze were used as working and counter electrodes in controlled-potential coulometry and macro scale electrolysis, respectively. The potential of the working electrode was measured against Ag/AgCl (AZAR electrode). All chemicals were purchased from commercial sources and used without further purification.

2.2. Characteristic of the products

***N,N*-diethylbenzo[d]oxazole-2-sulfonamide (SO1) ($C_{11}H_{14}N_2O_3S$).** Light yellow oil, yield: 59%, ^{1}H NMR (400 MHz, DMSO-d_6) δ/ppm: 7.48 (d, *J* = 8 Hz, 2H, aromatic), 7.25 (d, *J* = 8 Hz, 2H, aromatic), 2.94 (q, 4H, methylene), 1.17 (t, 6H, methyl). ^{13}C NMR (100 MHz, DMSO-d_6) δ/ppm: 11.0, 41.3, 109.7, 110.8, 123.4, 124.9, 132.2, 148.3, 180.2. IR (KBr) v/cm^{-1}: 2971, 2823, 2776, 1764, 1618, 1507, 1449, 1279, 1247, 1132, 1096, 1008, 931, 744, 647, 607. MS (EI, 70 eV) m/z (%): 256 (M, 3), 192 (3), 151 (100), 91 (26), 58 (62).

***N*-Cyclohexyl-2-benzoxazole sulfonamide (SO2) ($C_{13}H_{16}N_2O_3S$).** Light yellow oil, yield: 79%. ^{1}H NMR (500 MHz, DMSO-d_6) δ/ppm: 7.62 (d, *J* = 7.8, 1H, NH), 7.21 (d, *J* = 7.7 Hz, 1H, aromatic), 7.16 (d, *J* = 7.5 Hz, 1H, aromatic), 7.04 (t, *J* = 7.5 Hz, 1H, aromatic), 6.96 (t, *J* = 7.3 Hz, 1H, aromatic), 3.01 (s, 1H, CH), 1.92 (d, *J* = 10.1 Hz, 2H, CH), 1.70 (d, *J* = 12.1 Hz, 2H, CH), 1.55 (d, *J* = 12.8 Hz, 1H, CH), 1.37 - 1.14 (m, 5H, CH). ^{13}C NMR (100 MHz, DMSO-d_6) δ/ppm: 182.1, 150.8, 142.1, 123.2, 121.0, 113.5, 108.2, 49.9, 30.8, 25.0, 24.2. IR (KBr) v/cm^{-1}: 3476, 2935, 2854, 2588, 2523, 2048, 1890, 1759, 1698,

1643, 1538, 1507, 1464, 1431, 1381, 1346, 1252, 1132, 1114, 1070, 1003, 890, 741, 625, 605, 552, 450, 417. MS (EI, 70 eV) m/z (%): 279 (M, 3), 41 (75), 57 (86), 76 (16), 104 (25), 132 (7), 149 (100), 167 (15).

***N*-Piperidin-2-benzoxazole sulfonamide (SO3) ($C_{12}H_{14}N_2O_3S$).** Light yellow oil, yield: 62%. ^{1}H NMR (500 MHz, DMSO-d_6) δ/ppm: 7.31 (d, J = 7.9 Hz, 1H, aromatic), 7.21 (d, J = 7.7 Hz, 1H, aromatic), 7.12 (t, J = 7.1 Hz, 1H, aromatic), 7.06 (t, J = 7.1 Hz, 1H, aromatic), 3.09 - 2.73 (m, 4H, CH), 1.68 - 1.51 (m, 6H, CH). ^{13}C NMR (126 MHz, DMSO-d_6) δ/ppm: 181.6, 150.0, 138.3, 124.0, 122.2, 112.6, 109.0, 44.1, 22.7, 22.1. IR (KBr) v/cm^{-1}: 3445, 3049, 2941, 2855, 1774, 1640, 1578, 1501, 1451, 1424, 1248, 1131, 1069, 1004, 921, 743, 627, 552, 418. MS (EI, 70 eV) *m/z* (%): 266 (M, 0.2), 41 (32), 64 (74), 91 (65), 84 (62), 134 (48), 151 (100), 173 (10), 202 (35), 256 (10).

***N,N*-diethylbenzo[d]thiazole-2-sulfenamide (SE4) ($C_{11}H_{14}N_2S_2$).** Light yellow oil, yield: 65%. ^{1}H NMR (500 MHz, DMSO-d_6) δ/ppm: 7.95 (d, J = 7.9 Hz, 1H, aromatic), 7.76 (d, J = 8.1 Hz, 1H, aromatic), 7.39 (t, J = 7.7 Hz, 1H, aromatic), 7.28 (t, J = 7.6 Hz, 1H, aromatic), 3.08 (q, J = 7.0 Hz, 4H, methylene), 1.14 (t, J = 7.1 Hz, 6H, methyl). ^{13}C NMR (126 MHz, DMSO-d_6) δ/ppm: 178.3, 155.1, 134.9, 126.4, 124.1, 122.0, 121.6, 52.3, 13.7. IR (KBr) v/cm^{-1}: 2972, 2931, 2855, 1563, 1468, 1429, 1376, 1310, 1273, 1159, 1081, 1023, 1009, 756, 727, 669, 432. MS (EI, 70 eV) *m/z* (%): 239 (M, 33), 167 (20), 108 (4), 72 (100), 42 (15).

***N*-Cyclohexyl-2-benzothiazole sulfenamide (SE5) ($C_{13}H_{16}N_2S_2$).** White solid, yield: 88%, isolated yield: 53%. Melting Point: 95-97 °C. ^{1}H NMR (500 MHz, DMSO-d_6) δ/ppm: 7.98 (d, J = 8.5 Hz, 1H, aromatic), 7.73 (d, J = 8.1 Hz, 1H, aromatic), 7.41 (t, 1H, aromatic), 7.29 (t, 1H, aromatic), 5.49 (d, J = 5.8 Hz, 1H, NH), 2.77 (m, J = 9.2, 4.4 Hz, 1H, CH), 1.97 (s, 2H, CH), 1.70 (s, 2H, CH), 1.54 (d, J = 11.6 Hz, 1H, CH), 1.22 (t, 5H, CH). ^{13}C NMR (126 MHz, DMSO-d_6)

δ/ppm: 181.4, 155.3, 134.8, 126.4, 123.9, 122.1, 121.4, 59.9, 33.5, 25.8, 24.8. IR (KBr) v/cm^{-1}: 3443, 3222, 2930, 2850, 1560, 1463, 1427, 1316, 1241, 1187, 1068, 1012, 753, 726. MS (EI, 70 eV) m/z (%): 265 (M, 86), 41 (70), 55 (64), 83 (14), 98 (100), 122 (11), 149 (15), 167 (86), 182 (17), 221 (11).

***N*-Piperidin-2-benzothiazole sulfenamide (SE6) ($C_{12}H_{14}N_2S_2$).** Light yellow oil, yield: 74%. ^{1}H NMR (500 MHz, DMSO-d_6) δ/ppm: 8.00 (d, J = 7.9 Hz, 1H, aromatic), 7.77 (d, J = 8.1 Hz, 1H, aromatic), 7.41 (t, J = 7.6 Hz, 1H, aromatic), 7.30 (t, J = 7.6 Hz, 1H, aromatic), 3.17 - 2.86 (m, 4H, CH), 1.67 - 1.40 (m, 6H, CH). ^{13}C NMR (126 MHz, DMSO-d_6) δ/ppm: 176.9, 155.2, 135.0, 126.5, 124.2, 122.2, 121.7, 57.9, 27.4, 22.9. IR (KBr) v/cm^{-1}: 3064, 2939, 2847, 1559, 1453, 1467, 1427, 1362, 1310, 1271, 1157, 1126, 1081, 1008, 919, 856, 761, 729, 667, 429. MS (EI, 70 eV) m/z (%): 251 (M, 39.5), 42 (36), 69 (6.5), 55 (33), 84 (100), 108 (5.9), 167 (18.3).

3. Results and Discussion

3.1. Electrochemical study of 2-mercaptobenzoheterocyclic compounds

In this work, electrochemical oxidation of **MBO**, **MBT** and **MBI** have been studied in two stages. The first stage involves studying the electrochemical behavior of these compounds in order to better understand the oxidation mechanism, electrochemical properties of the compounds and produced intermediates. The second part involves the electrochemical study of these compounds in the presence of diethylamine, cyclohexanamine and piperidine in order to obtain the necessary information for synthesis of sulfonamide and sulfenamide compounds.

Fig. 1, part I, shows the cyclic voltammograms of **MBO** (1.0 mM) in aqueous phosphate buffer (c = 0.2 M, pH = 7.0) by changing the potential scan rate between 10 and 1000 mV/s. The Figure shows that at the scan rate of 10 mV/s, the voltammogram has two anodic peaks (A_1 and A_2) and one sharp and symmetric cathodic peak (C_1). The effect of

increasing scan rate on the voltammetric response is quite complex. At first with increasing scan rate from 10 to 50 mV/s, the anodic peak A_2 removed and both I_{pA1} and I_{pC1} increase linearly with *v*. With further increase in scan rate, I_{pA1} continues to increase linearly (I_{pA1} = 0.03 *v* + 1.80, R^2 = 0.9925) (Fig. 1 part II). In order to obtain further data on the adsorption/diffusion behavior of **MBO**, the log I_{pA1}changes were plotted against the log *v* (Fig. 1 part III).

[Figure 1]

The slope of the line is a measure of the adsorption/diffusion of **MBO** on the surface of electrode. It is found that when the slope of the line is equal to 0.5, the process is pure diffusion-controlled, however, when the slope is 1, the process is pure adsorption-controlled [45]. The slope of the line is 0.75, which are higher than 0.5 and less than one that confirms the adsorption-diffusion process for electrochemical oxidation of **MBO**. With increasing potential scan rate from 50 mV/s, the voltammetric behavior of peak C_1 is quite complex (Fig. 1 parts I and IV).

At low scan rates (10, 25 and 50 mV/s), the peak is sharp and symmetrical and increases linearly with v (characteristic of an adsorption peak [45]). However, with increasing potential scan rate, I_{pC1} changes abnormally (Fig. 1 part I). At high scan rates (500, 750 and 1000 mV/s) the cathodic peak C_1 becomes almost a normal diffusion peak and its current increases linearly with $v^{1/2}$ at high scan rates (characteristic of a diffusion peak [45]) (Fig. 1 part IV, inset).

Figure 2 part I compares the electrochemical behavior of **MBO** in water (phosphate buffer, pH = 7.0 and *c* = 0.2 M), at two different switching potentials. The Figure clearly shows that when the switching potential increases from 0.30 V to 0.65 V, the amount of adsorbed material and adsorption intensity have increased dramatically. Based on these results, it can

be concluded that the over-oxidation of **MBO** appears to lead to the formation of materials with a higher adsorption property.

Figure 2 part II compares peak C_1 in different water (phosphate buffer, pH = 8.0, *c* = 0.2 M)/ethanol mixtures. As can be seen, when the percentage of ethanol in the mixture is zero (curve a), the cathodic peak C_1 shows the characteristic of a complete adsorption peak. However, with increasing ethanol percentage in the solvent mixture, peak C_1 tends to become a normal diffusion peak (curve c).

[Figure 2]

Fig. 3 shows the linear sweep voltammograms of **MBO** at scan rate of 10 mV/s, in ethanol/H_2O (with different pH values) (20/80, v/v) mixture. As can be seen at all studied pHs, the voltammograms show an anodic peak (A_1) in the positive going scan. The shift of peaks towards negative potentials with increasing pH values is a sign of the participation of proton in the redox process. According to these data, and taking into account the previously reported data [27,46,47], we proposed the following mechanism for electrochemical oxidation of **MBO** at different pH solutions.

[Figure 3]

At pH values less than 3.5, the oxidation mechanism of **MBO** is shown in Eq. 1. According to this equation, two protonated **MBOs** become dimer after losing two electrons and four protons. At this condition, the slope for the *E*-pH line is 113 mV/pH, which is close to the theoretical value of 118 mV/pH for a two-electron/four-proton process.

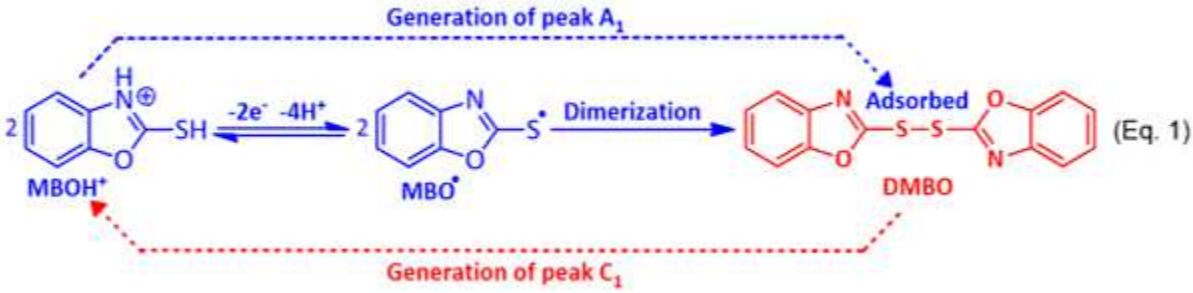

(Eq. 1)

At pH values more than 3.5 and less than 6.9, the oxidation mechanism of **MBO** is shown in Eq. 2. In this condition, the slope for the *E*-pH line is 53 mV/pH, which is close to the theoretical value of 59 mV/pH for a two-electron/two-proton process.

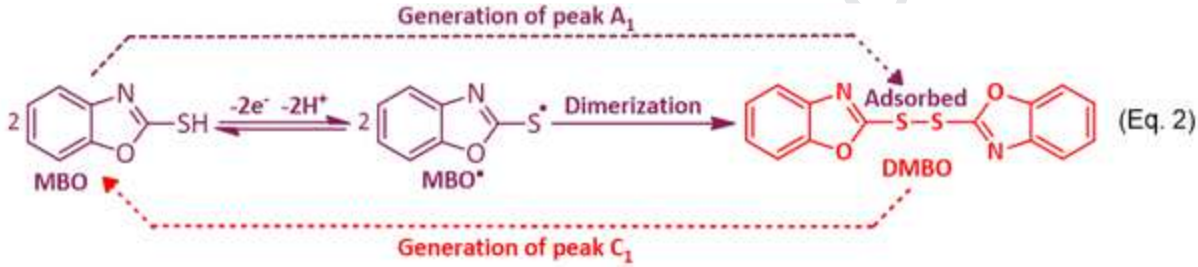

(Eq. 2)

At pH values more than 6.9, the oxidation mechanism of **MBO** is shown in Eq. 3. In this region (pH > 6.9), **MBO** is in its anionic form and in its redox process the proton is not exchanged. In addition, from data shown in Fig. 3 part II, we can conclude that the pK_a values for acid/base equilibria of **MBOH**$^+$/**MBO** and **MBO**/**MBO**$^-$ are 3.5 and 6.9, respectively (Eqs. 4 and 5). These data are in agreement with previously published data [46,48].

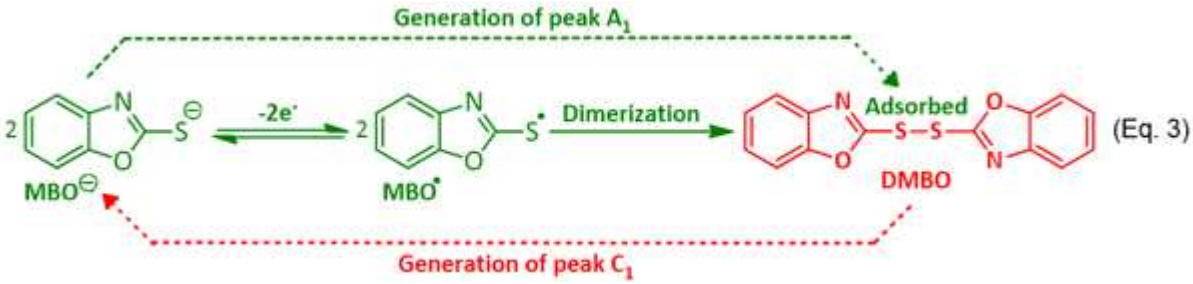

(Eq. 3)

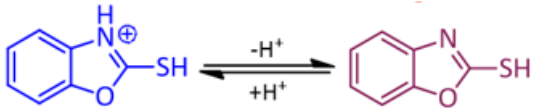

$pK_a = 3.5$ (Eq. 4)

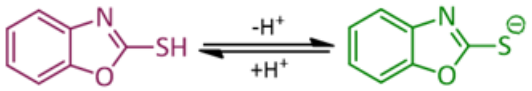

$pK_a = 6.9$ (Eq. 5)

According to our data, the anodic peak A_1 pertains to the oxidation of **MBO** (**MBOH**$^+$ and/or **MBO**$^-$) to the **MBO** radical (**MBO**$^\bullet$). At the next step, the reaction of two **MBO** radicals leads to the formation of 1,2-bis(benzo[d]oxazol-2-yl)disulfane dimer (**DMBO**). So, at slow or moderate potential scan rates, peak C_1 pertains to the reduction of adsorbed **DMBO** to **MBO** (Eqs. 1-3). At high scan rates, however, there is no sufficient time for dimerization reaction, so, diffusion peak C_1 is related to the reduction of **MBO**$^\bullet$ to **MBO**. The change of I_{pC1} at different pH is shown in Fig. 3, part III. As can be seen, with increasing pH from 1.4 to 5.0, the adsorption activity of **DMBO** increases. We think that the relative protonation of **DMBO** and formation of a more suitable medium for hydrogen bonding is important factor for less adsorption activity of **DMBO** in more acidic solutions. The adsorption activity of **DMBO** decreased with increasing pH from 5.0, so that at pH 9.0, peak C_1 shows the characteristic of a complete diffusion peak.

Figure 4 shows the cyclic voltammograms of **MBT** (curve a) and **MBI** (curve c) in comparison with **MBO** (curve b). As can be seen, these voltammograms are basically similar. However, they have some differences in detail. For example, the oxidation of **MBO** is higher than those of **MBT** and **MBI** due to the more electron donating ability of S and N atoms in the structure of **MBT** and **MBI** in comparison with O atom.

[Figure 4]

Other important differences in the voltammograms of **MBT**, **MBO** and **MBI** are different in adsorption ability of synthesized dimers and peak to peak separation ($\Delta E_p = E_{pA1} - E_{pC1}$). As can be seen, **MBT** shows largest peak-to-peak separation (ΔE_p = 0.68 V) and its dimer have highest adsorption activity. The result can be related to more adsorption activity of S atom in comparison with N and O atoms present in the structures of **MBO** and **MBI**. Figure 4

also shows that the lowest adsorption activity and peak-to-peak separation (ΔE_p = 0.13 V) belongs to **MBI**.

The effect of increasing potential scan rate on the cyclic voltammograms of **MBT** is shown in Fig. 5 part I. As can be seen, **MBT** shows a similar trend with that of **MBO** (Fig. 1). These experiments confirm previous results that at high scan rates, there is no sufficient time for dimerization reaction, so, peak C_1 is attributed to the reduction of **MBT**$^{\bullet}$ to **MBT**. At these scan rates, peak C_1 becomes like a normal diffusion peak and its current increases linearly with $v^{1/2}$.

[Figure 5]

The effect of increasing potential scan rate on the cyclic voltammograms of **MBI** is shown in Fig. 5 part II. Different with **MBO** and **MBT**, the cathodic peak C_1 shows a normal behavior with increasing scan rate. The presence of two N atoms in the structure of **MBI**, makes **MBI**$^{\bullet}$ more stable than **MBT**$^{\bullet}$ and **MBO**$^{\bullet}$. Consequently, we think that in the time scale of our experiments, **MBI** dimer is not formed and peak C_1 belongs to reduction of **MBI**$^{\bullet}$ to **MBI**.

Fig. 6 shows the linear sweep voltammograms of **MBT** at scan rate of 10 mV/s, in ethanol/H_2O (with different pH values) (20/80, v/v) mixture. The shift of peak A_1 towards negative potentials with increasing pH values confirmed the participation of proton in the redox process. According to the data presented in Fig. 6, the following equations for electrochemical oxidation of **MBT** at different pH values are proposed. At pHs less than 4.0, the oxidation mechanism of **MBT** is shown in Eq. 6. In this range of pH, the slope for the *E*-pH line is 53 mV/pH, which is close to the theoretical value of 59 mV/pH for a two-electron/two-proton process. At pH values more than 4.0 and less than 7.2, the oxidation mechanism of **MBT** is shown in Eq. 7. In this region of pH, the slope for the *E*-pH line is 85

mV/pH, which confirms the occurrence of a two-electron/three-proton process as shown in Eq. 7.

[Figure 6]

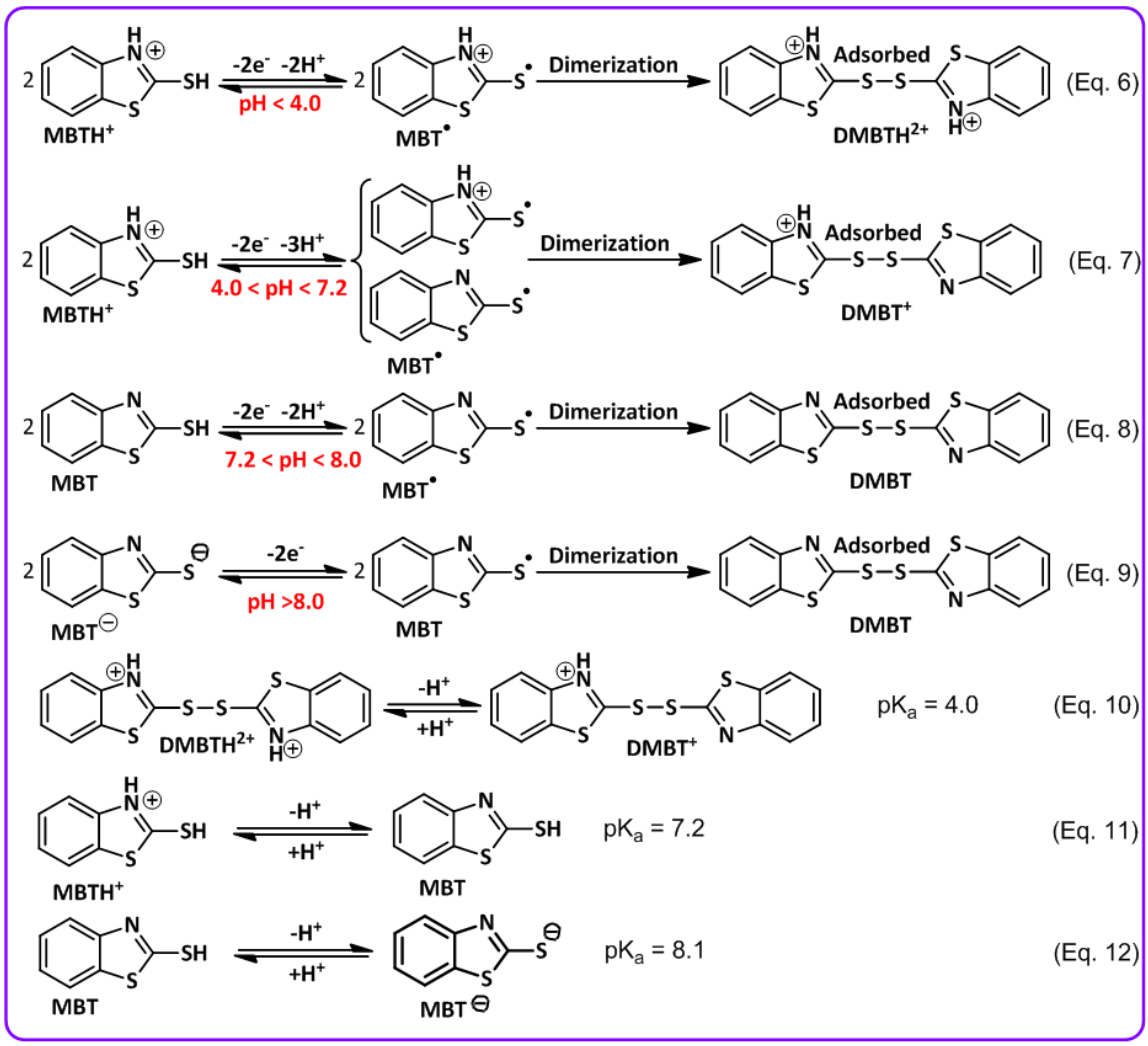

It is necessary to mention that the theoretical value for a two-electron/three-proton process is about 88 mV/pH. At pHs more than 7.2 and less than 8.0, the oxidation mechanism of **MBT** is shown in Eq. 8. In this narrow region of pH, the slope for the *E*-pH line is 50 mV/pH, which confirms the occurrence of a two-electron/two-proton process. In the basic region (pH > 8.0), **MBT** is in its anionic form (**MBT**$^-$) and so its redox process is not dependent on the pH (Eq. 9). In addition, from these data, we can determine the pK_a of the acid/base couples, **DMBTH**$^{2+}$/**DMBTH**$^+$, **MBTH**$^+$/**MBT** and **MBT**/**MBT**$^-$. The calculated pk_a

values are 4.0, 7.2 and 8.1, respectively (Eqs. 10-12). These data are in agreement with previously published data [48].

Similar research was conducted on **MBI**. Fig. 7 shows the linear sweep voltammograms of **MBI** in ethanol/H_2O (with different pH values) (20/80, v/v) mixture at scan rate of 10 mV/s. According to the data presented in Fig. 7, the following equations for electrochemical oxidation of **MBI** at different pH values are proposed. At pHs less than 7.9, the oxidation mechanism of **MBI** is shown in Eq. 13. In this range of pH, **MBI** is in its protonated form and the slope for the *E*-pH line is 35 mV/pH, which is close to the theoretical value of 29.5 mV/pH for a one-electron/two-proton process.

[Figure 7]

In the pH ranging from 7.9 to 9.9, the slope for the *E*-pH line is 67 mV/pH, which is close to the theoretical value of 59 mV/pH for a one-electron/one-proton process (Eq. 14). In the basic region (pH > 9.9), **MBI** is in its anionic form (**MBI**$^-$) and so the proton does not get involved in the redox process (Eq. 15). In addition, from these graphs we can calculate the pK_a values for of the acid/base couples, **MBIH**$^+$/**MBI** and **MBI**/**MBI**$^-$. The calculated pk_a values are 7.9 and 9.9, respectively (Eqs. 16 and 17). These data are in agreement with previously published data [48].

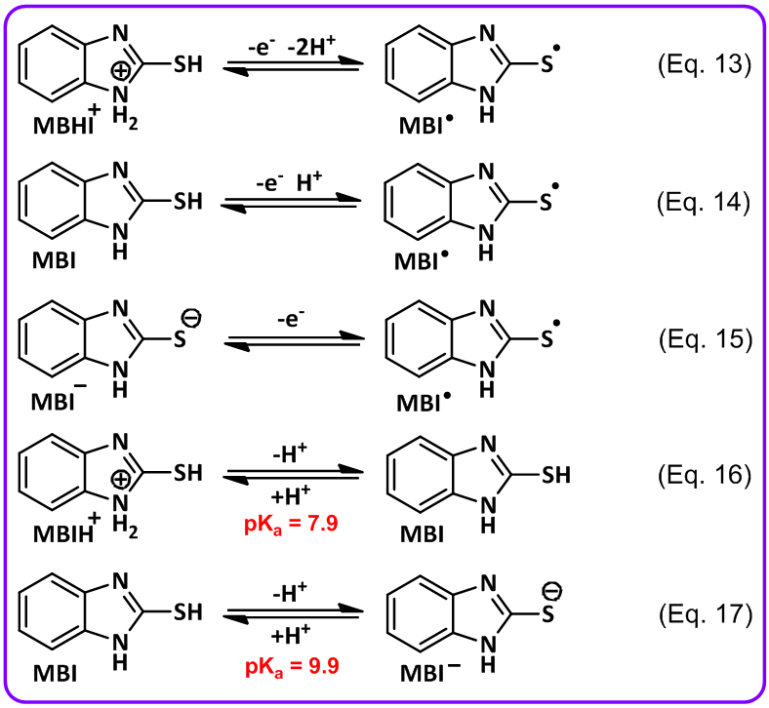

3.2. Electrochemical study of 2-mercaptobenzoheterocyclic compounds in the presence of diethylamine

In this part, to obtain the information needed for the synthesis of new compounds based on **MBO** oxidation, electrochemical study of **MBO** was carried out in the presence of diethylamine (**AM1**) to find the most suitable conditions for the synthesis as well as evaluation of the reaction mechanism. Cyclic voltammograms of **MBO** in the presence of **AM1** are shown in Fig. 8 (part I curve b) and have been compared with that of in the absence of **AM1** (curve a). Comparison of these voltammograms shows that the most important change is the removal of the cathode peak C_1. Since peak C_1 is related to the reduction of dimer (**DMBO**), its disappearance is a sign of the lack of dimer at the electrode surface. In other words, the occurrence of a fast chemical reaction between **AM1** and **DMBO**, removed the dimer from the electrode surface. Our data also show that I_{pC1} depends on the **AM1** concentration so that it decreases with increasing **AM1** concentration. Increasing the **AM1** concentration increases the reaction rate of amine with the dimer

results in the disappearance of the peak C_1 at high amine concentration. We also have found that there is a significant influence of potential sweep rate on the shape of the voltammogram (Fig. 8 part II). It is seen that the current of peak C_1 (I_{pC1}) increase with increasing potential scan rate due to the decrease in the time available for the reaction of amine with dimer at higher scan rates.

[Figure 8]

Constant current electrolysis was performed in water (pH=8.0)/ethanol mixture containing **MBO** and **AM1** at the current density of 0.26 mA cm^{-2} (10 mA). The electrolysis progress was monitored using cyclic voltammetry (Fig. 9) and thin layer chromatography. It was found that, proportional to the electrolysis progress, the anodic peak current (I_{pA1}) decreased. The electrolysis was ended when the peak A_1 decay more than 95% (after consumption of 190 C electricity, n_{app} = 3.9). In this condition, the spot of **MBO** disappeared on TLC.

By putting together voltammetric and amount of charge passed along with the results obtained from spectroscopic analysis of the product (mass spectroscopy and NMR), the mechanism shown in Scheme 2, is proposed for the electrochemical oxidation of **MBO** in the presence of **AM1**. According to Scheme 2, sulfonamide **SO1** is synthesized in four steps from **MBO**. First: electrolytic formation of **MBO$^{\bullet}$**, second: formation of dimer **DMBO**, third: nucleophilic addition of **AM1** to **DMBO**, S-S bond cleavage and formation of corresponding sulfenamide (**SE1**) and fourth: the air oxidation of sulfonamide [49-51] and converting it into the final product (**SO1**). The air oxidation of sulfonamide has caused the main product of **MBO** in the presence of **AM1** to be **SO1** and only a little amount of sulfenamide (**SE1**) was observed chromatographically. The role of oxygen in the oxidation of sulfenamide (**SE1**) is

confirmed by the fact that the number of electrons consumed in the synthesis of **SO1** is less than the required amount.

[Figure 9]

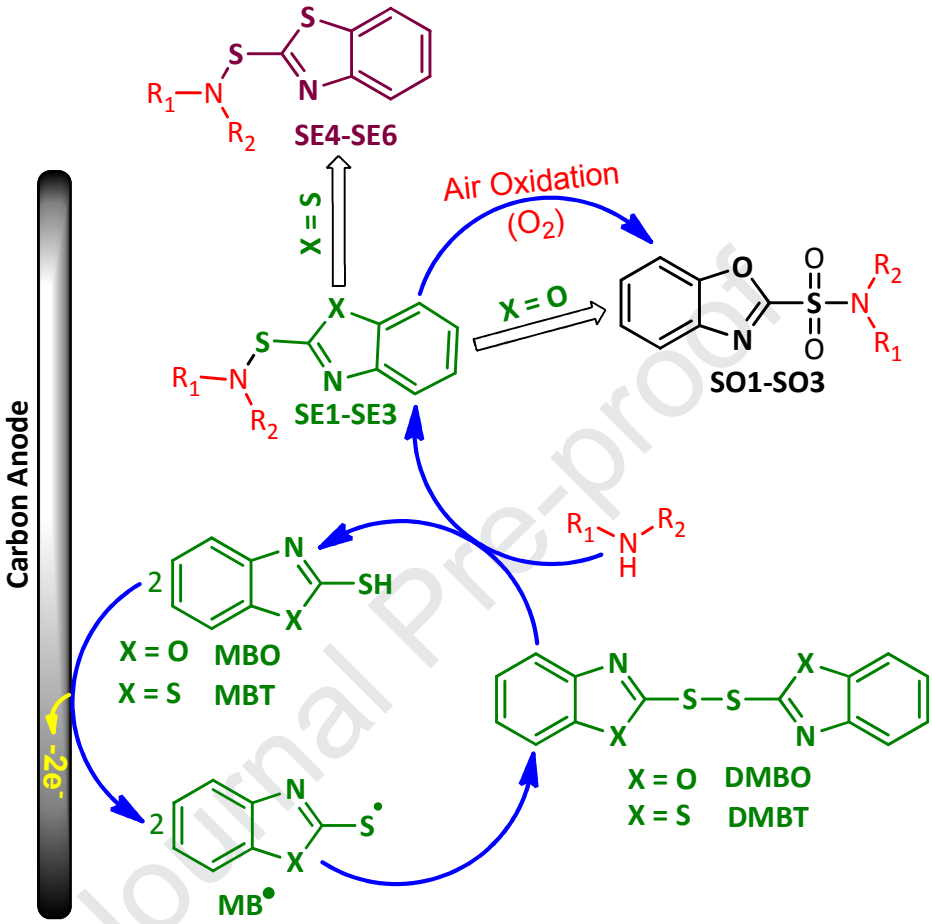

Scheme 2. Electrochemical oxidation pathway of **MBO** and **MBT** in the presence of the amines.

In the case of **MBT**, the same reaction mechanism was observed, however, the air oxidation process is not carried much. Therefore, when **MBT** is used as the starting material, the main product is sulfenamide (**SE**) and only small amounts of sulfonamide (**SO**) were observed (Scheme 2).

Different with **MBO** and **MBT**, when **MBI** is used as the starting material, as discussed in the preceding sections, the **MBI** dimer is not formed and we could not synthesize any sulfonamide or sulfenamide compounds from oxidation of **MBI** in the presence of amines.

3.3. Constant current electrolysis

Current density is one of the most important factors controlling yield and purity. The synthesis of **SO2** and **SE5**, were studied at different current densities ranging from 0.06 to 0.72 mA/cm^2, while other parameters (charge: 190 C, temperature: 298 K, **MBO** and **MBT** amount: 0.5 mmol and cyclohexylamine (**AM2**) amount: 1.5 mmol) remain constant (Fig. 10). Our results show that the highest yield for **SO2** (88%) and **SE5** (79%) were obtained at a current density of 0.26 and 0.52 mA/cm^2, respectively. In the synthesis of **SO2**, at the current densities lower than 0.26 mA/cm^2, the amount of **MBO** radicals produced per unit time decreases. As a result, they are less likely to react together to form **DMBO**. In such conditions, the **MBO** radicals participate either in the side reactions or in the back reaction in the cathode surface, therefore, despite equal charge consumption, the production yield is low. On the other hand, at the current densities higher than 0.26 mA/cm^2, the over oxidation of **DMBO** and/or **SE2** reduces the production yield.

[Figure 10]

*3.4. Electrochemical synthesis of sulfonamides (**SO1-SO3**) and sulfenamides (**SE4-SE6**)*

For the synthesis of sulfonamides **SO1**-**SO3**, an 80 ml solution containing phosphate buffer (pH = 8.0, *c* = 0.2 M)/ethanol (20/80 v/v) was pre-electrolyzed in an undivided cell. Then 0.5 mmol of **MBO**, 1.5 mmol of amine (**AM1**, **AM2** or **AM3**) was subjected to electrolysis at constant current of 10 mA (0.26 mA cm^{-2}), in an undivided cell. The progress of the electrolysis was followed by TLC using *n*-hexane/ethyl acetate (2:1) and also cyclic

voltammetry. At the end of electrolysis, the reaction mixture was filtered and then the ethanol was removed under vacuum. The residual was extracted with 3 x 10 ml of ethyl acetate. The extracted organic phase was dried over anhydrous sodium sulphate, filtered and evaporated under reduced pressure. The resulting residue was purified by flash chromatography on silica gel (eluent 2:1 *n*-hexane–ethyl acetate) to afford the corresponding sulfonamide (Table 1).

[Table 1]

For the synthesis of sulfenamides **SE4**-**SE6**, in a solution containing carbonate buffer (pH = 12.0, *c* = 0.2 M)/ethanol (20/80 v/v), **MBT** and amine (**AM1**, **AM2** or **AM3**) was subjected to electrolysis at constant current of 20 mA (0.52 mA cm^{-2}), in an undivided cell. Other conditions for the synthesis of sulfenamides **SE4**-**SE6**, are similar to the synthesis of sulfonamides (Table 1).

3.5. Scaling up experiments

In this part, we describe the large scale synthesis of **SO2** and **SE5**. Fig. 11 shows the electrochemical cell designed and manufactured for this purpose [52]. The working electrode (anode) used in large-scale electrolysis was an assembly of fifteen ordinary carbon plate (11 cm × 1.5 cm × 0.3 cm), placed beside of fifteen stainless steel plate cathode (11 cm× 1.5 cm × 0.1 cm). Under these conditions, the electrode surface increases up to 247 cm^2. In a typical procedure, for the large scale synthesis of **SO2**, 300 ml solution containing phosphate buffer (pH = 8.0, *c* = 0.2 M)/ethanol (20/80 v/v) was pre-electrolyzed in the cell; then 10 mmol of **MBO**, 30 mmol of **AM2** was subjected to electrolysis at the constant current of 0.22 mA cm^{-2} (yield 72%).

The large scale synthesis of **SE5** was carried out in a 300 ml solution containing carbonate buffer (pH = 12.0, *c* = 0.2 M)/ethanol (20/80 v/v), then 10 mmol of **MBT** and 30

mmol of **AM2** was subjected to electrolysis at the constant current of 0.51 mA cm^{-2} (yield 81%). Other conditions are similar to those of the previous section.

The large scale synthesis of **SE5** was carried out in a 300 ml solution containing carbonate buffer (pH = 12.0, *c* = 0.2 M)/ethanol (20/80 v/v), then 10 mmol of **MBT** and 30 mmol of **AM2** was subjected to electrolysis at the constant current of 0.51 mA cm^{-2} (yield 81%). Other conditions are similar to those of the previous section.

[Figure 11]

3.6. Antibacterial susceptibility

This part of the investigation was initiated to evaluate the antibacterial susceptibility of the synthesized sulfonamide (**SO1**-**SO3**) and sulfenamide (**SE4**-**SE6**) derivatives. Antobiogram studies revealed that all gram positive (*Bacillus cereus* and *Staphylococcus aureus*) and gram negative bacteria (*Escherichia coli* and *Salmonella enteritidis*) were sensitive to **SO2** and **SO3**. Gram positive bacteria were sensitive to **SE4** and **SE6** while, gram negative bacteria showed resistance to **SE4** and **SE6**. Gram negative bacteria were sensitive to **SE5** (see Supplementary Information). All bacteria was resistance to **SO1**. The results of antibacterial activity of **SO1**-**SO3** and **SE4**-**SE6** compounds are summarized in Table 2.

[Table 2]

4. Conclusion

In this work, an efficient and green strategy based on the electrochemical oxidation of 2-mercaptobenzoheterocyclic compounds in the presence of some amines was developed for the synthesis of some new sulfonamide (**SO**) and sulfenamide (**SE**) derivatives. All reactions were carried out in a simple cell, consisting of carbon and stainless steel electrodes in water/ethanol mixture under constant current condition, without using any catalyst. It is

also shown that the products can be easily synthesized in preparative scales with impressive yields. The product type is dependent upon the 2-mercaptobenzoheterocyclic type. When **MBO** is used as the starting material, sulfonamide compounds (**SO**) are the main products. Unlike **MBO**, when **MBT** is the starting material, then sulfenamide (**SE**) derivatives are the main products. It should be noted that Unlike **MBO** and **MBT**, upon the oxidation of **MBI** in the presence of amines, we could not isolate these two types of products. The product yields are dependent upon the current density. In this paper, also, the electrochemical behavior of **MBO**, **MBT** and **MBI** has been comprehensively investigated and unique information has been published.

Acknowledgements

The authors wish to acknowledge Iran National Science Foundation (INSF) for financial support of this work. We also acknowledge the Bu-Ali Sina University Research Council and Center of Excellence in Development of Environmentally Friendly Methods for Chemical Synthesis (CEDEFMCS) for their support of this work.

Appendix A. Supplementary data

Supplementary data including FT-IR, ^{1}H NMR ^{13}C NMR and MS spectra of **SO1-SO3** and **SE4-SE6** and antibacterial activity of products associated with this article can be found, in the online version, at http://dx.doi.org

Reference:

[1] R.J. Anderson, P.W. Groundwater, A. Todd, A.J. Worsley, Antibacterial agents: Chemistry, Mode of Action, Mechanisms of Resistance and Clinical Applications, John Wiley & Sons, Chichester, West Sussex (2012), pp. 105-124.

[2] S. Syed Shoaib Ahmad, G. Rivera, M. Ashfaq, Recent advances in medicinal chemistry of sulfonamides. Rational design as anti-tumoral, anti-bacterial and anti-inflammatory agents, Mini Rev. Med. Chem. 13 (2013) 70-86.

[3] A. Scozzafava, T. Owa, A. Mastrolorenzo, C.T. Supuran, Anticancer and antiviral sulfonamides, Curr. Med. Chem. 10 (2003) 925-953.

[4] C.T. Supuran, A. Casini, A. Scozzafava, Protease inhibitors of the sulfonamide type: anticancer, antiinflammatory, and antiviral agents, Med. Res. Rev. 23 (2003) 535-558.

[5] K.P. Rakesh, S.M. Wang, J. Leng, L. Ravindar, A.M. Asiri, H.M. Marwani, H. L. Qin, Recent development of sulfonyl or sulfonamide hybrids as potential anticancer agents: a key review. Anti-Cancer Agents Med. Chem. 18 (2018) 488–505.

[6] S.M. Pant, A. Mukonoweshuro, B. Desai, M.K. Ramjee, C.N. Selway, G.J. Tarver, A.G. Wright, K. Birchall, T.M. Chapman, T.A. Tervonen, J. Klefstrçm, Design, synthesis, and testing of potent, selective hepsin inhibitors via application of an automated closed-loop optimization platform. J. Med. Chem. 61 (2018) 4335-4347.

[7] H. Nishioka, N. Tooi, T. Isobe, N. Nakatsuji, K. Aiba, BMS-708163 and Nilotinib restore synaptic dysfunction in human embryonic stem cell-derived Alzheimer's disease models, Sci. Rep. 6 (2016) 33427.

[8] L.D. Pennington, M.D. Bartberger, M.D. Croghan, K.L. Andrews, K.S. Ashton, M.P. Bourbeau, J. Chen, S. Chmait, R. Cupples, C. Fotsch, J. Helmering, Discovery and structure-guided optimization of diarylmethanesulfonamide disrupters of glucokinase–glucokinase regulatory protein (GK–GKRP) binding: strategic use of a N→ S (nN→ σ* S–X) interaction for conformational constraint, J. Med. Chem. 58 (2015) 9663-9679.

[9] K.W. Gillman, J.E. Starrett Jr, M.F. Parker, K. Xie, J.J. Bronson, L.R. Marcin, K.E. McElhone, C.P. Bergstrom, R.A. Mate, R. Williams, J.E. Meredith Jr, Discovery and evaluation of

BMS-708163, a potent, selective and orally bioavailable γ-secretase inhibitor, ACS Med. Chem, 1(2010) 120-124.

[10] H. Sugimoto, M. Shichijo, T. Iino, Y. Manabe, A. Watanabe, M. Shimazaki, F. Gantner, K.B. Bacon, An orally bioavailable small molecule antagonist of CRTH2, ramatroban (BAY u3405), inhibits prostaglandin D2-induced eosinophil migration in vitro, J. Pharmacol. Exp. Ther. 305 (2003) 347-352

[11] M. Harmata, P. Zheng, C. Huang, M.G. Gomes, W. Ying, K.O. Ranyanil, G. Balan, N.L. Calkins, Expedient synthesis of sulfinamides from sulfonyl chlorides, J. Org. Chem. 72 (2007) 683-685.

[12] R. Sridhar, B. Srinivas, V.P. Kumar, M. Narender, K.R. Rao, β-Cyclodextrin-catalyzed monosulfonylation of amines and amino acids in water, Adv. Synth. Catal. 349 (2007) 1873–1876.

[13] D. Audisio, S. Messaoudi, J.F.O. Peyrat, J.D. Brion, M.D. Alami, A general copper powder-catalyzed Ullmann-type reaction of 3-halo-4(1*H*)-quinolones with various nitrogen-containing nucleophiles, J. Org. Chem. 76 (2011) 4995–5005.

[14] J. Yin, S.L. Buchwald, Pd-catalyzed intermolecular amidation of aryl halides: the discovery that xantphos can be trans-chelating in a palladium complex, J. Am. Chem. Soc. 124 (2002) 6043–6048.

[15] J. Baffoe, M.Y. Hoe, B.B. Touré, Copper-mediated *N*-heteroarylation of primary sulfonamides: Synthesis of mono-*N*-heteroaryl sulfonamides, Org. Lett. 12 (2010) 1532–1535.

[16] G. Burton, P. Cao, G. Li, R. Rivero, Palladium-catalyzed intermolecular coupling of aryl chlorides and sulfonamides under microwave irradiation, Org. Lett. 5 (2003) 4373–4376.

[17] W. Deng, L. Liu, C. Zhang, M. Liu, Q.X. Guo, Copper-catalyzed cross-coupling of sulfonamides with aryl iodides and bromides facilitated by amino acid ligands, Tetrahedron Lett. 46 (2005) 7295–7298.

[18] B.R. Rosen, J.C. Ruble, T.J. Beauchamp, A. Navarro, Mild Pd-catalyzed *N*-arylation of methanesulfonamide and related nucleophiles: Avoiding potentially genotoxic reagents and byproducts, Org. Lett. 13 (2011) 2564–2567.

[19] P.Y.S. Lam, G. Vincent, C.G. Clark, S. Deudon, P.K. Jadhav, Copper-catalyzed general C-N and C-O bond cross-coupling with arylboronic acid, Tetrahedron Lett. 42 (2001) 3415–3418.

[20] X.D. Tang, L.B. Huang, C.R. Qi, X. Wu, W.Q. Wu, H.F. Jiang, Copper-catalyzed sulfonamides formation from sodium sulfinates and amines, Chem. Commun. 49 (2013) 6102-6104.

[21] H. Zhu, Y. Shen, Q. Denga, T. Tu, Copper-catalyzed electrophilic amination of sodium sulfinates at room temperature, Chem. Commun. 51 (2015) 16573-16576.

[22] S.W. Wright, K.N. Hallstrom, A convenient preparation of heteroaryl sulfonamides and sulfonyl fluorides from heteroaryl thiols, J. Org. Chem. 71 (2006) 1080-1084.

[23] B. Nguyen, E.J. Emmett, M.C. Willis, Palladium-catalyzed aminosulfonylation of aryl halides, J. Am. Chem. Soc. 132 (2010) 16372- 16373.

[24] Y. Chen, P.R.D. Murray, A.T. Davies, M.C. Willis, The direct copper-catalyzed three-component synthesis of sulfonamides, J. Am. Chem. Soc. 140 (2018) 8781–8787.

[25] S. Ye, J. Wu, A palladium-catalyzed three-component coupling of arylboronic acids, sulfur dioxide and hydrazines, Chem. Commun. 48 (2012) 7753;

[26] D.Q. Zheng, Y.Y. An, Z.H. Li, J. Wu, Metal-free aminosulfonylation of aryldiazonium tetrafluoroborates with DABCO.$(SO_2)_2$ and hydrazines, Angew. Chem. Int. Ed. 53 (2014) 2451-2454.

[27] X. Wang, L. Xue, Z. Wang, A copper-catalyzed three-component reaction of triethoxysilanes, sulfur dioxide, and hydrazines, Org. Lett. 16 (2014) 4056-4058.

[28] N.W. Liu, S. Liang, G. Manolikakes, Visible-light photo redox catalyzed aminosulfonylation of diaryliodonium salts with sulfur dioxide and hydrazines, Adv. Synth. Catal. 359 (2017) 1308-1319.

[29] S. Ye, J. Wu, A palladium-catalyzed reaction of aryl halides, potassium metabisulfite, and hydrazines, Chem. Commun. 48 (2012) 10037.

[30] B. Mokhtari, D. Nematollahi, H. Salehzadeh, A tunable pair electrochemical strategy for the synthesis of new benzenesulfonamide derivatives, Sci. Rep. 9 (2019) Article number: 4537.

[31] S. Khazalpour, D. Nematollahi, A. Ahmad, B. Dowlati, Electroreductive nucleophile acceptor generation. Electrochemical synthesis of *N*-(4-(dimethylamino) phenyl) benzenesulfonamide, Electrochim. Acta 180 (2015) 909–913.

[32] G. Laudadio, E. Barmpoutsis, C. Schotten, L. Struik, S. Govaerts, D.L. Browne, T. Noël, Sulfonamide synthesis through electrochemical oxidative coupling of amines and thiols, J. Am. Chem. Soc. 141 (2019) 5664-5668.

[33] L. Craine, M. Raban, The chemistry of sulfonamides, Chem. Rev. 89 (1989) 689-712.

[34] A.J. Marzocca, M.A. Mansilla, Vulcanization kinetic of styrene–butadiene rubber by sulfur/TBBS, J. Appl. Polym. Sci. 101 (2006) 35-41.

[35] J.L. Shang, H. Guo, Z.S. Li, B. Ren, Z.M. Li, H.G. Dai, L.X. Zhang, J.G. Wang, Synthesis and evaluation of isatin-β-thiosemicarbazones as novel agents against antibiotic-resistant gram-positive bacterial species, Bioorg. Med. Chem. Lett. 23 (2013) 724-727.

[36] A.S. Karwa, A.R. Poreddy, B. Asmelash, T.S. Lin, R.B. Dorshow, R. Rajagopalan, Type 1 phototherapeutic agents. 2. Cancer cell viability and ESR Studies of Tricyclic Diarylamines, ACS Med. Chem. Lett. 211 (2011) 828-833.

[37] F.A. Davis, A.J. Friedman, E.W. Kluger, E.B. Skibo, E.R. Fretz, A.P. Milicia, W.C. LeMasters, M.D. Bentley, J.A. Lacadie, I.B. Douglass, Chemistry of the sulfur-nitrogen bond. 12. Metal-assisted synthesis of sulfenamide derivatives from aliphatic and aromatic disulfides, J. Org. Chem. 42 (1977) 967-972.

[38] K.M. Huttunen, J. Leppänen, K. Laine, J. Vepsäläinen, J. Rautio, Convenient microwave-assisted synthesis of lipophilic sulfenamide prodrugs of metformin, Eur. J. Pharm. Sci. 49 (2013) 624–628.

[39] E. Rattanangkool, W. Krailat, T. Vilaivan, P. Phuwapraisirisan, M. Sukwattanasinitt, S. Wacharasindhu, Hypervalent Iodine (III)-promoted metal-free S–H activation: an approach for the construction of S–S, S–N, and S–C bonds, Eur. J. Org. Chem. 2014 (2014) 4795-4804.

[40] H. Yakan, H. Kutuk, Comparison of conventional and microwave-assisted synthesis of some new sulfenamides under free catalyst and ligand, Monatsh. Chem. 149 (2018) 2047–2057.

[41] D.N.Harpp, T.G. Back, A general synthesis of sulfonamides, Tetrahedron Lett. 12 (1971) 4953-4956.

[42] M. Shimizu, H. Fukazawa, S. Shimada, Y. Abe, The synthesis and reaction of *N*-sulfenyl heterocycles: development of effective sulfenylating reagents, Tetrahedron 62 (2006) 2175-2182.

[43] N. Taniguchi, Copper-catalyzed formation of sulfur–nitrogen bonds by dehydrocoupling of thiols with amines, Eur. J. Org. Chem. 2010 (2010) 2670-2673.

[44] C. Sandford, M.A. Edwards, K.J. Klunder, D.P. Hickey, M. Li, K. Barman, M.S. Sigman, H.S. White, S.D. Minteer, A synthetic chemist's guide to electroanalytical tools for studying reaction mechanisms, Chem. Sci. 10 (2019) 6404-6422.

[45] A.J. Bard, L.R. Faulkner, Electrochemical Methods, 2nd edn, Wiley, New York (2001).

[46] R.N. Goyal and M.S. Verma, Electrochemical oxidation of 2-mercaptobenzoxazole, Indian J. Chem. 35A (1996) 281-287.

[47] A. Schaufuß, G. Wittstock, Oxidation of 2-mercaptobenzoxazole in aqueous solution: solid phase formation at glassy carbon electrodes, J. Solid State Electrochem. 3 (1999) 361-369.

[48] A.A. Ahmed Boraei, I.T. Ahmed, M.M.A. Hamed, Acid dissociation constants of some mercaptobenzazoles in aqueous-organic solvent mixtures, J. Chem. Eng. Data 41 (1996) 787-790.

[49] Q. Liu, L. Wang, H. Yue, J.S. Li, Z. Luo, W. Wei, Catalyst-free visible-light-initiated oxidative coupling of aryldiazo sulfones with thiols leading to unsymmetrical sulfoxides in air, Green Chem. 21 (2019) 1609-1613.

[50] F. Jensen, A. Greer, E.L. Clennan, Reaction of organic sulfides with singlet oxygen. A revised mechanism, J. Am. Chem. Soc. 120 (1998) 4439-4449.

[51] D.H. Kim, J. Lee, A. Lee, Visible-light-driven silver-catalyzed one-pot approach: A selective synthesis of diaryl sulfoxides and diaryl sulfones, Org. Lett. 20 (2018) 764-767.

[52] B. Karimi, M. Rafiee, S. Alizadeh, H. Vali, Eco-friendly electrocatalytic oxidation of alcohols on a novel electro generated TEMPO-functionalized MCM-41 modified electrode, Green Chem. 17 (2015) 991-1000.

Tables

Table 1. Products and conditions for the synthesis of sulfonamide (**SO**) and sulfenamide (**SE**) compounds.

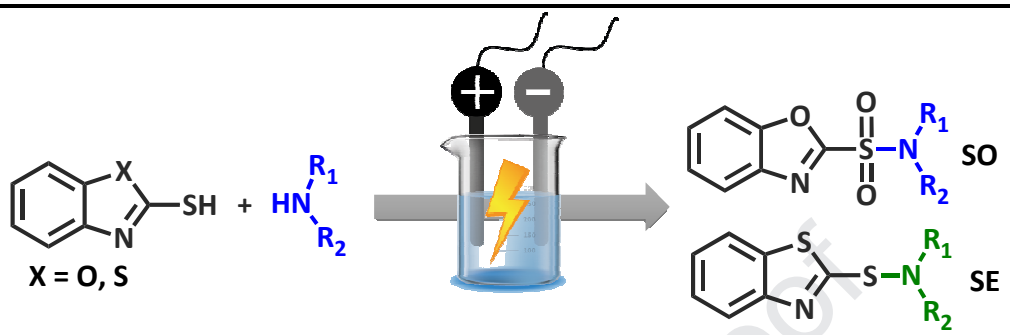

Undivided cell **.** Anode: carbon **.** Cathode: stainless steel

Phosphate buffer (X = O, pH = 8.0, X = S, pH = 12.0)/ethanol (20/80 v/v)

X = O, J = 0.26 mA cm^{-2} **.** X = S, J = 0.52 mA cm^{-2} Q = 190 C **.**

Room temperature

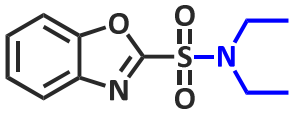 **SO1** Yield: 59%	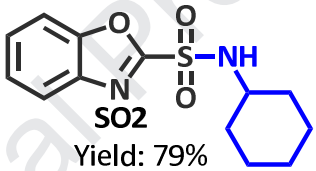 **SO2** Yield: 79%	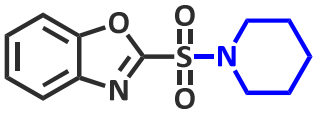 **SO3** Yield: 62%
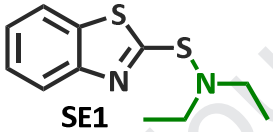 **SE1** Yield: 65%	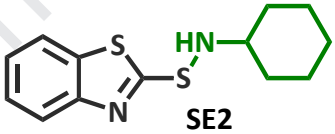 **SE2** Yield: 88%	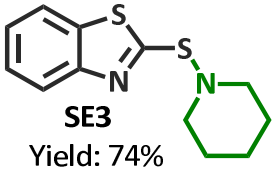 **SE3** Yield: 74%

Table 2. Antibacterial activity of **SO1**-**SO3** and **SE4**-**SE6**.

	Microorganism	Tetracyclne disc 30 µg[a]	well 30 µg[b]	Disc 30 µg	Activity
SO1	*Bacillus cereus*	32	12	11	(-)[c]
	Staphylococcus aureus	26	8	9	(-)
	Escherichia coli	20	8	9	(-)
	Salmonella enteritidis	18	7	10	(-)
SO2	*Bacillus cereus*	26	17	15	(+)[d]
	Staphylococcus aureus	29	19	16	(+)
	Escherichia coli	18	16	14	(+)
	Salmonella enteritidis	22	16	15	(+)
SO3	*Bacillus cereus*	29	16	14	(+)
	Staphylococcus aureus	23	17	14	(+)
	Escherichia coli	18	18	17	(+)
	Salmonella enteritidis	19	16	15	(+)
SE4	*Bacillus cereus*	30	19	17	(+)
	Staphylococcus aureus	27	16	15	(+)
	Escherichia coli	18	8	8	(-)
	Salmonella enteritidis	23	8	7	(-)
SE5	*Bacillus cereus*	35	18	17	(+)
	Staphylococcus aureus	28	9	9	(-)
	Escherichia coli	20	16	15	(+)
	Salmonella enteritidis	22	14	15	(+)
SE6	*Bacillus cereus*	28	18	14	(+)
	Staphylococcus aureus	26	16	15	(+)
	Escherichia coli	18	8	8	(-)
	Salmonella enteritidis	24	7	8	(-)

[a]Diameter of effective zone of inhibition (mm).

[b]Solvent well, DMSO + Tween 20.

[c]Negative activity.

[d]Positive activity

Figures

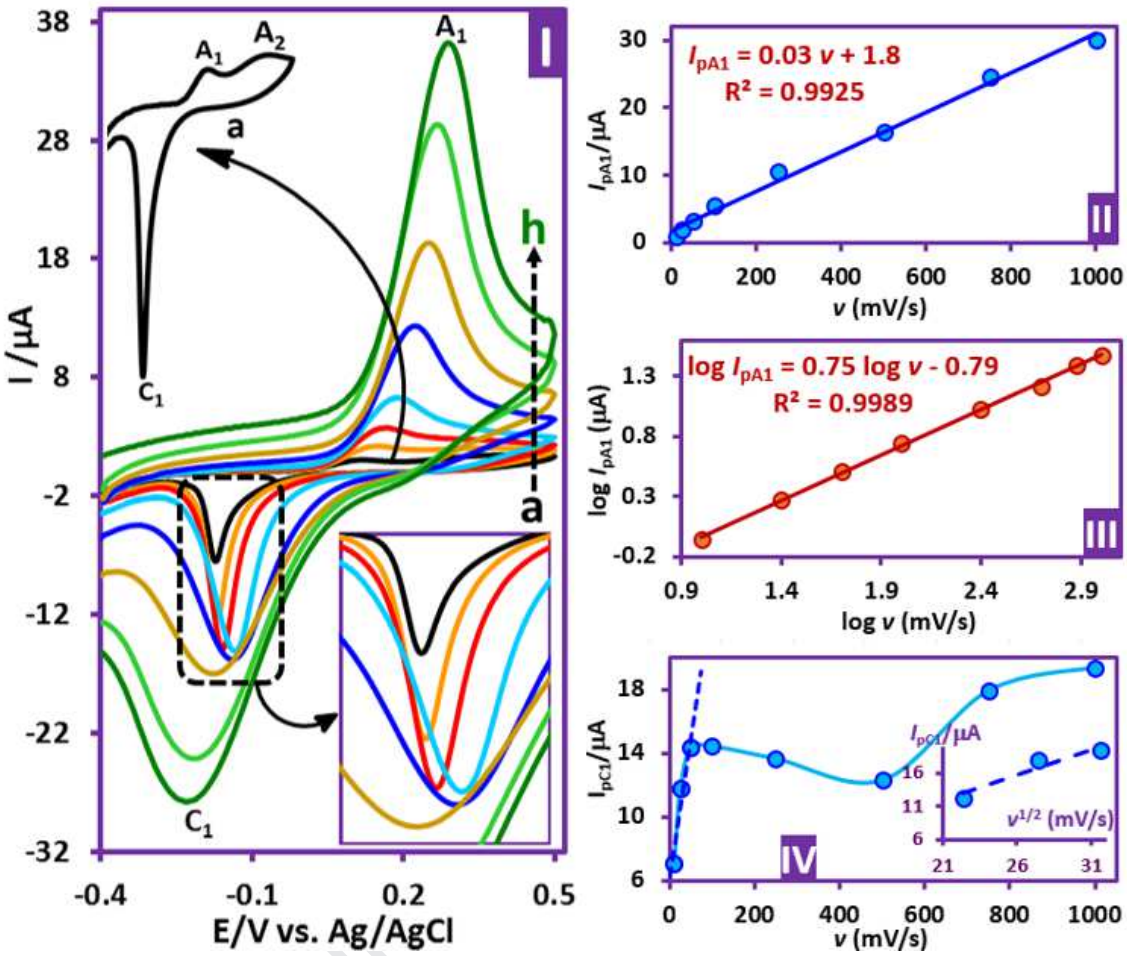

Figure 1. Part I. Cyclic voltammograms of **MBO** (1.0 mM) in aqueous phosphate buffer (*c* = 0.2 M, pH = 7.0), at GC electrode, at different scan rate and at room temperature. Scan rates from a to h are: 10, 25, 50, 100, 250, 500, 750 and 1000 mV/s. Part II, the plot of I_{pA1} versus scan rate. Part III, the plot of log I_{pA1} versus log *v*. Part IV, the plot of I_{pC1} versus scan rate.

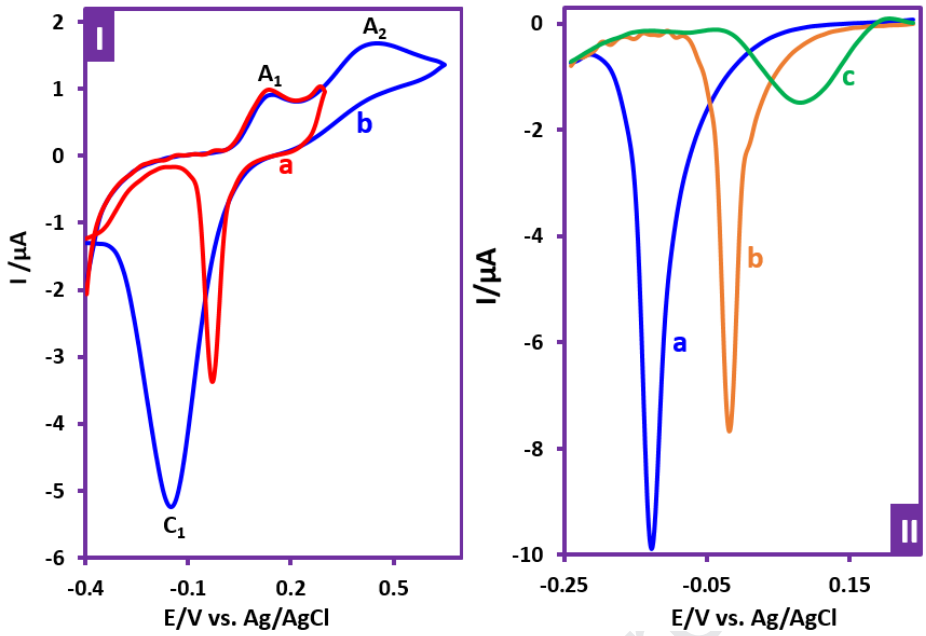

Figure 2. Part I: Cyclic voltammograms of **MBO** (1.0 mM) in water (phosphate buffer, pH = 7.0 and *c* = 0.2 M) at two different switching potentials. Switching potentials for "a" and "b" are 0.30 and 0.65 V vs. Ag/AgCl, respectively. Part II: Linear sweep voltammograms of **MBO** (1.0 mM) (peak C_1) in different ethanol/H_2O (phosphate buffer, pH = 8.0 and *c* = 0.2 M) mixtures a) 0%, b) 10% and c) 20% ethanol. Working electrode: GC electrode. Scan rate: 10 mV/s. Temperature = room temperature.

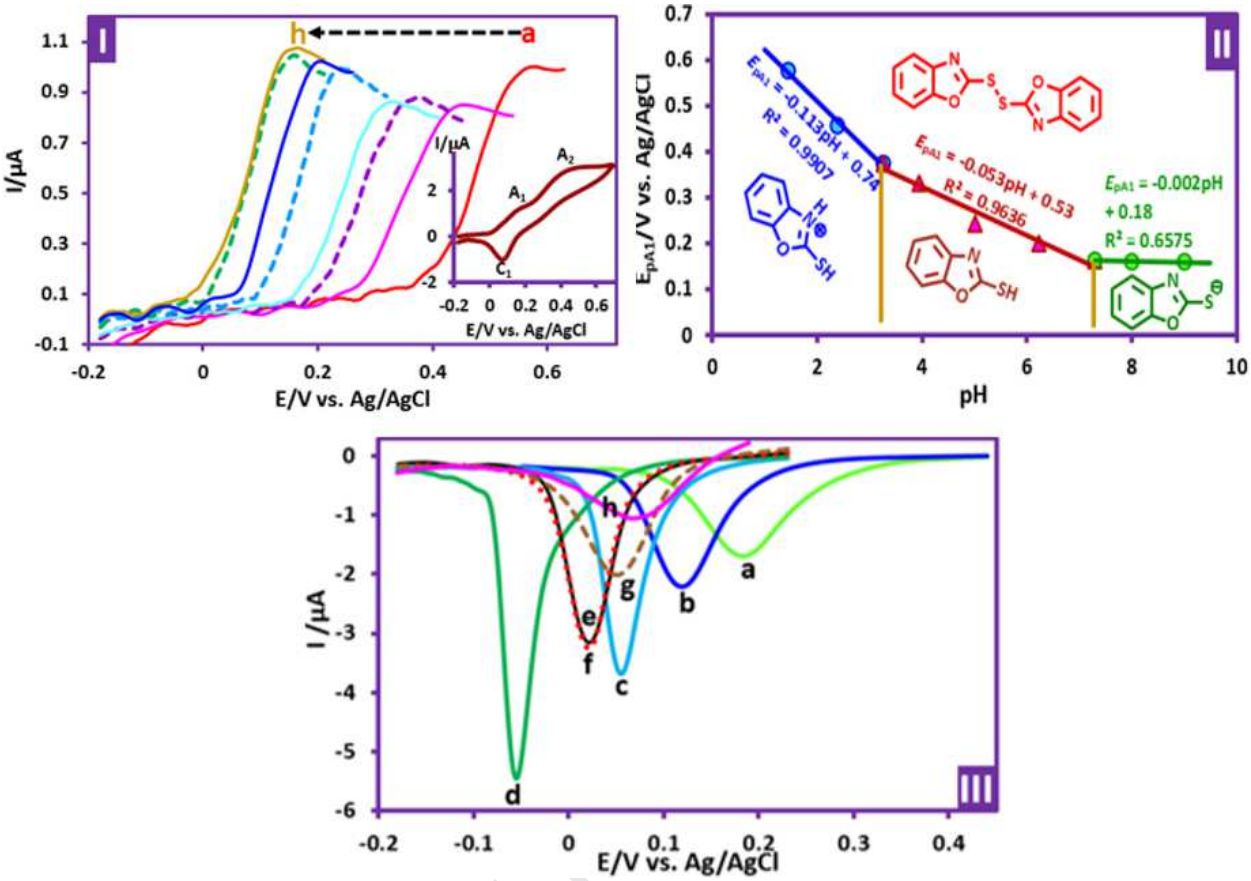

Figure 3. Part I: Linear sweep voltammograms of **MBO** (1.0 mM) in ethanol/H_2O (with different pH values) (20/80, v/v) mixture at GC electrode, at room temperature. Scan rate: 10 mV/s. pH values from a to h are: 1.4, 2.4, 3.3, 3.9, 5.0, 6.2, 7.3 and 8.0. Inset: cyclic voltammogram of **MBO** under above condition at pH = 9.00. Part II: The potential-pH diagram of **MBO**. Part III: The status of peak C_1 at different pHs. pH values from a to h are: 1.4, 2.4, 3.3, 5.0, 6.2, 7.3, 8.0 and 9.0.

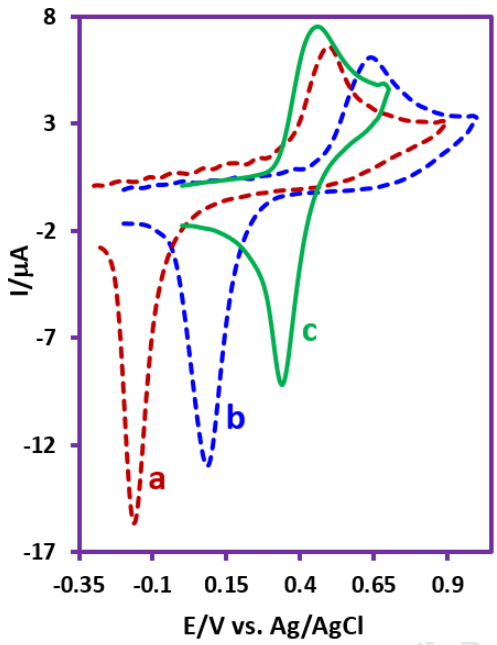

Figure 4. Cyclic voltammograms of 1.0 mM: (a) **MBT**, (b) **MBO** and (c) **MBI** in water ($HClO_4$, pH = 1.0 and *c* = 0.1 M)/ethanol (80/20) mixture at GC electrode, at room temperature. Scan rate: 100 mV/s.

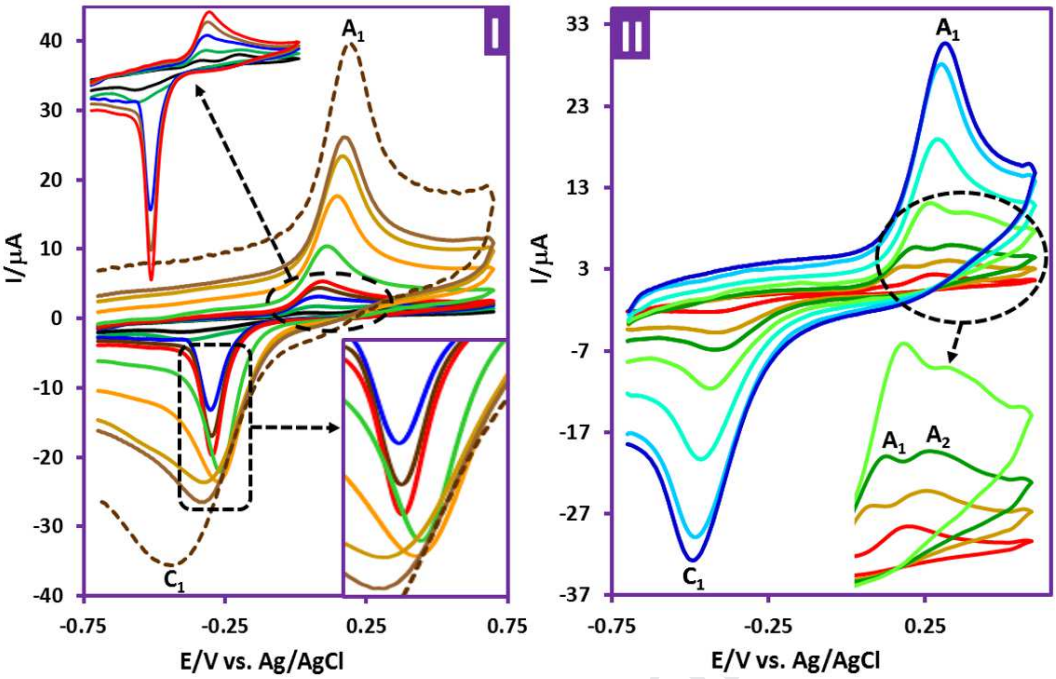

Figure 5. Cyclic voltammograms of 1.0 mM **MBT** (part I) and 1.0 mM **MBI** (part II) in water (phosphate buffer, pH = 8.0 and *c* = 0.2 M)/ethanol (80/20) mixture at GC electrode, at room temperature. Scan rates for **MBT** are: 10, 25, 50, 75, 100, 250, 500, 750, 1000 and 2000 mV/s. Scan rates for **MBI** are: 10, 50, 100, 250, 500, 750 and 1000 mV/s.

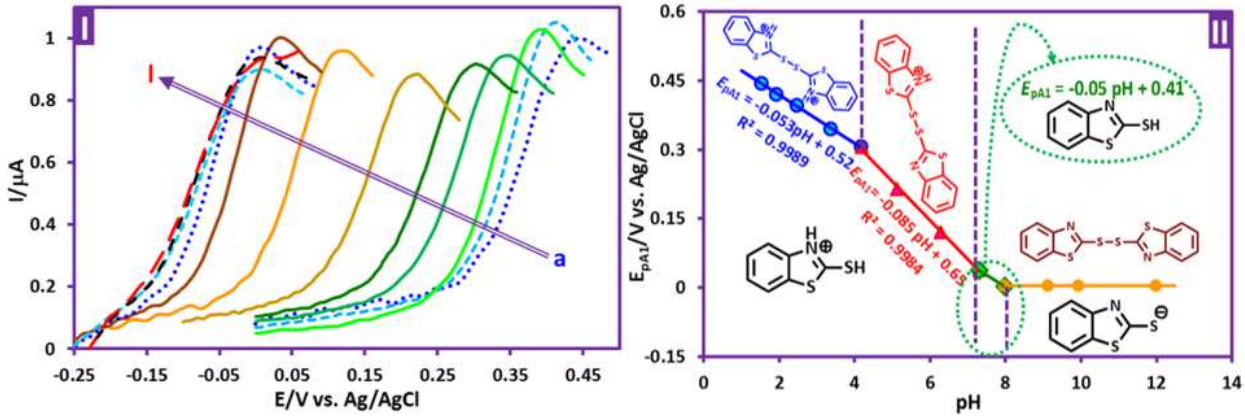

Figure 6. . Part I: Linear sweep voltammograms of **MBT** (1.0 mM) in ethanol/H_2O (with different pH values) (20/80, v/v) mixture at GC electrode, at room temperature. Scan rate: 10 mV/s. pH values from a to I are: 1.54, 1.93, 2.47, 3.37, 4.17, 5.12, 6.27, 7.31, 7.98, 9.13, 9.94 and 12.00. Part II: The potential-pH diagram of **MBT**.

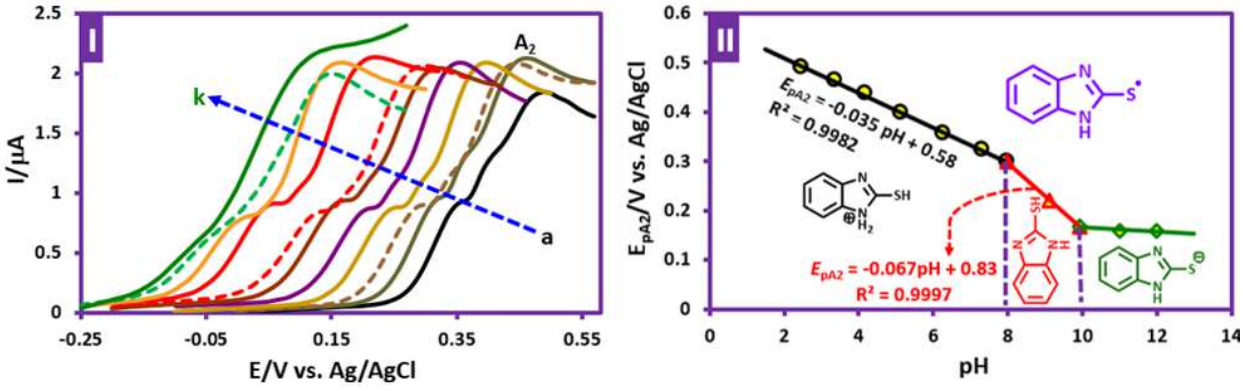

Figure 7. Part I: Linear sweep voltammograms of **MBI** (1.0 mM) in ethanol/H_2O (with different pH values) (20/80, v/v) mixture at GC electrode, at room temperature. Scan rate: 10 mV/s. pH values from a to k are: 2.47, 3.37, 4.17, 5.12, 6.27, 7.31, 7.98, 9.13, 9.94, 11.01 and 12.00. Part II: The potential-pH diagram of **MBI**.

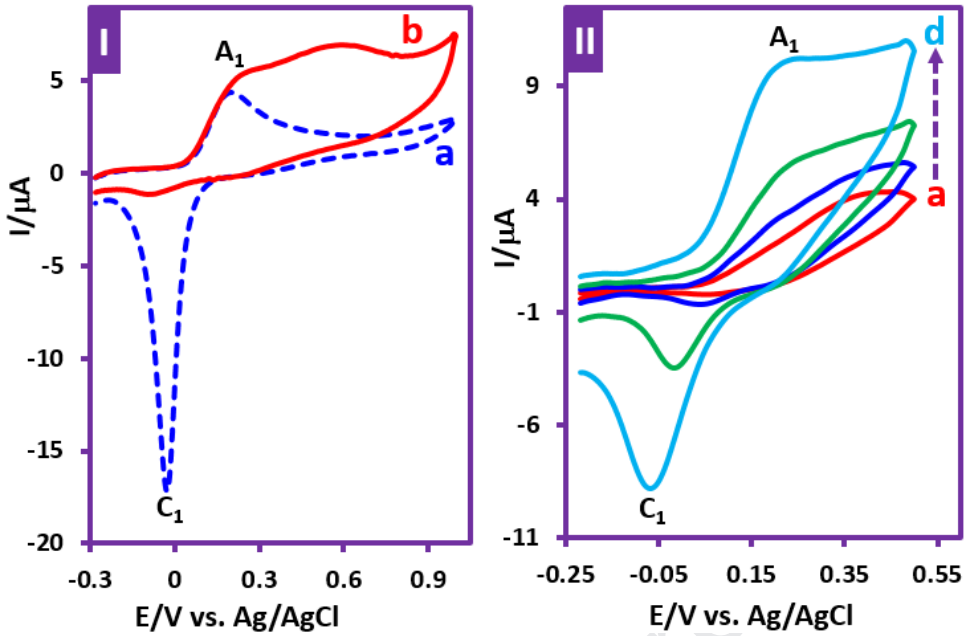

Figure 8. Part I: Cyclic voltammograms of **MBO** (1.0 mM) in the absence of **AM1** (curve a) and in the presence of **AM1** (2.5 mM) (curve b) at scan rate of 100 mV s^{-1}. Part II: Cyclic voltammograms of **MBO** (1.0 mM) in the presence of **AM1** (2.5 mM) at various scan rates. Scan rates from of a to d are: 10, 25, 100 and 250 mV s^{-1}. Solvent: ethanol/H_2O (pH = 8.0) (20/80, v/v) mixture at GC electrode and at room temperature.

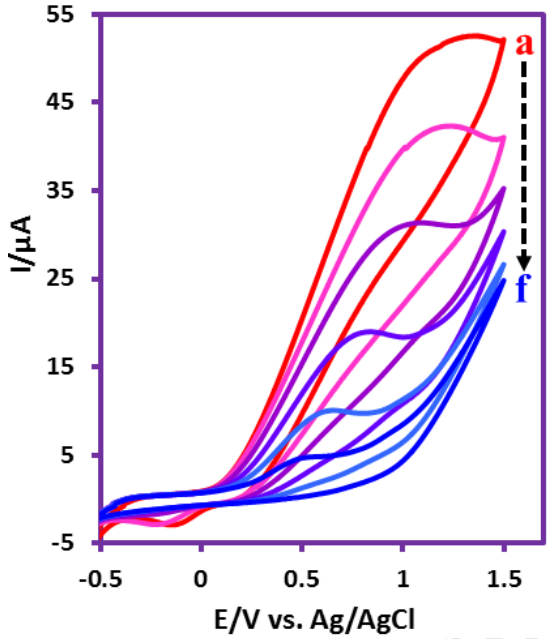

Figure 9. Cyclic voltammograms of **MBO** (0.5 mmol) in the presence of **AM1** (1.5 mmol) during the constant current electrolysis in water (pH=8.0)/ethanol mixture (20/80, v/v) in various time. Time from a to f is: 0, 60, 120, 180, 240 and 330 min. current density: 0.26 mA/cm^2. Scan rate: 100 mV/s at room temperature.

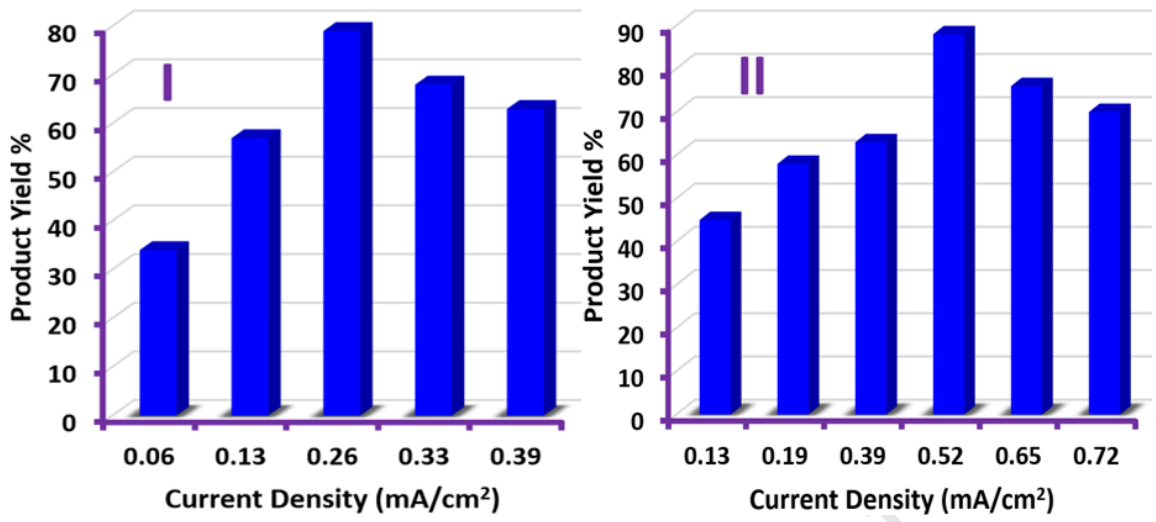

Figure 10. The effect of current density on the yield of **SO2** (part I) and **SE5** (part II). Charge passed: 190 C. **MBO** and **MBT** amount: 0.5 mmol. **AM2** amount: 1.5 mmol at room temperature.

Figure 11. Cell configuration in large scale synthesis.

A Comprehensive Electrochemical Study of 2-Mercaptobenzoheterocyclic Derivatives. Air-Assisted Electrochemical Synthesis of New Sulfonamide Derivatives

Nesa Yousefloui,[a] Saber Alizadeh,[a] Mahmood Masoudi-Khoram,[a] Davood Nematollahi[*a] and Hojjat Alizadeh[b]

E-Mail: nemat@basu.ac.ir

[a]Faculty of Chemistry, Bu-Ali Sina University, Hamedan, Iran. Zip Code 65178-38683

[b]Rooyana veterinary laboratory, Saqqez, Kurdistan, Iran

[*]Corresponding author. Tel.: + 0098 813 8271541; fax: +0098 813 8272404.

E-mail addresses: *nemat@basu.ac.ir, dnematollahi@yahoo.com* (D. Nematollahi).

Fax: +0098 813 8257407, Tel: +0098 813 8282807.

ABSTRACT

In this work, we have introduced a green air-assisted electrochemical method for the synthesis of new sulfonamide derivatives via oxidative coupling of heterocyclic thiols and amines. The synthetic method was designed based on the data collected from electrochemical oxidation of heterocyclic thiols, 2-mercaptobenzoxazole (**MBO**), 2-mercaptobenzothiazole (**MBT**) and 2-mercaptobenzimidazole (**MBI**) in the absence and presence of amines. The electrochemical results indicate that the oxidation of **MBO** and **MBT** lead to the formation of the corresponding dimers, which as an intermediate is essential for sulfonamide synthesis. The results also show that, in the time scale of our voltammetric experiments, oxidation of **MBI** does not lead to dimer formation. Our voltammetric studies suggest that the formed dimer is adsorbed on the electrode surface. The amount and intensity of adsorption depends on the type heterocyclic thiol, solvent, switching potential and solution pH. The mechanism of synthesis of sulfonamide compounds has been established based on the disappearing of the dimer reduction peak in the cyclic voltammogram of **MBO** in the presence of amines along with increasing the number of electrons transferred in this condition, as well as spectroscopic data of the products. These compounds have been successfully synthesized in water/ethanol mixture solutions in an undivided cell, at carbon rod electrodes, by constant current electrolysis at room temperature. The proposed method does not need to use toxic solvent, metal, catalyst and challenging workups. This method is easy to scale-up and the products have antibacterial activity.

Keywords: 2-Mercaptobenzoheterocyclic compounds, Sulfonamide derivatives, Green chemistry, Electrochemical synthesis, Cyclic voltammetry, Sulfenamide derivatives.

1. Introduction

Sulfonamides are the first group of antibiotics to be used systemically in the treatment of bacterial infections [1]. In addition, they are used as anticancer, anti-inflammatory and antiviral agents [2-6]. Some of them, also used for the treatment of type II diabetes [7], coronary artery disease and asthma [8], Alzheimer's disease [9] and respiratory diseases [10]. A literature survey reveals that the conventional methods for the synthesis of sulfonamides are the reaction of amines with sulfonyl chlorides [11,12] (Scheme 1, part I). Although some of these methods are efficient but they have disadvantages, such as the use of sulfonyl chlorides which are sensitive to hydrolysis, difficult to handle and not amenable to long-term storage. Transition metal catalyzed coupling reaction of primary sulfonamides and aryl halides or arylboronic acids is another method of sulfonamide synthesis [13-19] (Scheme 1, part II). These methods are also efficient but the main disadvantage of these methods is heavy metal pollution. The reaction of sodium sulfinates with amines in the presence of copper ions is another way to synthesize sulfonamides, which consequently creates the problem of metal pollution [20,21] (Scheme 1, part III). The oxidative chlorination of an aryl organosulfur compound is also another way to synthesize sulfonamides (Scheme 1, part IV). Although sulfonyl chlorides and transition metal are not used in this method, it has some drawbacks such as harsh acidic and low temperature conditions and harmful reagent [22]. Another method to synthesize sulfonamides, involves the combination of aryl halides, sulfur dioxide and amines [23-29] (Scheme 1, part IV). Although some of these methods are efficient but they may cause heavy metal pollution and are include strongly acidic/basic media, unsafe solvent, and compounds such as DABSO (SO_2 surrogate) that are expensive, unstable and unsafe.

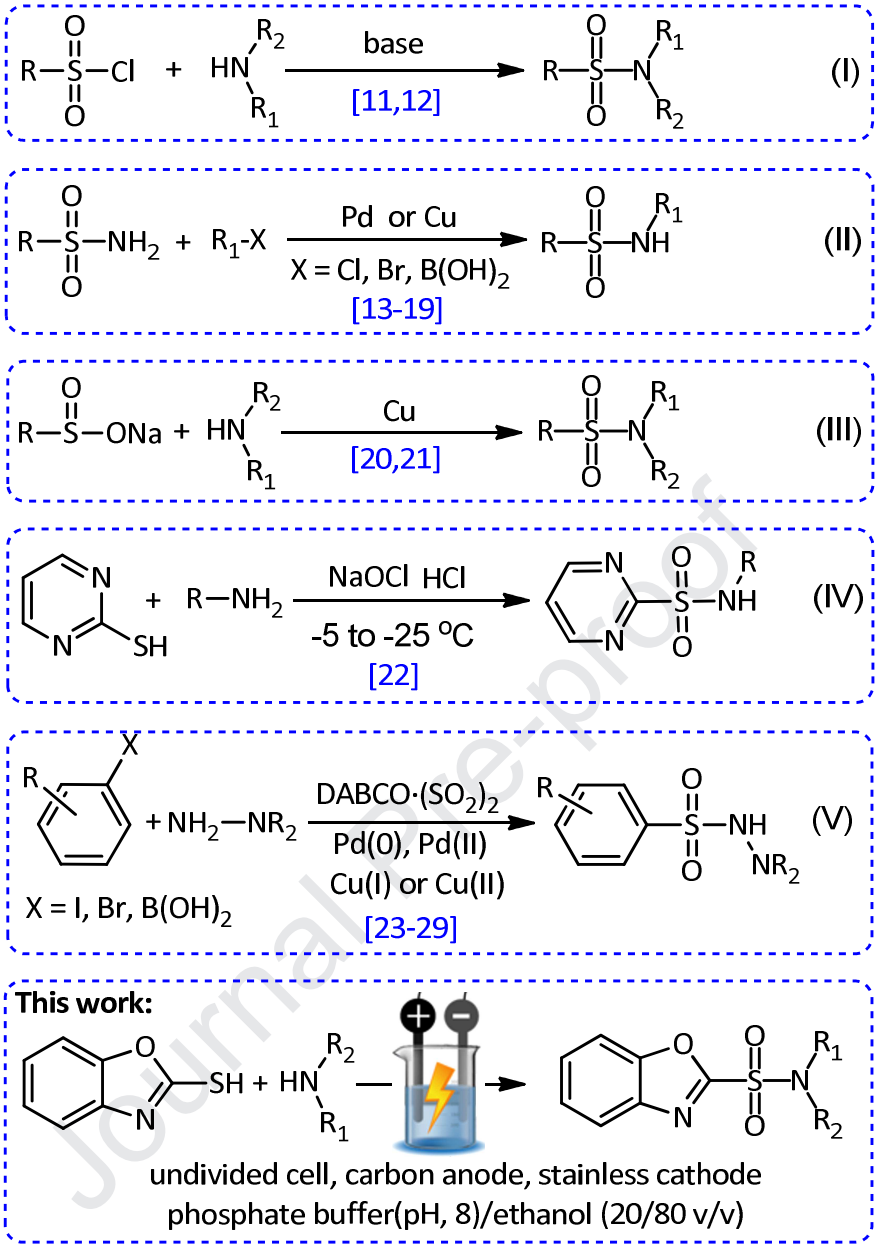

Scheme 1. Overview of the synthetic method for sulfonamides.

In addition to the chemical methods described above, we can list some interesting paper dealing with electrochemical synthesis of sulfonamides [30-32]. Although many problems have been addressed in these papers, there still exist problems associated with these papers including the use of toxic acetonitrile solvent, strong acidic media and the inability to synthesis of sulfonamide based on 2-mercaptobenzoheterocyclic compounds.

Another series of compounds synthesized in this study are sulfenamides. These compounds containing divalent sulfur bonded to trivalent nitrogen, which have been widely used in the vulcanization of rubbers as accelerator [33]. For example, *N-tert*-butyl-2-benzothiazole sulfenamide (TBBS) is the most widely used sulfonamide in the rubber industry as vulcanization accelerator [34]. In addition to rubber industry, sulfenamides are widely used in agriculture as plant growth regulators, pesticides and fungicides [33,35]. They have also shown many important biological activities such as antitumor, antiplatelet, antiasthmatic, antimicrobial and lipoxygenase activities [33,35,36].

Our literature survey shows that methods for the synthesis of sulfenamide consist of metal-assisted synthesis [37,38], hypervalent iodine(III) activated method [39], microwave-assisted synthesis [40], reaction of amines with thiophthalimides [41], transamination of *N*-unsubstituted sulfonamides [42], copper-catalyzed [43,44]. These methods, have the disadvantages such as heavy metal pollution, tedious work-up, low atom economy, safety problems, high temperatures, toxic and expensive reagents. However, the development of a simple and environmentally friendly methodology is still required for the synthesis of sulfonamide and sulfenamide compounds. The present work describes an air-assisted electrochemical method for the synthesis of titled compounds via electrochemical oxidation of 2-mercaptobenzoxazole in the presence of some amines under simple and green conditions, without toxic solvents and reagents, using carbon electrode in water/ethanol mixture. Another feature of the proposed method is its amenability to scaling up which is discussed in the text.

Electrochemistry is a powerful tool for studying reaction mechanisms [44]. In this paper a comprehensive study on the electrochemical behavior of 2-mercaptobenzoxazole (**MBO**), 2-mercaptobenzothiazole (**MBT**) and 2-mercaptobenzimidazole (**MBI**) in water/ethanol

mixture were carried out by cyclic voltammetry at glassy carbon electrode to report the detailed oxidation mechanism as well as detailed potential-pH properties and pK_a values of **MBO**, **MBT** and **MBI** and related compounds. This paper provides experimental details on the synthesis of sulfonamide and sulfenamide compounds with a comprehensive electrochemical data on the oxidation and acid/base behaviors of **MBO**, **MBT** and **MBI** and related compounds.

2. Experimental

2.1. Reagents and apparatus

2-Mercaptobenzoxazole (**MBO**) (95%), 2-mercapto benzothiazole (**MBT**) (97%), 2-mercaptobenzimidazole (**MBI**) (98%), diethylamine (**AM1**) (≥99.5%), cyclohexylamine (**AM2**) (≥99%), piperidine (**AM3**) (≥99%), sodium hydrogen phosphate (99%) and sodium dihydrogen phosphate (99%) were obtained from Sigma-Aldrich. Ethanol, sodium bicarbonate (98%), sodium carbonate (98%), hydrochloric acid (37%), sodium hydroxide (99%) were obtained from Merck (Darmstadt, Germany). These chemicals were used without further purification. The buffered solutions were prepared based on Kolthoff tables.

The glassy carbon electrode was polished using alumina slurry (3.0 – 0.1 µm). Melting points were measured with a Barnstead Electrothermal 9100 apparatus. IR spectra (KBr) were recorded on Perkin–Elmer GX FT-IR spectrometer. ^{1}H and ^{13}C NMR spectra were recorded on a Bruker Avance DRX-400 spectrometer at 400 MHz and INOVA 500 MHz. The mass spectra were recorded on MS Model: 5975C VL MSD with Tripe-Axis Detector. Cyclic voltammetry was performed using a Sama-500 potentiostat/galvanostat. Typical voltammetry experiments were carried out on a classical three electrode undivided cell configuration with a platinum auxiliary electrode and a glassy carbon (GC) working electrode (surface area = 1.8 mm^2). The working electrode potentials were measured versus Ag/AgCl (3M KCl) (all electrodes from AZAR

electrode). The Macro-scale electrolysis was carried out with a two electrode system under constant current condition by a dc power supply Dazheng ps-303D. The working electrode (anode) used in macro-scale electrolysis was an assembly of five ordinary soft carbon rods (38 cm^2), placed circularly around a stainless steel cylinder cathode (25 cm^2 area).

Autolab model PGSTAT302N potentiostat/galvanostat was used for preparative electrolysis, controlled-potential coulometry and cyclic voltammetry. A glassy carbon disc (1.8 mm^2 areas) and a platinum wire were used as working and counter electrodes, respectively. An assembly of four graphite rods (30 cm^2) and a large stainless steel gauze were used as working and counter electrodes in controlled-potential coulometry and macro scale electrolysis, respectively. The potential of the working electrode was measured against Ag/AgCl (AZAR electrode). All chemicals were purchased from commercial sources and used without further purification.

2.2. Characteristic of the products

***N,N*-diethylbenzo[d]oxazole-2-sulfonamide (SO1) ($C_{11}H_{14}N_2O_3S$).** Light yellow oil, yield: 59%, ^{1}H NMR (400 MHz, DMSO-d_6) δ/ppm: 7.48 (d, *J* = 8 Hz, 2H, aromatic), 7.25 (d, *J* = 8 Hz, 2H, aromatic), 2.94 (q, 4H, methylene), 1.17 (t, 6H, methyl). ^{13}C NMR (100 MHz, DMSO-d_6) δ/ppm: 11.0, 41.3, 109.7, 110.8, 123.4, 124.9, 132.2, 148.3, 180.2. IR (KBr) v/cm^{-1}: 2971, 2823, 2776, 1764, 1618, 1507, 1449, 1279, 1247, 1132, 1096, 1008, 931, 744, 647, 607. MS (EI, 70 eV) m/z (%): 256 (M, 3), 192 (3), 151 (100), 91 (26), 58 (62).

***N*-Cyclohexyl-2-benzoxazole sulfonamide (SO2) ($C_{13}H_{16}N_2O_3S$).** Light yellow oil, yield: 79%. ^{1}H NMR (500 MHz, DMSO-d_6) δ/ppm: 7.62 (d, *J* = 7.8, 1H, NH), 7.21 (d, *J* = 7.7 Hz, 1H, aromatic), 7.16 (d, *J* = 7.5 Hz, 1H, aromatic), 7.04 (t, *J* = 7.5 Hz, 1H, aromatic), 6.96 (t, *J* = 7.3 Hz, 1H, aromatic), 3.01 (s, 1H, CH), 1.92 (d, *J* = 10.1 Hz, 2H, CH), 1.70 (d, *J* = 12.1 Hz, 2H, CH), 1.55 (d, *J* = 12.8 Hz, 1H, CH), 1.37 - 1.14 (m, 5H, CH). ^{13}C NMR (100 MHz, DMSO-d_6) δ/ppm:

182.1, 150.8, 142.1, 123.2, 121.0, 113.5, 108.2, 49.9, 30.8, 25.0, 24.2. IR (KBr) v/cm^{-1}: 3476, 2935, 2854, 2588, 2523, 2048, 1890, 1759, 1698, 1643, 1538, 1507, 1464, 1431, 1381, 1346, 1252, 1132, 1114, 1070, 1003, 890, 741, 625, 605, 552, 450, 417. MS (EI, 70 eV) m/z (%): 279 (M, 3), 41 (75), 57 (86), 76 (16), 104 (25), 132 (7), 149 (100), 167 (15).

***N*-Piperidin-2-benzoxazole sulfonamide (SO3) ($C_{12}H_{14}N_2O_3S$).** Light yellow oil, yield: 62%. ^{1}H NMR (500 MHz, DMSO-d_6) δ/ppm: 7.31 (d, J = 7.9 Hz, 1H, aromatic), 7.21 (d, J = 7.7 Hz, 1H, aromatic), 7.12 (t, J = 7.1 Hz, 1H, aromatic), 7.06 (t, J = 7.1 Hz, 1H, aromatic), 3.09 - 2.73 (m, 4H, CH), 1.68 - 1.51 (m, 6H, CH). ^{13}C NMR (126 MHz, DMSO-d_6) δ/ppm: 181.6, 150.0, 138.3, 124.0, 122.2, 112.6, 109.0, 44.1, 22.7, 22.1. IR (KBr) v/cm^{-1}: 3445, 3049, 2941, 2855, 1774, 1640, 1578, 1501, 1451, 1424, 1248, 1131, 1069, 1004, 921, 743, 627, 552, 418. MS (EI, 70 eV) *m/z* (%): 266 (M, 0.2), 41 (32), 64 (74), 91 (65), 84 (62), 134 (48), 151 (100), 173 (10), 202 (35), 256 (10).

***N,N*-diethylbenzo[d]thiazole-2-sulfenamide (SE4) ($C_{11}H_{14}N_2S_2$).** Light yellow oil, yield: 65%. ^{1}H NMR (500 MHz, DMSO-d_6) δ/ppm: 7.95 (d, J = 7.9 Hz, 1H, aromatic), 7.76 (d, J = 8.1 Hz, 1H, aromatic), 7.39 (t, J = 7.7 Hz, 1H, aromatic), 7.28 (t, J = 7.6 Hz, 1H, aromatic), 3.08 (q, J = 7.0 Hz, 4H, methylene), 1.14 (t, J = 7.1 Hz, 6H, methyl). ^{13}C NMR (126 MHz, DMSO-d_6) δ/ppm: 178.3, 155.1, 134.9, 126.4, 124.1, 122.0, 121.6, 52.3, 13.7. IR (KBr) v/cm^{-1}: 2972, 2931, 2855, 1563, 1468, 1429, 1376, 1310, 1273, 1159, 1081, 1023, 1009, 756, 727, 669, 432. MS (EI, 70 eV) *m/z* (%): 239 (M, 33), 167 (20), 108 (4), 72 (100), 42 (15).

***N*-Cyclohexyl-2-benzothiazole sulfenamide (SE5) ($C_{13}H_{16}N_2S_2$).** White solid, yield: 88%, isolated yield: 53%. Melting Point: 95-97 ℃. ^{1}H NMR (500 MHz, DMSO-d_6) δ/ppm: 7.98 (d, J = 8.5 Hz, 1H, aromatic), 7.73 (d, J = 8.1 Hz, 1H, aromatic), 7.41 (t, 1H, aromatic), 7.29 (t, 1H, aromatic), 5.49 (d, J = 5.8 Hz, 1H, NH), 2.77 (m, J = 9.2, 4.4 Hz, 1H, CH), 1.97 (s, 2H, CH), 1.70

(s, 2H, CH), 1.54 (d, *J* = 11.6 Hz, 1H, CH), 1.22 (t, 5H, CH). ^{13}C NMR (126 MHz, DMSO-d_6) δ/ppm: 181.4, 155.3, 134.8, 126.4, 123.9, 122.1, 121.4, 59.9, 33.5, 25.8, 24.8. IR (KBr) *v*/cm^{-1}: 3443, 3222, 2930, 2850, 1560, 1463, 1427, 1316, 1241, 1187, 1068, 1012, 753, 726. MS (EI, 70 eV) m/z (%): 265 (M, 86), 41 (70), 55 (64), 83 (14), 98 (100), 122 (11), 149 (15), 167 (86), 182 (17), 221 (11).

***N*-Piperidin-2-benzothiazole sulfenamide (SE6) ($C_{12}H_{14}N_2S_2$).** Light yellow oil, yield: 74%. ^{1}H NMR (500 MHz, DMSO-d_6) δ/ppm: 8.00 (d, *J* = 7.9 Hz, 1H, aromatic), 7.77 (d, *J* = 8.1 Hz, 1H, aromatic), 7.41 (t, *J* = 7.6 Hz, 1H, aromatic), 7.30 (t, *J* = 7.6 Hz, 1H, aromatic), 3.17 - 2.86 (m, 4H, CH), 1.67 - 1.40 (m, 6H, CH). ^{13}C NMR (126 MHz, DMSO-d_6) δ/ppm: 176.9, 155.2, 135.0, 126.5, 124.2, 122.2, 121.7, 57.9, 27.4, 22.9. IR (KBr) *v*/cm^{-1}: 3064, 2939, 2847, 1559, 1453, 1467, 1427, 1362, 1310, 1271, 1157, 1126, 1081, 1008, 919, 856, 761, 729, 667, 429. MS (EI, 70 eV) m/z (%): 251 (M, 39.5), 42 (36), 69 (6.5), 55 (33), 84 (100), 108 (5.9), 167 (18.3).

3. Results and Discussion

3.1. Electrochemical study of 2-mercaptobenzoheterocyclic compounds

In this work, electrochemical oxidation of **MBO**, **MBT** and **MBI** have been studied in two stages. The first stage involves studying the electrochemical behavior of these compounds in order to better understand the oxidation mechanism, electrochemical properties of the compounds and produced intermediates. The second part involves the electrochemical study of these compounds in the presence of diethylamine, cyclohexanamine and piperidine in order to obtain the necessary information for synthesis of sulfonamide and sulfenamide compounds.

Fig. 1, part I, shows the cyclic voltammograms of **MBO** (1.0 mM) in aqueous phosphate buffer (c = 0.2 M, pH = 7.0) by changing the potential scan rate between 10 and 1000 mV/s. The Figure shows that at the scan rate of 10 mV/s, the voltammogram has two anodic peaks (A_1 and A_2) and one sharp and symmetric cathodic peak (C_1). The effect of increasing scan rate on the voltammetric response is quite complex. At first with increasing scan rate from 10 to 50 mV/s, the anodic peak A_2 removed and both I_{pA1} and I_{pC1} increase linearly with v. With further increase in scan rate, I_{pA1} continues to increase linearly (I_{pA1} = 0.03 v + 1.80, R^2 = 0.9925) (Fig. 1 part II). In order to obtain further data on the adsorption/diffusion behavior of **MBO**, the log I_{pA1}changes were plotted against the log v (Fig. 1 part III).

[Figure 1]

The slope of the line is a measure of the adsorption/diffusion of **MBO** on the surface of electrode. It is found that when the slope of the line is equal to 0.5, the process is pure diffusion-controlled, however, when the slope is 1, the process is pure adsorption-controlled [45]. The slope of the line is 0.75, which are higher than 0.5 and less than one that confirms the adsorption-diffusion process for electrochemical oxidation of **MBO**. With increasing potential scan rate from 50 mV/s, the voltammetric behavior of peak C_1 is quite complex (Fig. 1 parts I and IV).

At low scan rates (10, 25 and 50 mV/s), the peak is sharp and symmetrical and increases linearly with v (characteristic of an adsorption peak [45]). However, with increasing potential scan rate, I_{pC1} changes abnormally (Fig. 1 part I). At high scan rates (500, 750 and 1000 mV/s) the cathodic peak C_1 becomes almost a normal diffusion peak and its current increases linearly with $v^{1/2}$ at high scan rates (characteristic of a diffusion peak [45]) (Fig. 1 part IV, inset).

Figure 2 part I compares the electrochemical behavior of **MBO** in water (phosphate buffer, pH = 7.0 and *c* = 0.2 M), at two different switching potentials. The Figure clearly shows that when the switching potential increases from 0.30 V to 0.65 V, the amount of adsorbed material and adsorption intensity have increased dramatically. Based on these results, it can be concluded that the over-oxidation of **MBO** appears to lead to the formation of materials with a higher adsorption property.

Figure 2 part II compares peak C_1 in different water (phosphate buffer, pH = 8.0, *c* = 0.2 M)/ethanol mixtures. As can be seen, when the percentage of ethanol in the mixture is zero (curve a), the cathodic peak C_1 shows the characteristic of a complete adsorption peak. However, with increasing ethanol percentage in the solvent mixture, peak C_1 tends to become a normal diffusion peak (curve c).

[Figure 2]

Fig. 3 shows the linear sweep voltammograms of **MBO** at scan rate of 10 mV/s, in ethanol/H_2O (with different pH values) (20/80, v/v) mixture. As can be seen at all studied pHs, the voltammograms show an anodic peak (A_1) in the positive going scan. The shift of peaks towards negative potentials with increasing pH values is a sign of the participation of proton in the redox process. According to these data, and taking into account the previously reported data [27,46,47], we proposed the following mechanism for electrochemical oxidation of **MBO** at different pH solutions.

[Figure 3]

At pH values less than 3.5, the oxidation mechanism of **MBO** is shown in Eq. 1. According to this equation, two protonated **MBOs** become dimer after losing two electrons and four protons. At this condition, the slope for the *E*-pH line is 113 mV/pH, which is close to the theoretical value of 118 mV/pH for a two-electron/four-proton process.

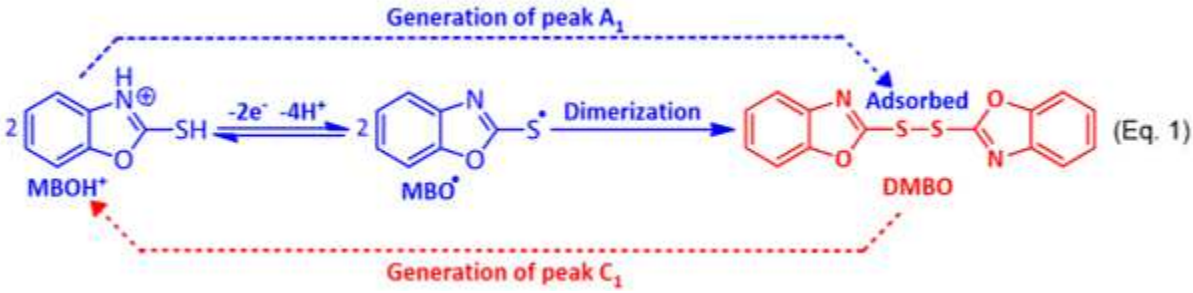

(Eq. 1)

At pH values more than 3.5 and less than 6.9, the oxidation mechanism of **MBO** is shown in Eq. 2. In this condition, the slope for the *E*-pH line is 53 mV/pH, which is close to the theoretical value of 59 mV/pH for a two-electron/two-proton process.

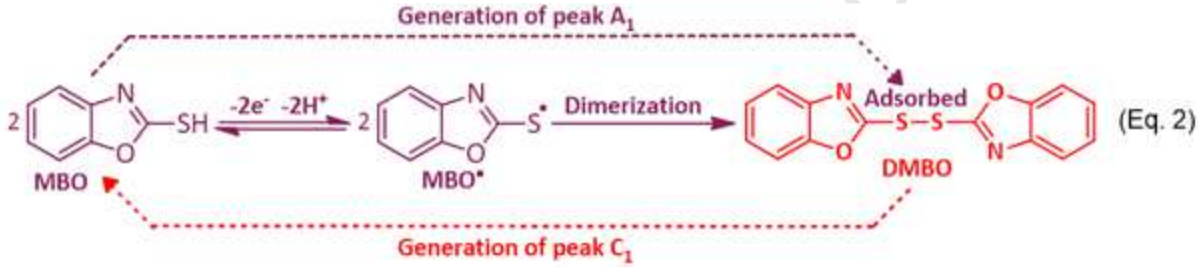

(Eq. 2)

At pH values more than 6.9, the oxidation mechanism of **MBO** is shown in Eq. 3. In this region (pH > 6.9), **MBO** is in its anionic form and in its redox process the proton is not exchanged. In addition, from data shown in Fig. 3 part II, we can conclude that the pK_a values for acid/base equilibria of **MBOH**$^+$/**MBO** and **MBO**/**MBO**$^-$ are 3.5 and 6.9, respectively (Eqs. 4 and 5). These data are in agreement with previously published data [46,48].

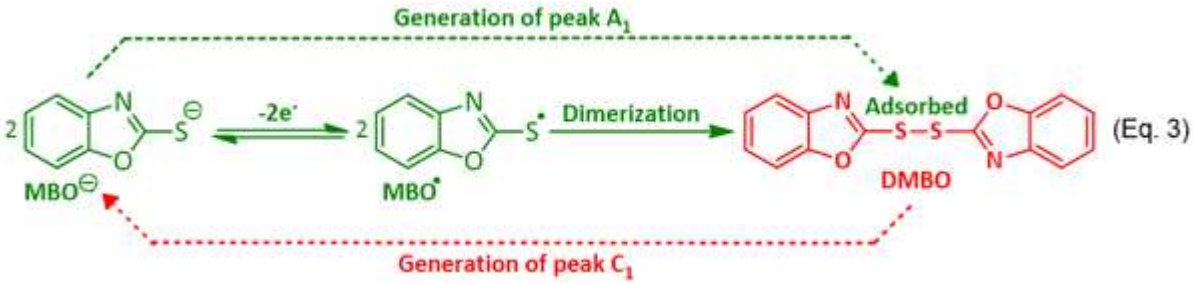

(Eq. 3)

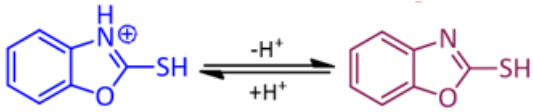

$pK_a = 3.5$ (Eq. 4)

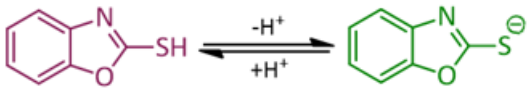

$pK_a = 6.9$ (Eq. 5)

According to our data, the anodic peak A_1 pertains to the oxidation of **MBO** (**MBOH**$^+$ and/or **MBO**$^-$) to the **MBO** radical (**MBO**$^\bullet$). At the next step, the reaction of two **MBO** radicals leads to the formation of 1,2-bis(benzo[d]oxazol-2-yl)disulfane dimer (**DMBO**). So, at slow or moderate potential scan rates, peak C_1 pertains to the reduction of adsorbed **DMBO** to **MBO** (Eqs. 1-3). At high scan rates, however, there is no sufficient time for dimerization reaction, so, diffusion peak C_1 is related to the reduction of **MBO**$^\bullet$ to **MBO**. The change of I_{pC1} at different pH is shown in Fig. 3, part III. As can be seen, with increasing pH from 1.4 to 5.0, the adsorption activity of **DMBO** increases. We think that the relative protonation of **DMBO** and formation of a more suitable medium for hydrogen bonding is important factor for less adsorption activity of **DMBO** in more acidic solutions. The adsorption activity of **DMBO** decreased with increasing pH from 5.0, so that at pH 9.0, peak C_1 shows the characteristic of a complete diffusion peak.

Figure 4 shows the cyclic voltammograms of **MBT** (curve a) and **MBI** (curve c) in comparison with **MBO** (curve b). As can be seen, these voltammograms are basically similar. However, they have some differences in detail. For example, the oxidation of **MBO** is higher than those of **MBT** and **MBI** due to the more electron donating ability of S and N atoms in the structure of **MBT** and **MBI** in comparison with O atom.

[Figure 4]

Other important differences in the voltammograms of **MBT**, **MBO** and **MBI** are different in adsorption ability of synthesized dimers and peak to peak separation ($\Delta E_p = E_{pA1} - E_{pC1}$). As can be seen, **MBT** shows largest peak-to-peak separation (ΔE_p = 0.68 V) and its dimer have highest adsorption activity. The result can be related to more adsorption activity of S atom in comparison with N and O atoms present in the structures of **MBO** and **MBI**. Figure 4

also shows that the lowest adsorption activity and peak-to-peak separation (ΔE_p = 0.13 V) belongs to **MBI**.

The effect of increasing potential scan rate on the cyclic voltammograms of **MBT** is shown in Fig. 5 part I. As can be seen, **MBT** shows a similar trend with that of **MBO** (Fig. 1). These experiments confirm previous results that at high scan rates, there is no sufficient time for dimerization reaction, so, peak C_1 is attributed to the reduction of **MBT**$^{\bullet}$ to **MBT**. At these scan rates, peak C_1 becomes like a normal diffusion peak and its current increases linearly with $v^{1/2}$.

[Figure 5]

The effect of increasing potential scan rate on the cyclic voltammograms of **MBI** is shown in Fig. 5 part II. Different with **MBO** and **MBT**, the cathodic peak C_1 shows a normal behavior with increasing scan rate. The presence of two N atoms in the structure of **MBI**, makes **MBI**$^{\bullet}$ more stable than **MBT**$^{\bullet}$ and **MBO**$^{\bullet}$. Consequently, we think that in the time scale of our experiments, **MBI** dimer is not formed and peak C_1 belongs to reduction of **MBI**$^{\bullet}$ to **MBI**.

Fig. 6 shows the linear sweep voltammograms of **MBT** at scan rate of 10 mV/s, in ethanol/H_2O (with different pH values) (20/80, v/v) mixture. The shift of peak A_1 towards negative potentials with increasing pH values confirmed the participation of proton in the redox process. According to the data presented in Fig. 6, the following equations for electrochemical oxidation of **MBT** at different pH values are proposed. At pHs less than 4.0, the oxidation mechanism of **MBT** is shown in Eq. 6. In this range of pH, the slope for the *E*-pH line is 53 mV/pH, which is close to the theoretical value of 59 mV/pH for a two-electron/two-proton process. At pH values more than 4.0 and less than 7.2, the oxidation mechanism of **MBT** is shown in Eq. 7. In this region of pH, the slope for the *E*-pH line is 85

mV/pH, which confirms the occurrence of a two-electron/three-proton process as shown in Eq. 7.

[Figure 6]

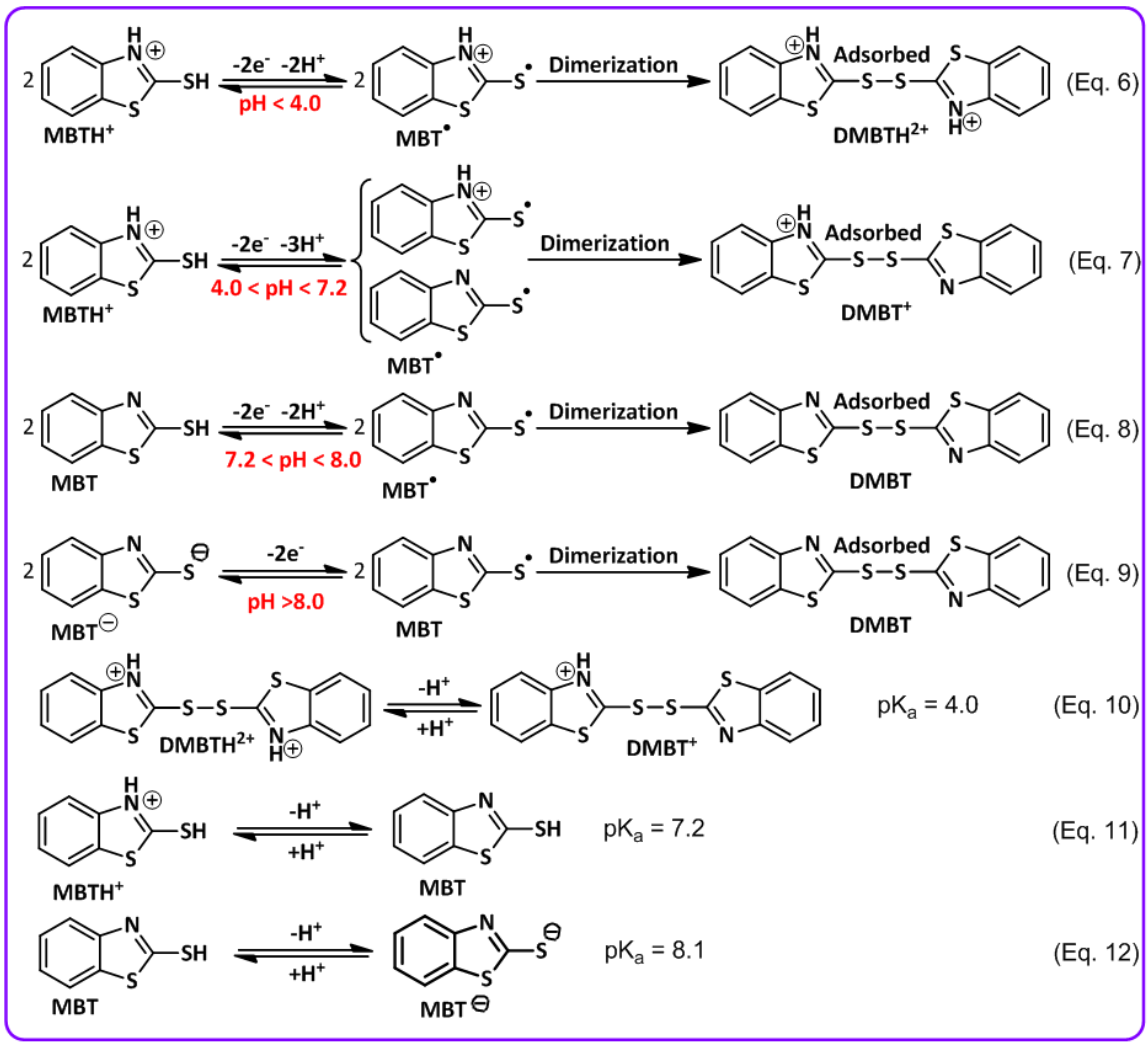

It is necessary to mention that the theoretical value for a two-electron/three-proton process is about 88 mV/pH. At pHs more than 7.2 and less than 8.0, the oxidation mechanism of **MBT** is shown in Eq. 8. In this narrow region of pH, the slope for the *E*-pH line is 50 mV/pH, which confirms the occurrence of a two-electron/two-proton process. In the basic region (pH > 8.0), **MBT** is in its anionic form (**MBT**$^-$) and so its redox process is not dependent on the pH (Eq. 9). In addition, from these data, we can determine the pK_a of the acid/base couples, **DMBTH**$^{2+}$/**DMBTH**$^+$, **MBTH**$^+$/**MBT** and **MBT**/**MBT**$^-$. The calculated pk_a

values are 4.0, 7.2 and 8.1, respectively (Eqs. 10-12). These data are in agreement with previously published data [48].

Similar research was conducted on **MBI**. Fig. 7 shows the linear sweep voltammograms of **MBI** in ethanol/H_2O (with different pH values) (20/80, v/v) mixture at scan rate of 10 mV/s. According to the data presented in Fig. 7, the following equations for electrochemical oxidation of **MBI** at different pH values are proposed. At pHs less than 7.9, the oxidation mechanism of **MBI** is shown in Eq. 13. In this range of pH, **MBI** is in its protonated form and the slope for the *E*-pH line is 35 mV/pH, which is close to the theoretical value of 29.5 mV/pH for a one-electron/two-proton process.

[Figure 7]

In the pH ranging from 7.9 to 9.9, the slope for the *E*-pH line is 67 mV/pH, which is close to the theoretical value of 59 mV/pH for a one-electron/one-proton process (Eq. 14). In the basic region (pH > 9.9), **MBI** is in its anionic form (**MBI**$^-$) and so the proton does not get involved in the redox process (Eq. 15). In addition, from these graphs we can calculate the pK_a values for of the acid/base couples, **MBIH**$^+$/**MBI** and **MBI**/**MBI**$^-$. The calculated pk_a values are 7.9 and 9.9, respectively (Eqs. 16 and 17). These data are in agreement with previously published data [48].

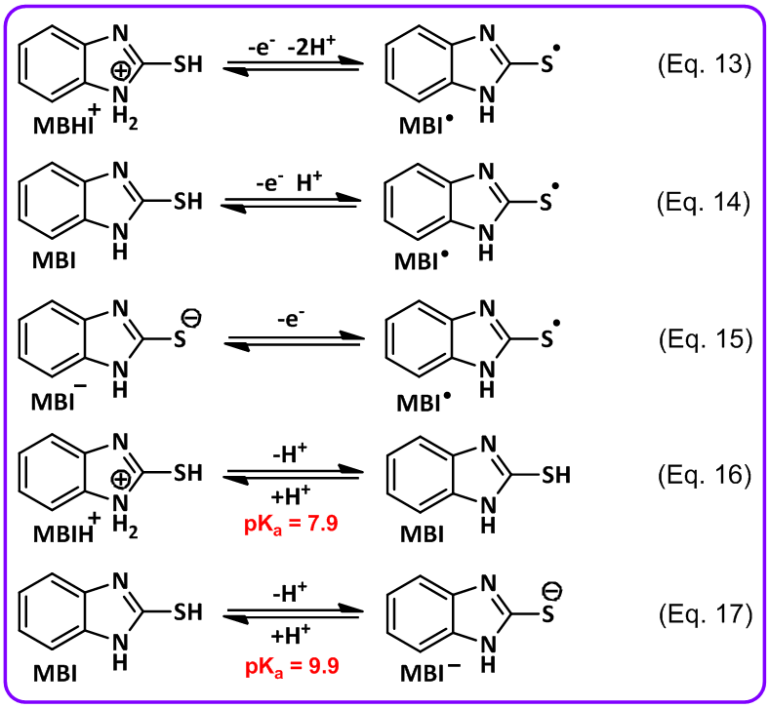

3.2. Electrochemical study of 2-mercaptobenzoheterocyclic compounds in the presence of diethylamine

In this part, to obtain the information needed for the synthesis of new compounds based on **MBO** oxidation, electrochemical study of **MBO** was carried out in the presence of diethylamine (**AM1**) to find the most suitable conditions for the synthesis as well as evaluation of the reaction mechanism. Cyclic voltammograms of **MBO** in the presence of **AM1** are shown in Fig. 8 (part I curve b) and have been compared with that of in the absence of **AM1** (curve a). Comparison of these voltammograms shows that the most important change is the removal of the cathode peak C_1. Since peak C_1 is related to the reduction of dimer (**DMBO**), its disappearance is a sign of the lack of dimer at the electrode surface. In other words, the occurrence of a fast chemical reaction between **AM1** and **DMBO**, removed the dimer from the electrode surface. Our data also show that I_{pC1} depends on the **AM1** concentration so that it decreases with increasing **AM1** concentration. Increasing the **AM1** concentration increases the reaction rate of amine with the dimer

results in the disappearance of the peak C_1 at high amine concentration. We also have found that there is a significant influence of potential sweep rate on the shape of the voltammogram (Fig. 8 part II). It is seen that the current of peak C_1 (I_{pC1}) increase with increasing potential scan rate due to the decrease in the time available for the reaction of amine with dimer at higher scan rates.

[Figure 8]

Constant current electrolysis was performed in water (pH=8.0)/ethanol mixture containing **MBO** and **AM1** at the current density of 0.26 mA cm^{-2} (10 mA). The electrolysis progress was monitored using cyclic voltammetry (Fig. 9) and thin layer chromatography. It was found that, proportional to the electrolysis progress, the anodic peak current (I_{pA1}) decreased. The electrolysis was ended when the peak A_1 decay more than 95% (after consumption of 190 C electricity, n_{app} = 3.9). In this condition, the spot of **MBO** disappeared on TLC.

By putting together voltammetric and amount of charge passed along with the results obtained from spectroscopic analysis of the product (mass spectroscopy and NMR), the mechanism shown in Scheme 2, is proposed for the electrochemical oxidation of **MBO** in the presence of **AM1**. According to Scheme 2, sulfonamide **SO1** is synthesized in four steps from **MBO**. First: electrolytic formation of **MBO$^{\bullet}$**, second: formation of dimer **DMBO**, third: nucleophilic addition of **AM1** to **DMBO**, S-S bond cleavage and formation of corresponding sulfenamide (**SE1**) and fourth: the air oxidation of sulfonamide [49-51] and converting it into the final product (**SO1**). The air oxidation of sulfonamide has caused the main product of **MBO** in the presence of **AM1** to be **SO1** and only a little amount of sulfenamide (**SE1**) was observed chromatographically. The role of oxygen in the oxidation of sulfenamide (**SE1**) is

confirmed by the fact that the number of electrons consumed in the synthesis of **SO1** is less than the required amount.

[Figure 9]

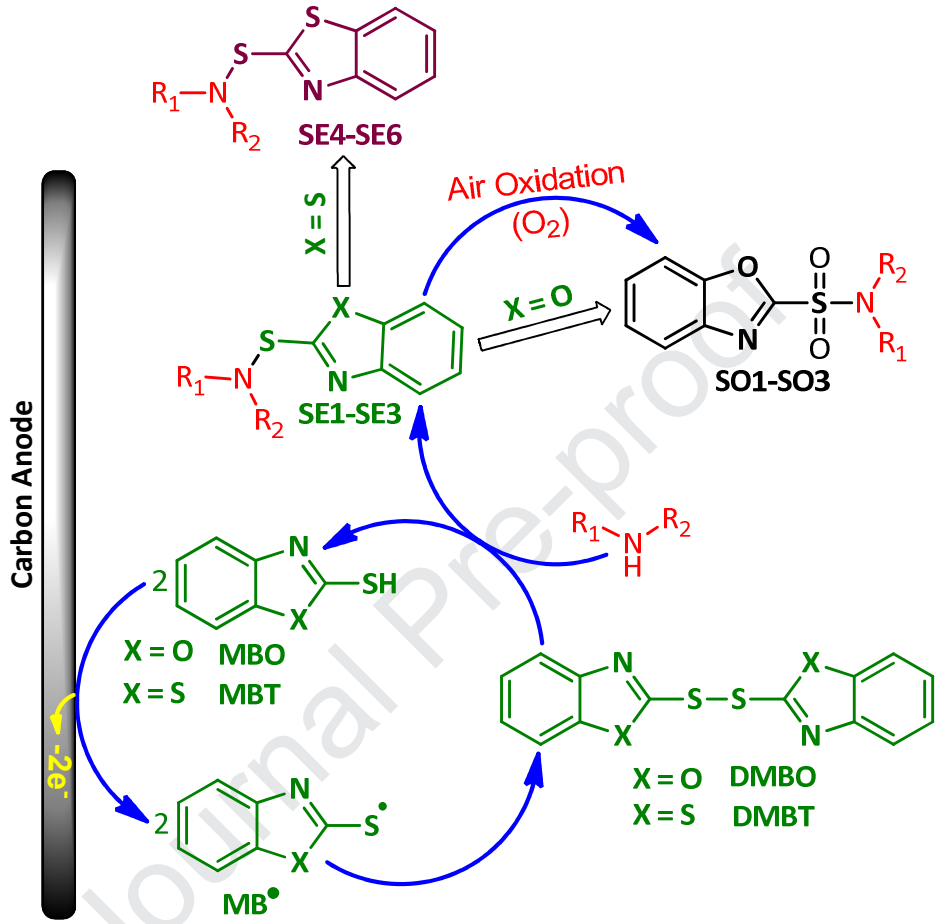

Scheme 2. Electrochemical oxidation pathway of **MBO** and **MBT** in the presence of the amines.

In the case of **MBT**, the same reaction mechanism was observed, however, the air oxidation process is not carried much. Therefore, when **MBT** is used as the starting material, the main product is sulfenamide (**SE**) and only small amounts of sulfonamide (**SO**) were observed (Scheme 2).

Different with **MBO** and **MBT**, when **MBI** is used as the starting material, as discussed in the preceding sections, the **MBI** dimer is not formed and we could not synthesize any sulfonamide or sulfenamide compounds from oxidation of **MBI** in the presence of amines.

3.3. Constant current electrolysis

Current density is one of the most important factors controlling yield and purity. The synthesis of **SO2** and **SE5**, were studied at different current densities ranging from 0.06 to 0.72 mA/cm^2, while other parameters (charge: 190 C, temperature: 298 K, **MBO** and **MBT** amount: 0.5 mmol and cyclohexylamine (**AM2**) amount: 1.5 mmol) remain constant (Fig. 10). Our results show that the highest yield for **SO2** (88%) and **SE5** (79%) were obtained at a current density of 0.26 and 0.52 mA/cm^2, respectively. In the synthesis of **SO2**, at the current densities lower than 0.26 mA/cm^2, the amount of **MBO** radicals produced per unit time decreases. As a result, they are less likely to react together to form **DMBO**. In such conditions, the **MBO** radicals participate either in the side reactions or in the back reaction in the cathode surface, therefore, despite equal charge consumption, the production yield is low. On the other hand, at the current densities higher than 0.26 mA/cm^2, the over oxidation of **DMBO** and/or **SE2** reduces the production yield.

[Figure 10]

*3.4. Electrochemical synthesis of sulfonamides (**SO1-SO3**) and sulfenamides (**SE4-SE6**)*

For the synthesis of sulfonamides **SO1**-**SO3**, an 80 ml solution containing phosphate buffer (pH = 8.0, *c* = 0.2 M)/ethanol (20/80 v/v) was pre-electrolyzed in an undivided cell. Then 0.5 mmol of **MBO**, 1.5 mmol of amine (**AM1**, **AM2** or **AM3**) was subjected to electrolysis at constant current of 10 mA (0.26 mA cm^{-2}), in an undivided cell. The progress of the electrolysis was followed by TLC using *n*-hexane/ethyl acetate (2:1) and also cyclic

voltammetry. At the end of electrolysis, the reaction mixture was filtered and then the ethanol was removed under vacuum. The residual was extracted with 3 x 10 ml of ethyl acetate. The extracted organic phase was dried over anhydrous sodium sulphate, filtered and evaporated under reduced pressure. The resulting residue was purified by flash chromatography on silica gel (eluent 2:1 *n*-hexane–ethyl acetate) to afford the corresponding sulfonamide (Table 1).

[Table 1]

For the synthesis of sulfenamides **SE4**-**SE6**, in a solution containing carbonate buffer (pH = 12.0, *c* = 0.2 M)/ethanol (20/80 v/v), **MBT** and amine (**AM1**, **AM2** or **AM3**) was subjected to electrolysis at constant current of 20 mA (0.52 mA cm^{-2}), in an undivided cell. Other conditions for the synthesis of sulfenamides **SE4**-**SE6**, are similar to the synthesis of sulfonamides (Table 1).

3.5. Scaling up experiments

In this part, we describe the large scale synthesis of **SO2** and **SE5**. Fig. 11 shows the electrochemical cell designed and manufactured for this purpose [52]. The working electrode (anode) used in large-scale electrolysis was an assembly of fifteen ordinary carbon plate (11 cm × 1.5 cm × 0.3 cm), placed beside of fifteen stainless steel plate cathode (11 cm× 1.5 cm × 0.1 cm). Under these conditions, the electrode surface increases up to 247 cm^2. In a typical procedure, for the large scale synthesis of **SO2**, 300 ml solution containing phosphate buffer (pH = 8.0, *c* = 0.2 M)/ethanol (20/80 v/v) was pre-electrolyzed in the cell; then 10 mmol of **MBO**, 30 mmol of **AM2** was subjected to electrolysis at the constant current of 0.22 mA cm^{-2} (yield 72%).

The large scale synthesis of **SE5** was carried out in a 300 ml solution containing carbonate buffer (pH = 12.0, *c* = 0.2 M)/ethanol (20/80 v/v), then 10 mmol of **MBT** and 30

mmol of **AM2** was subjected to electrolysis at the constant current of 0.51 mA cm^{-2} (yield 81%). Other conditions are similar to those of the previous section.

The large scale synthesis of **SE5** was carried out in a 300 ml solution containing carbonate buffer (pH = 12.0, *c* = 0.2 M)/ethanol (20/80 v/v), then 10 mmol of **MBT** and 30 mmol of **AM2** was subjected to electrolysis at the constant current of 0.51 mA cm^{-2} (yield 81%). Other conditions are similar to those of the previous section.

[Figure 11]

3.6. Antibacterial susceptibility

This part of the investigation was initiated to evaluate the antibacterial susceptibility of the synthesized sulfonamide (**SO1**-**SO3**) and sulfenamide (**SE4**-**SE6**) derivatives. Antobiogram studies revealed that all gram positive (*Bacillus cereus* and *Staphylococcus aureus*) and gram negative bacteria (*Escherichia coli* and *Salmonella enteritidis*) were sensitive to **SO2** and **SO3**. Gram positive bacteria were sensitive to **SE4** and **SE6** while, gram negative bacteria showed resistance to **SE4** and **SE6**. Gram negative bacteria were sensitive to **SE5** (see Supplementary Information). All bacteria was resistance to **SO1**. The results of antibacterial activity of **SO1**-**SO3** and **SE4**-**SE6** compounds are summarized in Table 2.

[Table 2]

4. Conclusion

In this work, an efficient and green strategy based on the electrochemical oxidation of 2-mercaptobenzoheterocyclic compounds in the presence of some amines was developed for the synthesis of some new sulfonamide (**SO**) and sulfenamide (**SE**) derivatives. All reactions were carried out in a simple cell, consisting of carbon and stainless steel electrodes in water/ethanol mixture under constant current condition, without using any catalyst. It is

also shown that the products can be easily synthesized in preparative scales with impressive yields. The product type is dependent upon the 2-mercaptobenzoheterocyclic type. When **MBO** is used as the starting material, sulfonamide compounds (**SO**) are the main products. Unlike **MBO**, when **MBT** is the starting material, then sulfenamide (**SE**) derivatives are the main products. It should be noted that Unlike **MBO** and **MBT**, upon the oxidation of **MBI** in the presence of amines, we could not isolate these two types of products. The product yields are dependent upon the current density. In this paper, also, the electrochemical behavior of **MBO**, **MBT** and **MBI** has been comprehensively investigated and unique information has been published.

Acknowledgements

The authors wish to acknowledge Iran National Science Foundation (INSF) for financial support of this work. We also acknowledge the Bu-Ali Sina University Research Council and Center of Excellence in Development of Environmentally Friendly Methods for Chemical Synthesis (CEDEFMCS) for their support of this work.

Appendix A. Supplementary data

Supplementary data including FT-IR, ^{1}H NMR ^{13}C NMR and MS spectra of **SO1-SO3** and **SE4-SE6** and antibacterial activity of products associated with this article can be found, in the online version, at http://dx.doi.org

Reference:

[1] R.J. Anderson, P.W. Groundwater, A. Todd, A.J. Worsley, Antibacterial agents: Chemistry, Mode of Action, Mechanisms of Resistance and Clinical Applications, John Wiley & Sons, Chichester, West Sussex (2012), pp. 105-124.

[2] S. Syed Shoaib Ahmad, G. Rivera, M. Ashfaq, Recent advances in medicinal chemistry of sulfonamides. Rational design as anti-tumoral, anti-bacterial and anti-inflammatory agents, Mini Rev. Med. Chem. 13 (2013) 70-86.

[3] A. Scozzafava, T. Owa, A. Mastrolorenzo, C.T. Supuran, Anticancer and antiviral sulfonamides, Curr. Med. Chem. 10 (2003) 925-953.

[4] C.T. Supuran, A. Casini, A. Scozzafava, Protease inhibitors of the sulfonamide type: anticancer, antiinflammatory, and antiviral agents, Med. Res. Rev. 23 (2003) 535-558.

[5] K.P. Rakesh, S.M. Wang, J. Leng, L. Ravindar, A.M. Asiri, H.M. Marwani, H. L. Qin, Recent development of sulfonyl or sulfonamide hybrids as potential anticancer agents: a key review. Anti-Cancer Agents Med. Chem. 18 (2018) 488–505.

[6] S.M. Pant, A. Mukonoweshuro, B. Desai, M.K. Ramjee, C.N. Selway, G.J. Tarver, A.G. Wright, K. Birchall, T.M. Chapman, T.A. Tervonen, J. Klefstrçm, Design, synthesis, and testing of potent, selective hepsin inhibitors via application of an automated closed-loop optimization platform. J. Med. Chem. 61 (2018) 4335-4347.

[7] H. Nishioka, N. Tooi, T. Isobe, N. Nakatsuji, K. Aiba, BMS-708163 and Nilotinib restore synaptic dysfunction in human embryonic stem cell-derived Alzheimer's disease models, Sci. Rep. 6 (2016) 33427.

[8] L.D. Pennington, M.D. Bartberger, M.D. Croghan, K.L. Andrews, K.S. Ashton, M.P. Bourbeau, J. Chen, S. Chmait, R. Cupples, C. Fotsch, J. Helmering, Discovery and structure-guided optimization of diarylmethanesulfonamide disrupters of glucokinase–glucokinase regulatory protein (GK–GKRP) binding: strategic use of a N→ S (nN→ σ* S–X) interaction for conformational constraint, J. Med. Chem. 58 (2015) 9663-9679.

[9] K.W. Gillman, J.E. Starrett Jr, M.F. Parker, K. Xie, J.J. Bronson, L.R. Marcin, K.E. McElhone, C.P. Bergstrom, R.A. Mate, R. Williams, J.E. Meredith Jr, Discovery and evaluation of

BMS-708163, a potent, selective and orally bioavailable γ-secretase inhibitor, ACS Med. Chem, 1(2010) 120-124.

[10] H. Sugimoto, M. Shichijo, T. Iino, Y. Manabe, A. Watanabe, M. Shimazaki, F. Gantner, K.B. Bacon, An orally bioavailable small molecule antagonist of CRTH2, ramatroban (BAY u3405), inhibits prostaglandin D2-induced eosinophil migration in vitro, J. Pharmacol. Exp. Ther. 305 (2003) 347-352

[11] M. Harmata, P. Zheng, C. Huang, M.G. Gomes, W. Ying, K.O. Ranyanil, G. Balan, N.L. Calkins, Expedient synthesis of sulfinamides from sulfonyl chlorides, J. Org. Chem. 72 (2007) 683-685.

[12] R. Sridhar, B. Srinivas, V.P. Kumar, M. Narender, K.R. Rao, β-Cyclodextrin-catalyzed monosulfonylation of amines and amino acids in water, Adv. Synth. Catal. 349 (2007) 1873–1876.

[13] D. Audisio, S. Messaoudi, J.F.O. Peyrat, J.D. Brion, M.D. Alami, A general copper powder-catalyzed Ullmann-type reaction of 3-halo-4(1*H*)-quinolones with various nitrogen-containing nucleophiles, J. Org. Chem. 76 (2011) 4995–5005.

[14] J. Yin, S.L. Buchwald, Pd-catalyzed intermolecular amidation of aryl halides: the discovery that xantphos can be trans-chelating in a palladium complex, J. Am. Chem. Soc. 124 (2002) 6043–6048.

[15] J. Baffoe, M.Y. Hoe, B.B. Touré, Copper-mediated *N*-heteroarylation of primary sulfonamides: Synthesis of mono-*N*-heteroaryl sulfonamides, Org. Lett. 12 (2010) 1532–1535.

[16] G. Burton, P. Cao, G. Li, R. Rivero, Palladium-catalyzed intermolecular coupling of aryl chlorides and sulfonamides under microwave irradiation, Org. Lett. 5 (2003) 4373–4376.

[17] W. Deng, L. Liu, C. Zhang, M. Liu, Q.X. Guo, Copper-catalyzed cross-coupling of sulfonamides with aryl iodides and bromides facilitated by amino acid ligands, Tetrahedron Lett. 46 (2005) 7295–7298.

[18] B.R. Rosen, J.C. Ruble, T.J. Beauchamp, A. Navarro, Mild Pd-catalyzed *N*-arylation of methanesulfonamide and related nucleophiles: Avoiding potentially genotoxic reagents and byproducts, Org. Lett. 13 (2011) 2564–2567.

[19] P.Y.S. Lam, G. Vincent, C.G. Clark, S. Deudon, P.K. Jadhav, Copper-catalyzed general C-N and C-O bond cross-coupling with arylboronic acid, Tetrahedron Lett. 42 (2001) 3415–3418.

[20] X.D. Tang, L.B. Huang, C.R. Qi, X. Wu, W.Q. Wu, H.F. Jiang, Copper-catalyzed sulfonamides formation from sodium sulfinates and amines, Chem. Commun. 49 (2013) 6102-6104.

[21] H. Zhu, Y. Shen, Q. Denga, T. Tu, Copper-catalyzed electrophilic amination of sodium sulfinates at room temperature, Chem. Commun. 51 (2015) 16573-16576.

[22] S.W. Wright, K.N. Hallstrom, A convenient preparation of heteroaryl sulfonamides and sulfonyl fluorides from heteroaryl thiols, J. Org. Chem. 71 (2006) 1080-1084.

[23] B. Nguyen, E.J. Emmett, M.C. Willis, Palladium-catalyzed aminosulfonylation of aryl halides, J. Am. Chem. Soc. 132 (2010) 16372- 16373.

[24] Y. Chen, P.R.D. Murray, A.T. Davies, M.C. Willis, The direct copper-catalyzed three-component synthesis of sulfonamides, J. Am. Chem. Soc. 140 (2018) 8781–8787.

[25] S. Ye, J. Wu, A palladium-catalyzed three-component coupling of arylboronic acids, sulfur dioxide and hydrazines, Chem. Commun. 48 (2012) 7753;

[26] D.Q. Zheng, Y.Y. An, Z.H. Li, J. Wu, Metal-free aminosulfonylation of aryldiazonium tetrafluoroborates with DABCO.$(SO_2)_2$ and hydrazines, Angew. Chem. Int. Ed. 53 (2014) 2451-2454.

[27] X. Wang, L. Xue, Z. Wang, A copper-catalyzed three-component reaction of triethoxysilanes, sulfur dioxide, and hydrazines, Org. Lett. 16 (2014) 4056-4058.

[28] N.W. Liu, S. Liang, G. Manolikakes, Visible-light photo redox catalyzed aminosulfonylation of diaryliodonium salts with sulfur dioxide and hydrazines, Adv. Synth. Catal. 359 (2017) 1308-1319.

[29] S. Ye, J. Wu, A palladium-catalyzed reaction of aryl halides, potassium metabisulfite, and hydrazines, Chem. Commun. 48 (2012) 10037.

[30] B. Mokhtari, D. Nematollahi, H. Salehzadeh, A tunable pair electrochemical strategy for the synthesis of new benzenesulfonamide derivatives, Sci. Rep. 9 (2019) Article number: 4537.

[31] S. Khazalpour, D. Nematollahi, A. Ahmad, B. Dowlati, Electroreductive nucleophile acceptor generation. Electrochemical synthesis of *N*-(4-(dimethylamino) phenyl) benzenesulfonamide, Electrochim. Acta 180 (2015) 909–913.

[32] G. Laudadio, E. Barmpoutsis, C. Schotten, L. Struik, S. Govaerts, D.L. Browne, T. Noël, Sulfonamide synthesis through electrochemical oxidative coupling of amines and thiols, J. Am. Chem. Soc. 141 (2019) 5664-5668.

[33] L. Craine, M. Raban, The chemistry of sulfonamides, Chem. Rev. 89 (1989) 689-712.

[34] A.J. Marzocca, M.A. Mansilla, Vulcanization kinetic of styrene–butadiene rubber by sulfur/TBBS, J. Appl. Polym. Sci. 101 (2006) 35-41.

[35] J.L. Shang, H. Guo, Z.S. Li, B. Ren, Z.M. Li, H.G. Dai, L.X. Zhang, J.G. Wang, Synthesis and evaluation of isatin-β-thiosemicarbazones as novel agents against antibiotic-resistant gram-positive bacterial species, Bioorg. Med. Chem. Lett. 23 (2013) 724-727.

[36] A.S. Karwa, A.R. Poreddy, B. Asmelash, T.S. Lin, R.B. Dorshow, R. Rajagopalan, Type 1 phototherapeutic agents. 2. Cancer cell viability and ESR Studies of Tricyclic Diarylamines, ACS Med. Chem. Lett. 211 (2011) 828-833.

[37] F.A. Davis, A.J. Friedman, E.W. Kluger, E.B. Skibo, E.R. Fretz, A.P. Milicia, W.C. LeMasters, M.D. Bentley, J.A. Lacadie, I.B. Douglass, Chemistry of the sulfur-nitrogen bond. 12. Metal-assisted synthesis of sulfenamide derivatives from aliphatic and aromatic disulfides, J. Org. Chem. 42 (1977) 967-972.

[38] K.M. Huttunen, J. Leppänen, K. Laine, J. Vepsäläinen, J. Rautio, Convenient microwave-assisted synthesis of lipophilic sulfenamide prodrugs of metformin, Eur. J. Pharm. Sci. 49 (2013) 624–628.

[39] E. Rattanangkool, W. Krailat, T. Vilaivan, P. Phuwapraisirisan, M. Sukwattanasinitt, S. Wacharasindhu, Hypervalent Iodine (III)-promoted metal-free S–H activation: an approach for the construction of S–S, S–N, and S–C bonds, Eur. J. Org. Chem. 2014 (2014) 4795-4804.

[40] H. Yakan, H. Kutuk, Comparison of conventional and microwave-assisted synthesis of some new sulfenamides under free catalyst and ligand, Monatsh. Chem. 149 (2018) 2047–2057.

[41] D.N.Harpp, T.G. Back, A general synthesis of sulfonamides, Tetrahedron Lett. 12 (1971) 4953-4956.

[42] M. Shimizu, H. Fukazawa, S. Shimada, Y. Abe, The synthesis and reaction of *N*-sulfenyl heterocycles: development of effective sulfenylating reagents, Tetrahedron 62 (2006) 2175-2182.

[43] N. Taniguchi, Copper-catalyzed formation of sulfur–nitrogen bonds by dehydrocoupling of thiols with amines, Eur. J. Org. Chem. 2010 (2010) 2670-2673.

[44] C. Sandford, M.A. Edwards, K.J. Klunder, D.P. Hickey, M. Li, K. Barman, M.S. Sigman, H.S. White, S.D. Minteer, A synthetic chemist's guide to electroanalytical tools for studying reaction mechanisms, Chem. Sci. 10 (2019) 6404-6422.

[45] A.J. Bard, L.R. Faulkner, Electrochemical Methods, 2nd edn, Wiley, New York (2001).

[46] R.N. Goyal and M.S. Verma, Electrochemical oxidation of 2-mercaptobenzoxazole, Indian J. Chem. 35A (1996) 281-287.

[47] A. Schaufuß, G. Wittstock, Oxidation of 2-mercaptobenzoxazole in aqueous solution: solid phase formation at glassy carbon electrodes, J. Solid State Electrochem. 3 (1999) 361-369.

[48] A.A. Ahmed Boraei, I.T. Ahmed, M.M.A. Hamed, Acid dissociation constants of some mercaptobenzazoles in aqueous-organic solvent mixtures, J. Chem. Eng. Data 41 (1996) 787-790.

[49] Q. Liu, L. Wang, H. Yue, J.S. Li, Z. Luo, W. Wei, Catalyst-free visible-light-initiated oxidative coupling of aryldiazo sulfones with thiols leading to unsymmetrical sulfoxides in air, Green Chem. 21 (2019) 1609-1613.

[50] F. Jensen, A. Greer, E.L. Clennan, Reaction of organic sulfides with singlet oxygen. A revised mechanism, J. Am. Chem. Soc. 120 (1998) 4439-4449.

[51] D.H. Kim, J. Lee, A. Lee, Visible-light-driven silver-catalyzed one-pot approach: A selective synthesis of diaryl sulfoxides and diaryl sulfones, Org. Lett. 20 (2018) 764-767.

[52] B. Karimi, M. Rafiee, S. Alizadeh, H. Vali, Eco-friendly electrocatalytic oxidation of alcohols on a novel electro generated TEMPO-functionalized MCM-41 modified electrode, Green Chem. 17 (2015) 991-1000.

Tables

Table 1. Products and conditions for the synthesis of sulfonamide (**SO**) and sulfenamide (**SE**) compounds.

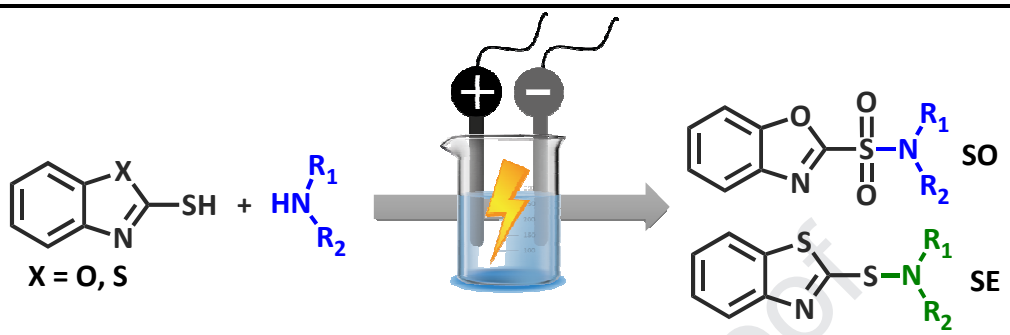

Undivided cell . Anode: carbon . Cathode: stainless steel
Phosphate buffer (X = O, pH = 8.0, X = S, pH = 12.0)/ethanol (20/80 v/v)
X = O, J = 0.26 mA cm^{-2} . X = S, J = 0.52 mA cm^{-2} Q = 190 C .
Room temperature

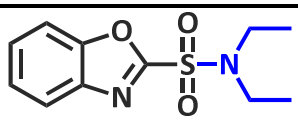 **SO1** Yield: 59%	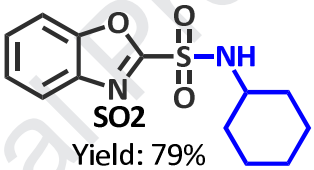 **SO2** Yield: 79%	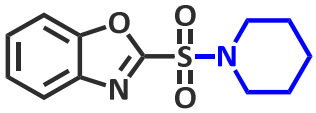 **SO3** Yield: 62%
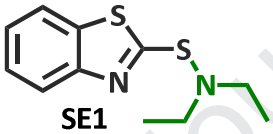 **SE1** Yield: 65%	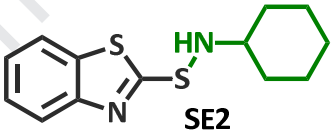 **SE2** Yield: 88%	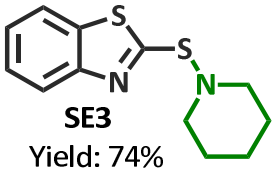 **SE3** Yield: 74%

Table 2. Antibacterial activity of **SO1**-**SO3** and **SE4**-**SE6**.

	Microorganism	Tetracyclne disc 30 µg[a]	well 30 µg[b]	Disc 30 µg	Activity
SO1	*Bacillus cereus*	32	12	11	(-)[c]
	Staphylococcus aureus	26	8	9	(-)
	Escherichia coli	20	8	9	(-)
	Salmonella enteritidis	18	7	10	(-)
SO2	*Bacillus cereus*	26	17	15	(+)[d]
	Staphylococcus aureus	29	19	16	(+)
	Escherichia coli	18	16	14	(+)
	Salmonella enteritidis	22	16	15	(+)
SO3	*Bacillus cereus*	29	16	14	(+)
	Staphylococcus aureus	23	17	14	(+)
	Escherichia coli	18	18	17	(+)
	Salmonella enteritidis	19	16	15	(+)
SE4	*Bacillus cereus*	30	19	17	(+)
	Staphylococcus aureus	27	16	15	(+)
	Escherichia coli	18	8	8	(-)
	Salmonella enteritidis	23	8	7	(-)
SE5	*Bacillus cereus*	35	18	17	(+)
	Staphylococcus aureus	28	9	9	(-)
	Escherichia coli	20	16	15	(+)
	Salmonella enteritidis	22	14	15	(+)
SE6	*Bacillus cereus*	28	18	14	(+)
	Staphylococcus aureus	26	16	15	(+)
	Escherichia coli	18	8	8	(-)
	Salmonella enteritidis	24	7	8	(-)

[a]Diameter of effective zone of inhibition (mm).

[b]Solvent well, DMSO + Tween 20.

[c]Negative activity.

[d]Positive activity

Figures

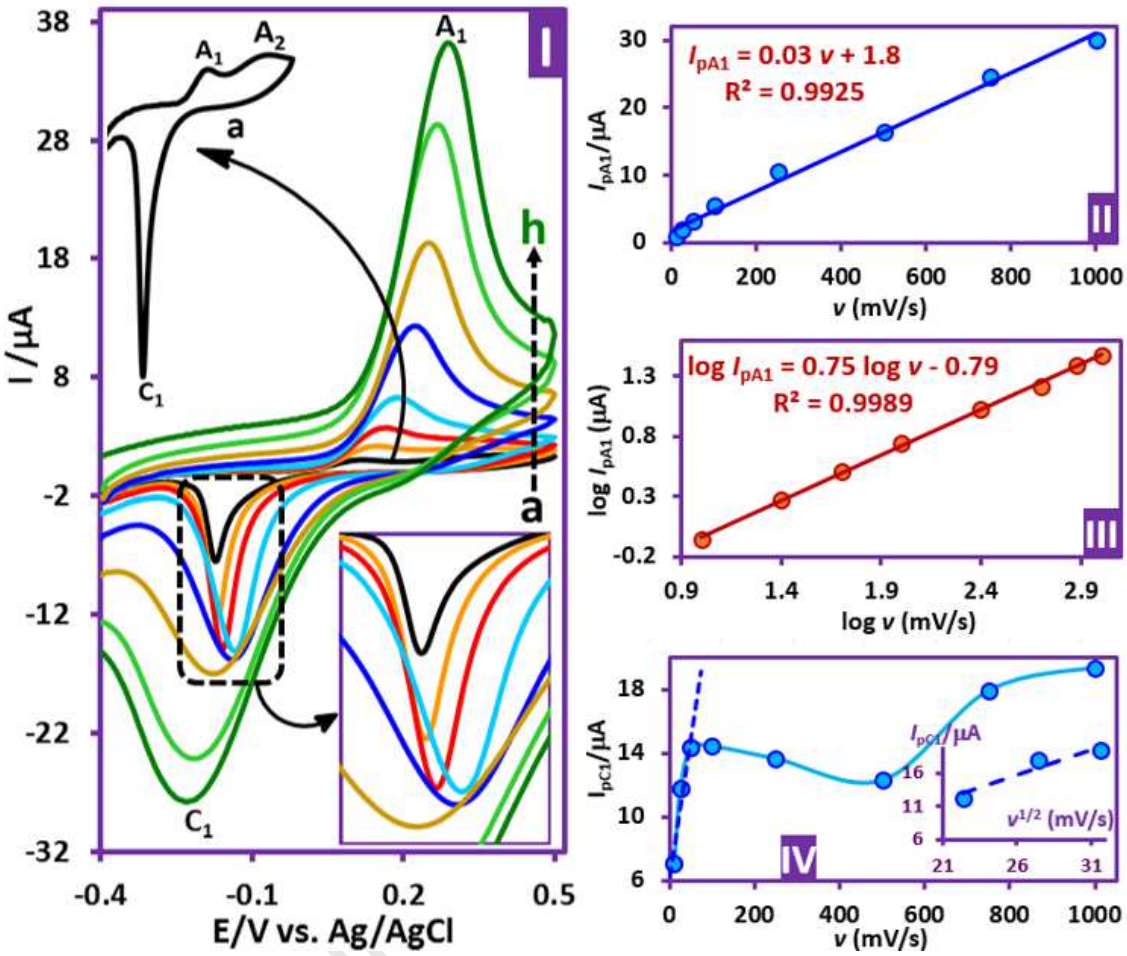

Figure 1. Part I. Cyclic voltammograms of **MBO** (1.0 mM) in aqueous phosphate buffer (*c* = 0.2 M, pH = 7.0), at GC electrode, at different scan rate and at room temperature. Scan rates from a to h are: 10, 25, 50, 100, 250, 500, 750 and 1000 mV/s. Part II, the plot of I_{pA1} versus scan rate. Part III, the plot of log I_{pA1} versus log *v*. Part IV, the plot of I_{pC1} versus scan rate.

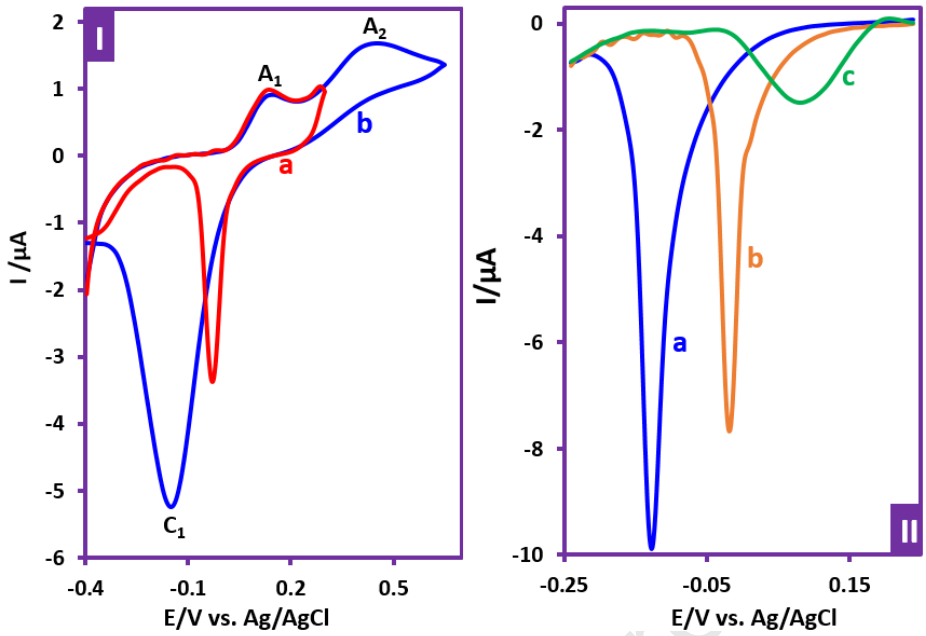

Figure 2. Part I: Cyclic voltammograms of **MBO** (1.0 mM) in water (phosphate buffer, pH = 7.0 and *c* = 0.2 M) at two different switching potentials. Switching potentials for "a" and "b" are 0.30 and 0.65 V vs. Ag/AgCl, respectively. Part II: Linear sweep voltammograms of **MBO** (1.0 mM) (peak C_1) in different ethanol/H_2O (phosphate buffer, pH = 8.0 and *c* = 0.2 M) mixtures a) 0%, b) 10% and c) 20% ethanol. Working electrode: GC electrode. Scan rate: 10 mV/s. Temperature = room temperature.

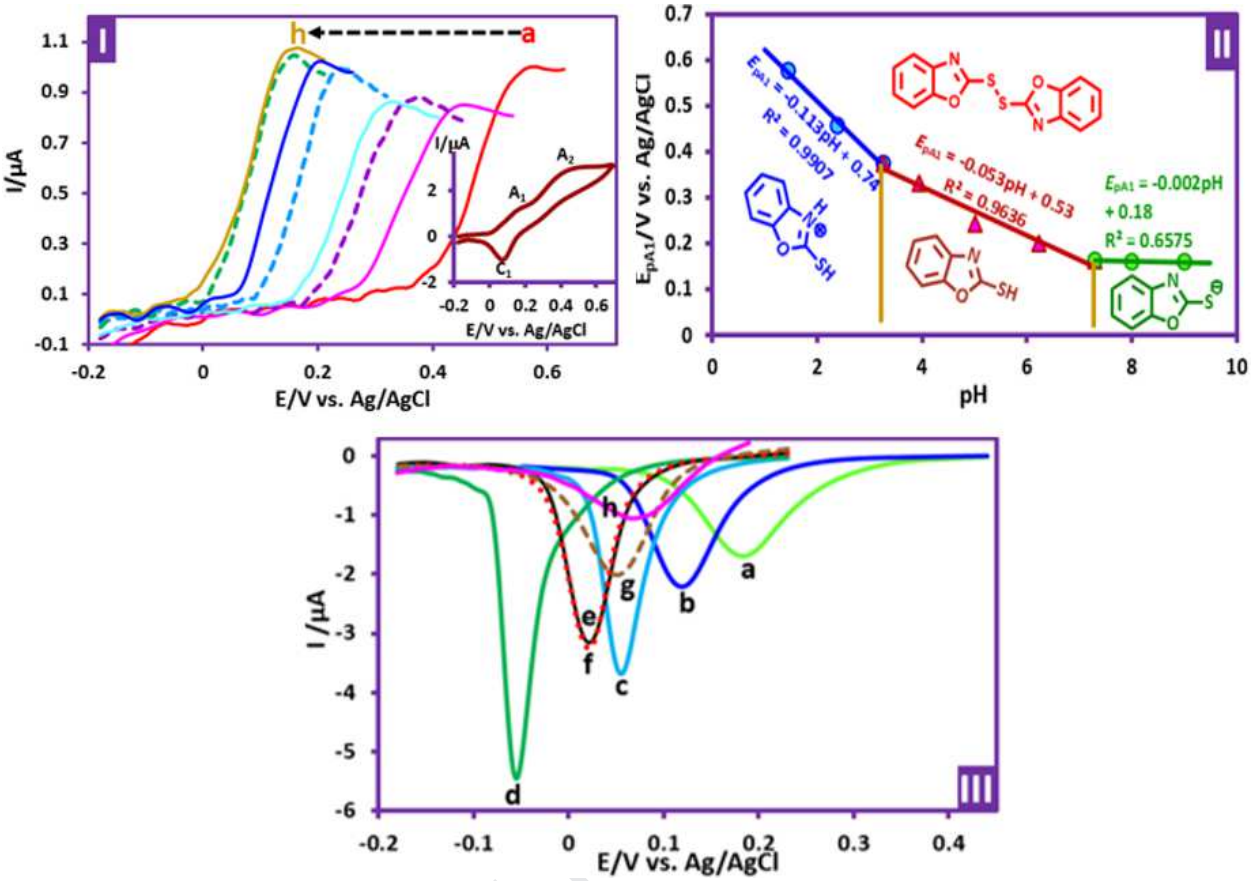

Figure 3. Part I: Linear sweep voltammograms of **MBO** (1.0 mM) in ethanol/H_2O (with different pH values) (20/80, v/v) mixture at GC electrode, at room temperature. Scan rate: 10 mV/s. pH values from a to h are: 1.4, 2.4, 3.3, 3.9, 5.0, 6.2, 7.3 and 8.0. Inset: cyclic voltammogram of **MBO** under above condition at pH = 9.00. Part II: The potential-pH diagram of **MBO**. Part III: The status of peak C_1 at different pHs. pH values from a to h are: 1.4, 2.4, 3.3, 5.0, 6.2, 7.3, 8.0 and 9.0.

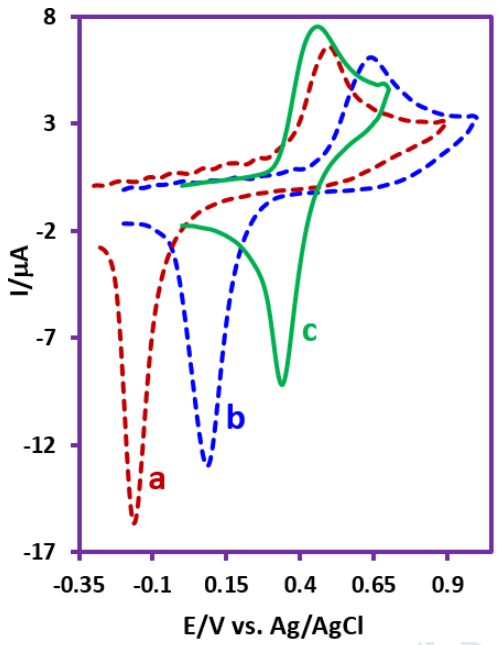

Figure 4. Cyclic voltammograms of 1.0 mM: (a) **MBT**, (b) **MBO** and (c) **MBI** in water ($HClO_4$, pH = 1.0 and *c* = 0.1 M)/ethanol (80/20) mixture at GC electrode, at room temperature. Scan rate: 100 mV/s.

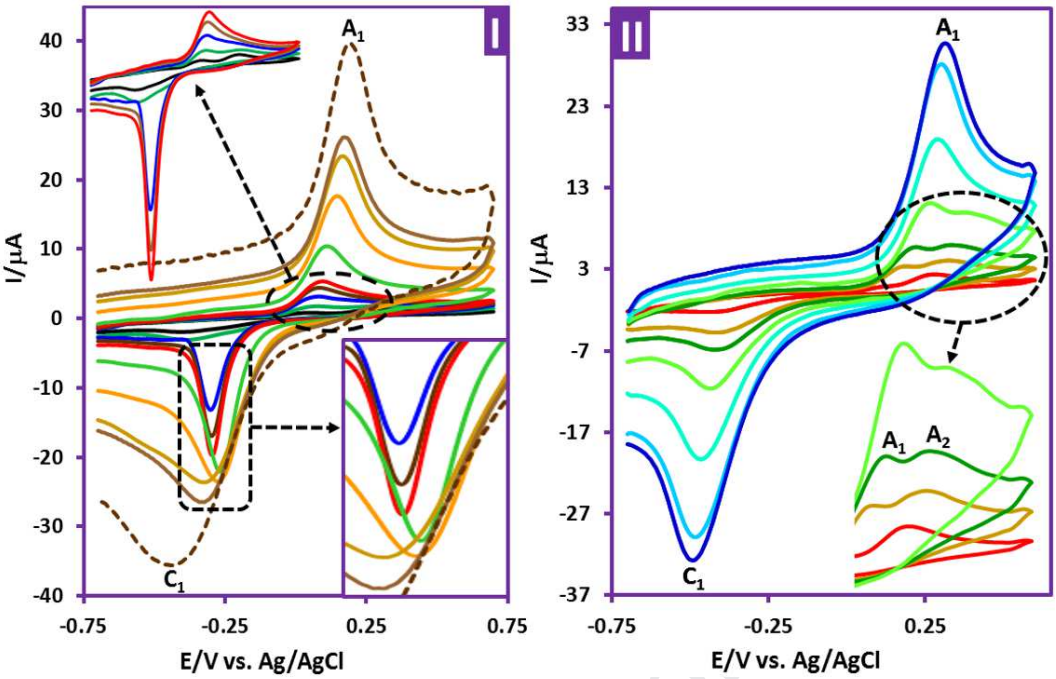

Figure 5. Cyclic voltammograms of 1.0 mM **MBT** (part I) and 1.0 mM **MBI** (part II) in water (phosphate buffer, pH = 8.0 and *c* = 0.2 M)/ethanol (80/20) mixture at GC electrode, at room temperature. Scan rates for **MBT** are: 10, 25, 50, 75, 100, 250, 500, 750, 1000 and 2000 mV/s. Scan rates for **MBI** are: 10, 50, 100, 250, 500, 750 and 1000 mV/s.

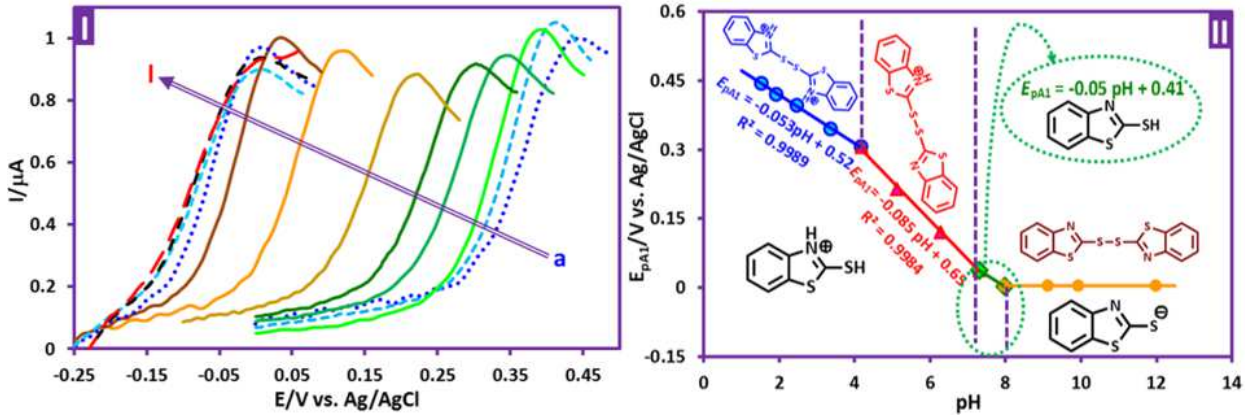

Figure 6. . Part I: Linear sweep voltammograms of **MBT** (1.0 mM) in ethanol/H_2O (with different pH values) (20/80, v/v) mixture at GC electrode, at room temperature. Scan rate: 10 mV/s. pH values from a to I are: 1.54, 1.93, 2.47, 3.37, 4.17, 5.12, 6.27, 7.31, 7.98, 9.13, 9.94 and 12.00. Part II: The potential-pH diagram of **MBT**.

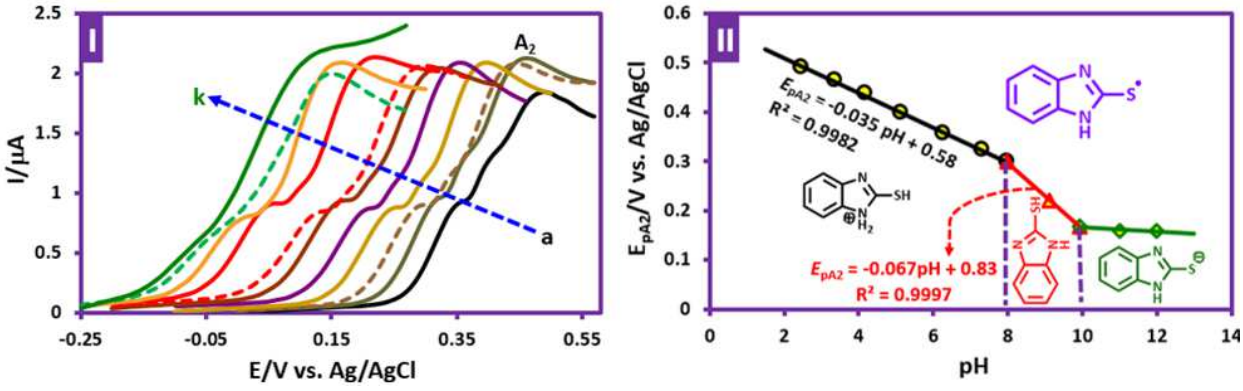

Figure 7. Part I: Linear sweep voltammograms of **MBI** (1.0 mM) in ethanol/H_2O (with different pH values) (20/80, v/v) mixture at GC electrode, at room temperature. Scan rate: 10 mV/s. pH values from a to k are: 2.47, 3.37, 4.17, 5.12, 6.27, 7.31, 7.98, 9.13, 9.94, 11.01 and 12.00. Part II: The potential-pH diagram of **MBI**.

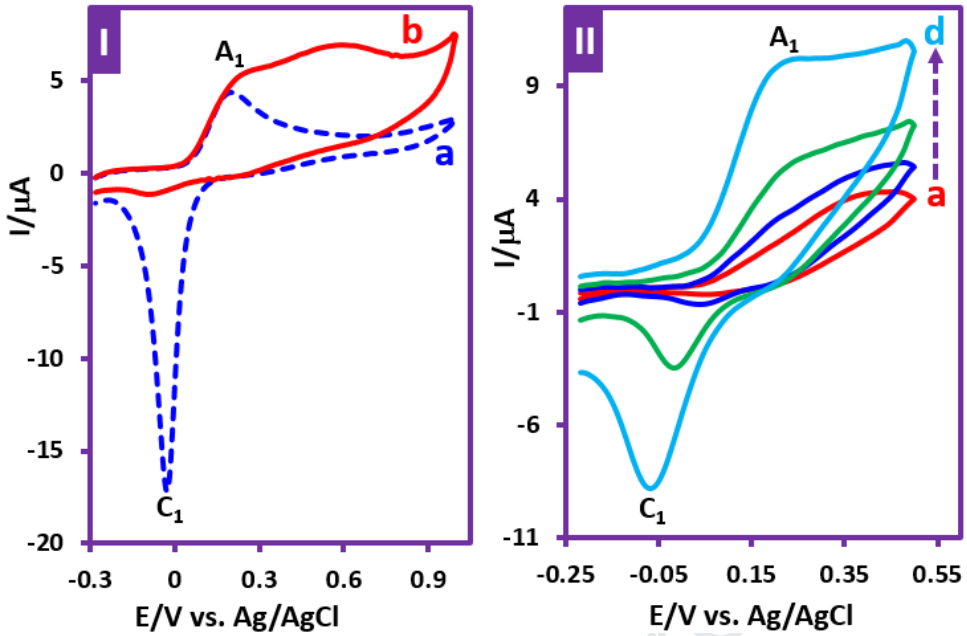

Figure 8. Part I: Cyclic voltammograms of **MBO** (1.0 mM) in the absence of **AM1** (curve a) and in the presence of **AM1** (2.5 mM) (curve b) at scan rate of 100 mV s^{-1}. Part II: Cyclic voltammograms of **MBO** (1.0 mM) in the presence of **AM1** (2.5 mM) at various scan rates. Scan rates from of a to d are: 10, 25, 100 and 250 mV s^{-1}. Solvent: ethanol/H_2O (pH = 8.0) (20/80, v/v) mixture at GC electrode and at room temperature.

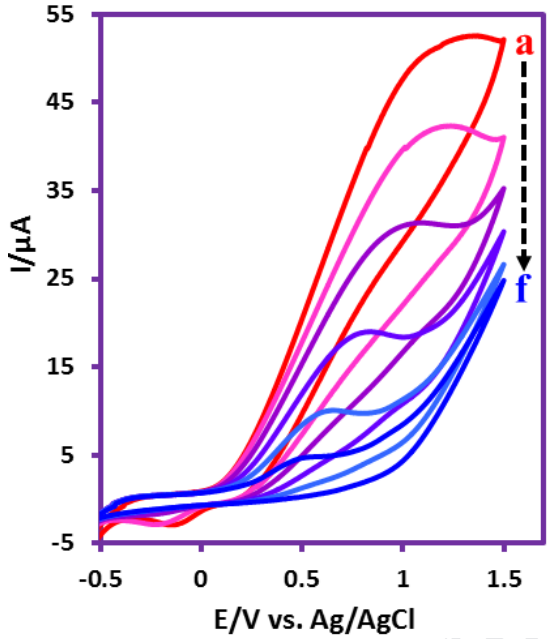

Figure 9. Cyclic voltammograms of **MBO** (0.5 mmol) in the presence of **AM1** (1.5 mmol) during the constant current electrolysis in water (pH=8.0)/ethanol mixture (20/80, v/v) in various time. Time from a to f is: 0, 60, 120, 180, 240 and 330 min. current density: 0.26 mA/cm^2. Scan rate: 100 mV/s at room temperature.

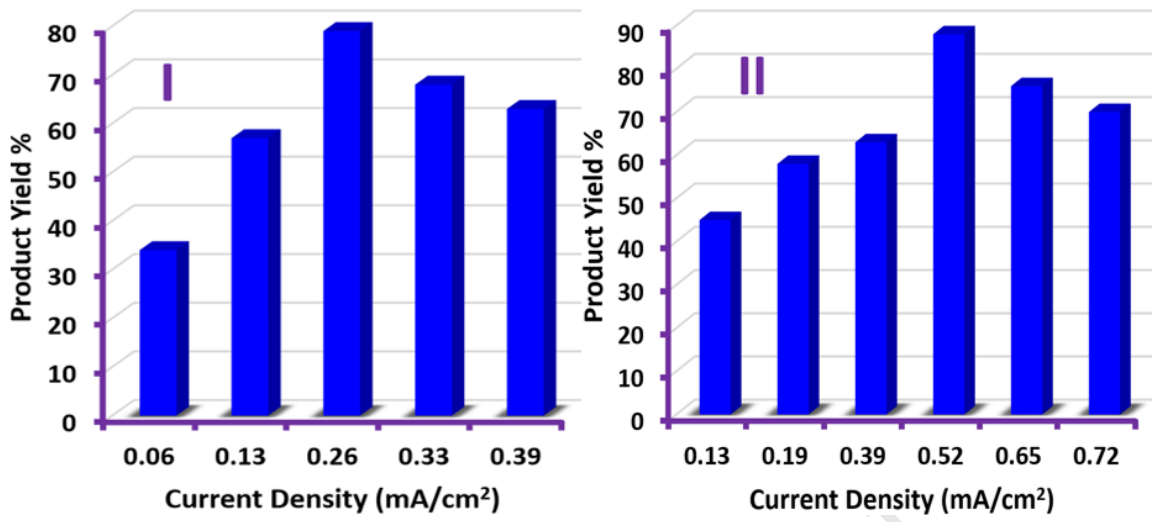

Figure 10. The effect of current density on the yield of **SO2** (part I) and **SE5** (part II). Charge passed: 190 C. **MBO** and **MBT** amount: 0.5 mmol. **AM2** amount: 1.5 mmol at room temperature.

Figure 11. Cell configuration in large scale synthesis.

Tables

Table 1. Products and conditions for the synthesis of sulfonamide (**SO**) and sulfenamide (**SE**) compounds.

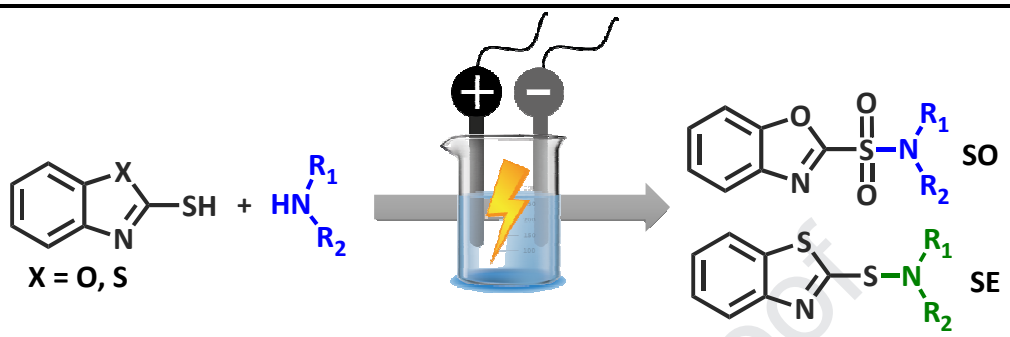

Undivided cell . Anode: carbon. Cathode: stainless steel
Phosphate buffer (X = O, pH = 8.0, X = S, pH = 12.0)/ethanol (20/80 v/v)
X = O, J = 0.26 mA cm^{-2}. X = S, J = 0.52 mA cm^{-2} Q = 190 C.
Room temperature

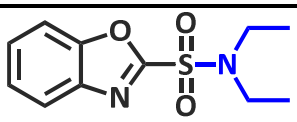 **SO1** Yield: 59%	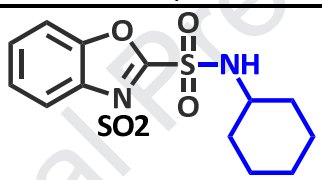 **SO2** Yield: 79%	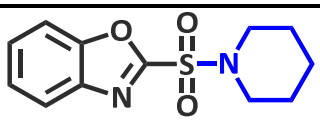 **SO3** Yield: 62%
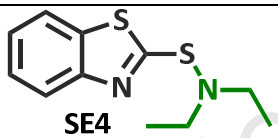 **SE4** Yield: 65%	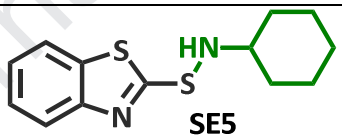 **SE5** Yield: 88%	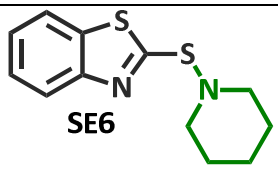 **SE6** Yield: 74%

Table 2. Antibacterial activity of **SO1**-**SO3** and **SE4**-**SE6**.

	Microorganism	Tetracyclne disc 30 µg[a]	well 30 µg[b]	Disc 30 µg	Activity
SO1	*Bacillus cereus*	32	12	11	(-)[c]
	Staphylococcus aureus	26	8	9	(-)
	Escherichia coli	20	8	9	(-)
	Salmonella enteritidis	18	7	10	(-)
SO2	*Bacillus cereus*	26	17	15	(+)[d]
	Staphylococcus aureus	29	19	16	(+)
	Escherichia coli	18	16	14	(+)
	Salmonella enteritidis	22	16	15	(+)
SO3	*Bacillus cereus*	29	16	14	(+)
	Staphylococcus aureus	23	17	14	(+)
	Escherichia coli	18	18	17	(+)
	Salmonella enteritidis	19	16	15	(+)
SE4	*Bacillus cereus*	30	19	17	(+)
	Staphylococcus aureus	27	16	15	(+)
	Escherichia coli	18	8	8	(-)
	Salmonella enteritidis	23	8	7	(-)
SE5	*Bacillus cereus*	35	18	17	(+)
	Staphylococcus aureus	28	9	9	(-)
	Escherichia coli	20	16	15	(+)
	Salmonella enteritidis	22	14	15	(+)
SE6	*Bacillus cereus*	28	18	14	(+)
	Staphylococcus aureus	26	16	15	(+)
	Escherichia coli	18	8	8	(-)
	Salmonella enteritidis	24	7	8	(-)

[a]Diameter of effective zone of inhibition (mm).

[b]Solvent well, DMSO + Tween 20.

[c]Negative activity.

[d]Positive activity

Declaration of interests

☒ The authors declare that they have no known competing financial interests or personal relationships that could have appeared to influence the work reported in this paper.

☐The authors declare the following financial interests/personal relationships which may be considered as potential competing interests: